

PRESSURE PROBES FOR FLUID MEASUREMENT

S. H. CHUE

Universiti Sains Malaysia*

Summary—The material contained in this monograph has been divided into six main sections, in accordance with the specific applications of the pitot tube and other allied pressure probes, viz. for impact pressure, static pressure, dynamic pressure, flow direction and vector velocity, skin friction as well as flow measurements. In most instances, as far as it could be managed, the author has tried to incorporate both theoretical and experimental aspects on the various factors influencing the accuracy of the pressure probes. It is, therefore, hoped that this monograph can serve as a useful sequel to the monograph by Bryer and Pankhurst, entitled "Pressure-probe Methods for Determining Wind Speed and Flow Direction", adding further details on topics discussed therein and other topics not already included.

It is the intention of the author to exclude discussions on the use of pressure probes for static-pressure fluctuation measurements. This is a highly specialized field of application and the only reliable measurements at the present seem to be those of Elliott (*J. Fluid Mech.*, 53 (1972) p. 351).

The author takes great pleasure in acknowledging the assistance rendered by Mr. P. Bradshaw of Imperial College in the preparation of this manuscript, for his advice and suggestions on matters related to this paper, and is also grateful to him and Prof. Küchemann for suggesting several extra references.

LIST OF SYMBOLS

c_f	skin friction coefficient
C_m	most probable molecular speed
C_p	pressure coefficient
d	inner diameter of round pitot; diameter of static hole
D	outer diameter of round pitot; d/D ratio
f	skin friction coefficient for pipe flow
h	internal height of flattened pitot
H	external height of flattened pitot
ℓ	depth of static hole
L	characteristic length; length of pitot tube
p	static pressure; if subscripted, pressure registered at particular orifice
P	impact or stagnation pressure
P_0	total pressure
q	dynamic pressure; resultant velocity
q'	resultant turbulent velocity
r	inner radius of round pitot
R	outer radius of round pitot; specific gas constant
S	speed ratio
T	absolute temperature
T_0	total temperature
u	longitudinal velocity component;
U	velocity under measurement
v	transverse velocity component
w	transverse velocity component; inner width of flattened pitot
W	outer width of flattened pitot
u', v', w'	turbulent velocity components
(-)	mean or averaged value

Greek symbols

α	shear parameter; yaw angle
γ	specific heat ratio
δ	displacement correction
Δ	shock stand-off distance
$\Delta()$	difference in ()
ϵ	average height of equivalent sand roughness
θ	pitch angle; semi-vertex angle of conical probes; critical angle subtended by static and stagnation orifices at centre of cylinder or sphere

λ	boundary layer thickness; mean free path; thermal conductivity
μ	dynamic viscosity
ν	kinematic viscosity
Π	inner pressure gradient parameter, $= \frac{\nu}{\rho u^3} \frac{dp}{dx}$
ρ	fluid density
τ	wall shear stress
ϕ	roll angle
ψ	pitch angle

Subscripts

c	cavity behind static pressure orifice
m	measured value
p	pipe
∞	free stream value
1	free stream condition
2	condition behind normal shock

1.1. Introduction

That a tube bent to face the oncoming stream and of sufficient stem length to bring the fluid to rest registers the total or impact pressure of the stream was first recognized by Pitot in 1732. Since then this simple device, which has been christened the pitot tube, has remained one of the simplest and most widely used instruments for measuring the impact pressure. Its main disadvantage, which is also true of many other pressure anemometers, is that it involves the insertion of a probe into the stream. This is bound to disturb the flow to a certain extent, and the disturbance will be propagated upstream through the main flow in subsonic streams and transmitted upstream through the boundary layer which interacts with the shock generated by the probe in the case of supersonic flows. In order to minimize this inherent error, it is therefore necessary to keep the disturbance sufficiently small so that it would not cause significant modification of the stream characteristics ahead of the probe such that the pressure at the mouth of the probe be-

*Present address: R. J. Brown & Associates (Far East) Pte. Ltd., International Consultants, P.O. Box 72, Farrer Road Post Office, Singapore 11.

comes different from that of the undisturbed flow.

In addition, other inherent errors are involved. These are caused by deviations from the assumptions made in deriving the fundamental equation governing the flow along a streamline. This is known as the Bernoulli equation, which can be written in the following general form*

$$\frac{u^2}{2} + \int \frac{dp}{\rho} = \left[\int \frac{dp}{\rho} \right]_{u=0}. \quad (1)$$

Strictly speaking, this equation applies under the following conditions: (i) the tube is so narrow that only one streamline is brought to rest, (ii) the flow is inviscid.

Though (i) is not strictly fulfilled for practical probes, the ability of pitot tubes to determine the true impact pressure for a wide range of nose shapes has been taken for granted for a long time. This perhaps owes its origin to the optimistic statement made by Zahn⁽¹⁴⁰⁾ in 1903: "Almost any size and form of nozzle will convey the impact perfectly, provided it squarely faces the wind." Strictly speaking, this observation for a practical probe should apply only in an uniform velocity flow field such as that obtained in a wind tunnel or at the centre-line of a pipe, as a less restricted form of condition (i) would require, where the impact orifice could be assumed to sense fluid particles having equal velocities over its entire cross-sectional area.

For a real fluid, (ii) introduces the viscosity effect on the pitot reading, which has to be determined by means of calibration since present theoretical knowledge is still inadequate to predict the calibration function for pitots of arbitrary nose configurations.

The non-conformity of practical situations to conditions (i) and (ii) has given rise to a host of adjustments on the impact reading if high accuracy is to be required, especially at low Reynolds numbers. These will be discussed in detail in the following sections.

1.2. Calibration of Impact Tubes: the Effect of Viscosity or Reynolds Number

As mentioned in the previous section, the Bernoulli equation holds only in inviscid flow. Real fluids, however, have been found to possess certain amount of viscosity. This certainly alters the flow round the probe to some extent so that the pressure at the mouth of the tube would not correspond to that computed with this equation. The prediction of the deviation from the Bernoulli equation by theory is no simple matter and generally we have to resort to experimentation.

The basis of calibration has been discussed to

some detail in Bryer and Pankhurst. In what follows, we shall therefore confine ourselves on the features displayed by these results.

1.2.1. Calibration in incompressible flow

Results from incompressible calibration tests are often plotted in dimensionless form. The pressure coefficient defined by

$$C_p = \frac{P_m - p}{\frac{1}{2}\rho u^2} \quad (2)$$

is often used to eliminate the effect of free stream pressure intensity. Since this definition requires also the static pressure, it has to be independently determined or deduced from other considerations. As a consequence, theoretical results have also been put into the same form to facilitate comparison.

A wide variety of theoretical solutions has been reported to account for the behaviour of the pitot tube at low Reynolds numbers. Earlier solutions were necessarily obtained using various simplifying assumptions, such as those of Stokes, Oseen or Prandtl. The beauty of these solutions lies in the fact that they can be neatly written in a closed form.

In addition, in the past decade numerical solutions obtained by solving the full Navier-Stokes equations have been reported. These solutions, however, are still not to be used for predicting the calibration function or pressure coefficient for practical purposes as they are all invariably obtained for some simple situations, while actual operating conditions may well involve other effects coupled to the viscous one as evident from the fact that no two sets of experimental data are identical.

Nevertheless, it is beneficial for us to first examine some of these theoretical solutions before proceeding to look at the experimental results. Figures 1 and 2 show two closed form solutions obtained by using the boundary layer approximation; the first was by Homann⁽⁵⁵⁾ for flow near the stagnation point of a sphere and the second by Lin and Schaaf⁽⁷⁷⁾ for an impact tube with hemispherical nose having its longitudinal axis placed parallel to the direction of the flow. These are given by

For the sphere

$$C_p = 1 + \frac{6}{Re + 0.455\sqrt{Re}}. \quad (3)$$

For the hemispherical nose impact tube

$$C_p = 1 + \frac{7.25}{Re + 0.455\sqrt{Re}} \quad (4)$$

where Re is based on the radius of the sphere or nose.

Also shown in these figures are the numerical solutions obtained by Lester⁽⁷³⁾ for the flow over a semi-infinite square-ended cylinder of radius 1 cm situated on the axis of a circular pipe of radius 20 cm. The solution based on the external radius

* Occasionally, when two points of measurement are at appreciably different levels, it becomes necessary to include the gravity head term.

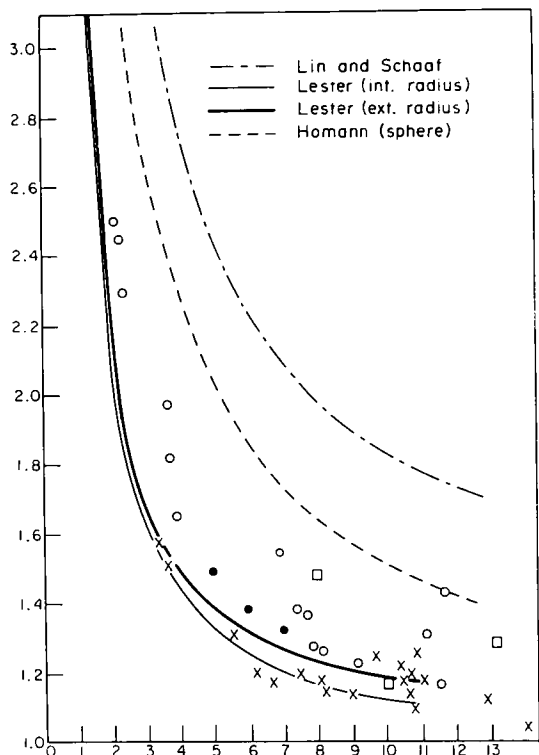


FIG. 1. Calibration function for square-ended pitots at low Reynolds number (based on external radius).

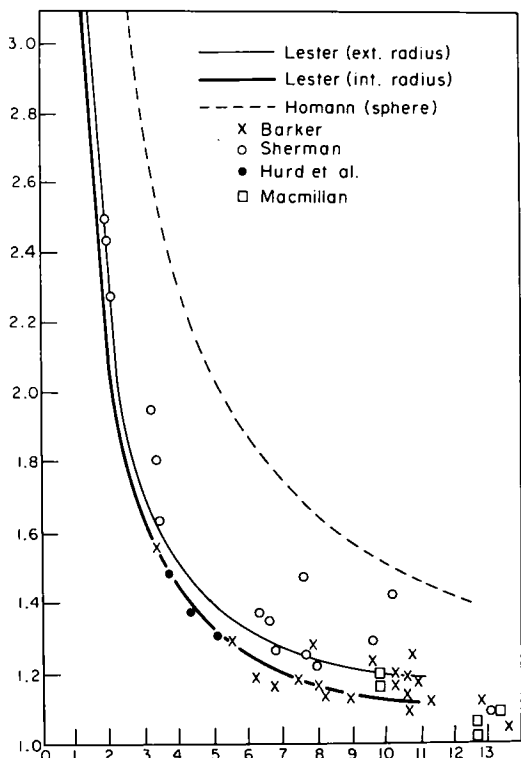


FIG. 2. Calibration function for square-ended pitots at low Reynolds number (based on internal radius).

was obtained with no orifice in the cylinder while that for the internal radius by assuming the walls to be infinitely thin so that the effect of the orifice

could be observed. In addition, the experimental data of several investigators have also been plotted for comparison, a topic which we shall return to later. From these figures, it can be deduced, assuming the mode of calibration does not influence the results, that the head-tip geometry does influence the calibration factor, C_p ; since C_p is smaller for square-ended tubes than for spherical or hemispherical heads over the range of Reynolds numbers reported, i.e. from $Re = 1$ to 14. This trend is expected to continue into the high Reynolds number range until their differences become indiscernible. It is difficult to specify the exact range of validity of these approximate solutions. Evidence suggests that Homann's results are accurate down to $Re = 10$, as the values of C_p agree quite well with the numerical results reported by Jensen⁽⁶²⁾ obtained by solving the complete Navier-Stokes equations for low Reynolds numbers, up to $Re = 20$.

Also observed is that the presence of a full orifice at the impact end decreases the value of C_p . As the two numerical solutions represent the limiting solutions for zero and full orifice sizes, it is therefore expected that the calibration curves for practical orifice bores will lie within the region bracketed by these two solutions; and the trend is that increasing orifice size decreases the value of C_p .

Bearing these theoretical observations in mind, we can now proceed to examine the various experimental calibration results.

The earliest experimental work on the effects of viscosity on pitot measurements was that of Miss Barker,⁽⁵⁾ who conducted tests with straight cylindrical tubes in Poiseuille flow. Whether the Reynolds number is based on the external or internal radius of the tube is not completely clear and later investigators have interpreted them in the manner that suits them best. The essential result of this investigation, which has come to be known as the Barker condition, that $UR/\nu > 3$ for C_p to be unity is not extensive enough to cover a reasonable range of operational Reynolds numbers. Reynolds numbers of the order of 30, corresponding to a velocity of 360 cm/sec in atmospheric air using a tube of 0.25 mm diameter, are rarely encountered except in exploration of a boundary layer and at low densities. Furthermore, the validity of this condition is marred by the large scatter in the results.

Later investigators generally carried their calibration measurements up to much higher operational Reynolds numbers. Figures 3 and 4 show some of these test results in the form of faired calibration curves. The experimental data have been omitted for the sake of clarity. The lower Reynolds number portion of some of these data have been displayed earlier in Figs. 1 and 2. A casual inspection of Fig. 3 shows that even for probes having the same head-tip shape, the calibration curves can differ quite considerably. Such a large difference cannot possibly be explained on the difference of orifice

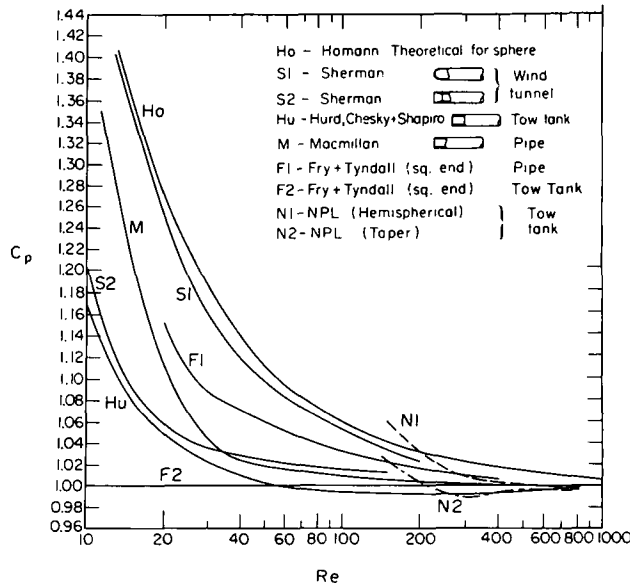


FIG. 3. Calibration function for pitots of various nose shapes (Reynolds number based on external radius).

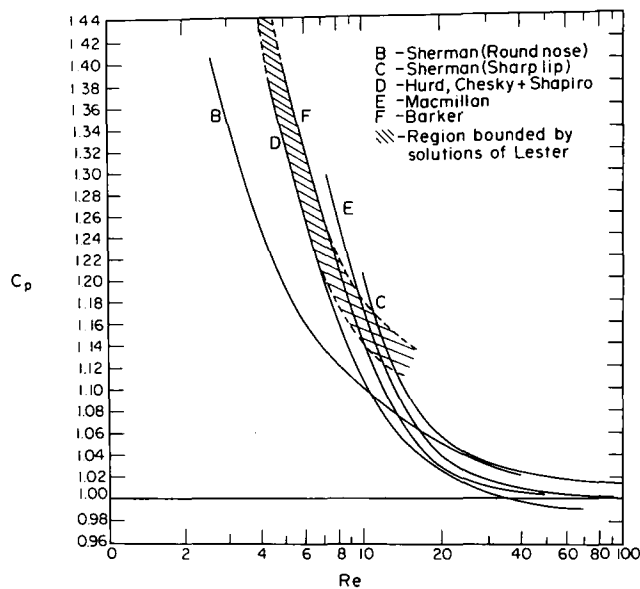


FIG. 4. Calibration function for pitots of various nose shapes (Reynolds number based on internal radius).

geometry as has been predicted by theory. The only plausible explanation remaining is that these calibration results are sensitive to the mode of calibration used in obtaining them. In other words, the calibration factor used for the correction of a measurement also depends on the operating conditions. Whether such is the case has not been conclusively affirmed. If such is the case, corresponding calibration results ought to be used for practical purposes. It is rather fortuitous that this disagreement in the calibration factor is limited to $Re_R < 300$ for all cases reported. For $Re_R > 300$, the calibration coefficient, C_p , is generally within $\pm 2\%$ of unity so that velocity measurements can be made

up to an accuracy of $\pm 1\%$, if this is the only correction involved.

Reynolds numbers of the order of 300 corresponds to an air speed of about 1.2 m/sec for standard NPL pitot-static tubes of external diameter about 8 mm under normal atmospheric conditions, and approximately one-thirteenth this speed for water. When using smaller tubes, the velocity limit will be raised according to the relation $UD = \text{constant}$. These results have vindicated the pitot tube as a convenient and reliable instrument for industrial purposes. However, it has still not been widely adopted for low-speed measurements. This is, perhaps, due to the many diversified functions

reported for C_p at low Reynolds numbers. As will be seen later, this should not hamper the use of the pitot tube at low speeds.

One of the major contentions among experimental investigators in the past is whether the calibration factor should decrease below unity over a certain range of Reynolds numbers. Folsom⁽³²⁾ even went so far to suggest that the more reliable tests have tended to show no values less than unity. However, comparison of all towing tank calibration results, such as those reported for the NPL tapered-nose and hemispherical-nose tubes⁽⁹³⁾ as well as the results of Hurd *et al.*⁽⁵⁹⁾ shows that C_p decreases below unity over a certain range of Reynolds numbers. Though the lower limit does not necessarily coincide due to the strong influence of the nose, it seems that the upper limit of this range is rather precisely located at $Re_R = 1650$. This no doubt provides an important piece of evidence in support of the earlier remark that C_p is sensitive to the mode of calibration. MacMillan⁽⁸³⁾ suggested that this phenomenal behaviour of C_p is possibly due to the increase in the correction for swirl in the tank, which could only be determined for large Reynolds numbers. However, this explanation is not satisfactory in view of the fact that this phenomenon extends to rather high Reynolds numbers, usually very close to the highest reported values.

Generally, calibration tests for round pitots carried out in pipes show no decrease of C_p below unity. Such tests have been reported by Barker,⁽⁵⁾ Fry and Tyndall⁽¹³⁾ and MacMillan.⁽⁸³⁾ All these investigations were carried out with square-ended pitots. Even so, their calibration curves differ considerably, as is evident from Fig. 3. The work of Sherman⁽¹²²⁾ was carried out at subsonic and supersonic air streams in a wind tunnel. Subsonic tests were obtained for two types of probes having source-shaped and sharp-lip head tips in the range $0.1 \leq M \leq 0.7$ and $1 \leq Re_R \leq 400$. No decrease of C_p below unity has been observed, though a slight decrease of C_p below unity was noted in supersonic results for the sharp-lip probe.

Having discussed the calibration results from the point of view of calibration methods, we now return to consider these results from a different angle: their agreement with available theoretical solutions.

The experimental results of Homann⁽⁵⁵⁾ and Sherman for the hemispherical and source-shaped head-tips generally agree well with Homann's theory in the range where this solution is supposedly quite accurate, i.e. for $Re_R > 10$. For the hemispherical nose pitot, Merriam and Spaulding⁽⁸⁸⁾ had investigated experimentally the effect of orifice size over the range $0.2 < d/D < 0.74$. They found that the size of the orifice has no effect on the magnitude of the impact pressure measured at zero yaw; though, on the other hand, to obtain the true impact pressure, the problem of alignment in yaw is much more

critical for smaller orifice sizes. On this basis, the use of the internal radius for computing the Reynolds number, as has been done in Fig. 4 for curve B, for the hemispherical or source-shaped pitot is not justifiable. This is rather obvious from a comparison of the various curves presented in the same figure, which singles out curve B as somewhat peculiar.

Calibration data for square-ended nose shapes have been shown in Figs. 1 and 2 for the low Reynolds number range; and faired curves through these data are shown in Figs. 3 and 4 to much higher Reynolds numbers. In the low Reynolds number (based on external radius) range, the disagreement among these curves are generally too large to be accounted for by the difference in orifice size as predicted by theory. However, when the internal radius is used, it can be seen from Fig. 2 that though the actual experimental data have quite a large scatter, within the limits of this scatter the data can be said to be quite consistent with theory considering the influence of orifice size on the calibration factor, despite the fact that they were obtained by different investigators. The trend of this agreement can be more clearly observed from Fig. 4.

Also evident from Fig. 4 is the fact that basing the Reynolds number on the internal or orifice radius of the pitot reduces the divergence among the different sets of data significantly enough to make them fall within the limiting solutions for zero and full orifice size predicted by Lester's theory, see, for instance, curves D and F. It is further evident that Sherman's data should not be interpreted on the basis of equal internal and external radius as the internal radius would act as the more significant dimension due to the re-entrant nature of the funnel-shaped tip.

Since the viscous influence is of an asymptotic nature, it seems there would be no theoretical justification for the pressure coefficient to decrease below unity. This may either be caused by the mode of calibration, as has been suggested earlier, or, as proposed by Lester, be due to the orifice effect outweighing the viscous effect over a certain range of Reynolds numbers. However, the experiment of Merriam and Spaulding cited earlier seems to have discounted this later influence for the hemispherical nose pitot for which C_p also decrease below unity in the NPL whirling-arm calibrations. It is interesting to note that all towing-tank calibration results decrease below unity over a certain range of Reynolds numbers. In this connection, it behoves us to note that both theoretical and experimental results for supersonic and hypersonic streams reported in Section 1.8.1 indicate that such decrease occurs and is caused by the shock weakening effect. In view of the analogy existing between compressible and open-channel flows, this observation in high-speed flow may be quoted to substantiate the incompressible towing-tank data to some extent. It may even be possible to explain the

reduced pressure on the forward portion of the probe on the basis of interaction of the surface waves generated in front of the probe in towing-tank tests on the effect of viscosity.

In recapitulation, it can be said that for accuracy of velocity measurements to $\pm 1\%$ whether C_p decreases below unity over a certain range of Reynolds numbers does not really matter, because over this range all calibration curves are within $\pm 2\%$ of unity. For the lower Reynolds number range, it appears that corrections made on the basis of the available theoretical solutions is quite adequate for hemispherical-nose probes, irrespective of their orifice size provided it lies in the range $0.2 < d/D < 0.74$. On the other hand, for square-ended pitots there appears to be a family of calibration curves, depending on the d/D ratio. But, at present, this family of curves has not been fully and finally established. In lieu of better calibration information, the results of Hurd *et al.* are recommended for general correction purposes on account of their good agreement with Lester's low Reynolds number solution (based on the internal radius) as well as their small experimental scatter. For this purpose, their results have been reproduced in Fig. 5. As the original data are plotted on the external radius basis, we have to transform the Reynolds number computed with the internal radius of a given pitot by dividing it by the d/D ratio used by Hurd *et al.*, i.e. 0.74, before the correction factor is

read from Fig. 5. It should be pointed out that in so doing we have ignored the parametric influence due to the d/D ratio on the calibration results. For a small difference in this value between the given probe and that tested by Hurd *et al.*, this influence is, however, rather small.

Impact tubes with square-ended flattened sections have also come into common use, especially in measurements close to a wall. Normal dimensions of such pitots lie within the ranges $0.3 < h/H < 0.6$ and $3 < W/H < 11$. Their calibration curves would in addition depend on the aspect ratio, W/H , of the tube, which no doubt will be more significant than the effect of orifice size, given by h/H . Calibration tests of such pitots have been reported by MacMillan.⁽⁸⁴⁾ His results show that for $W/H > 7$ the effect of aspect ratio becomes negligible when the pressure coefficient is plotted against Reynolds number based on the internal height of the probe. This collaborates an earlier result for square-ended round pitots: that the inner dimension is better choice for correlating calibration results. Another noteworthy point about these results is that now C_p decreases below unity over a certain range of Reynolds numbers even though MacMillan had found no such decrease for round pitots in an earlier investigation using the same experimental set-up.⁽⁸³⁾ For the purpose of effecting low Reynolds number correction, the reader is referred to Bryer and Pankhurst for the calibration function.

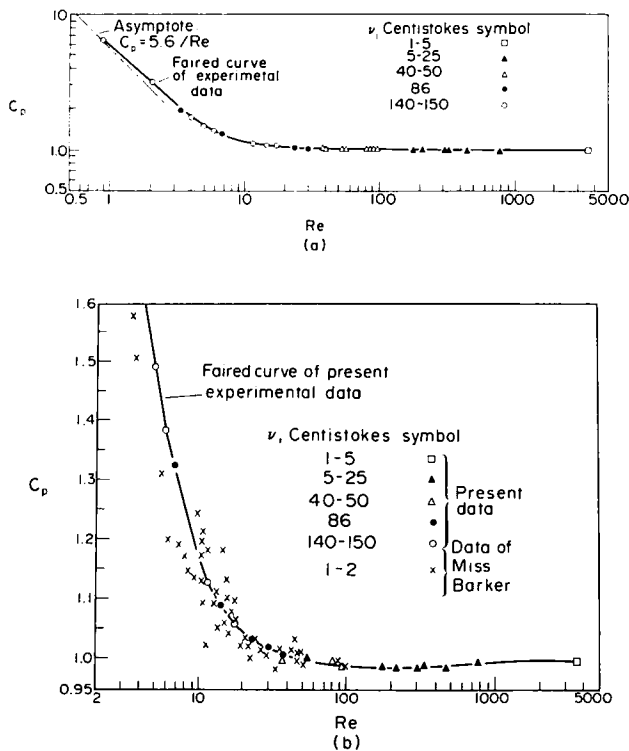


FIG. 5. Recommended calibration function for square-ended pitots. (Reynolds number to be computed with internal radius and divided by 0.74 before reading from graphs.) (a) Data over entire Reynolds number range. (b) Data for upper Reynolds number range.

1.2.2. Calibration in subsonic flow

For compressible flows, the stagnation of the fluid at the mouth of the pitot tube may be assumed to take place with such rapidity that heat transfer and frictional effects are negligible. This assumption has been checked experimentally by Walchner⁽¹³⁴⁾ and found to be true to within 0.2% up to Mach one. Thus, eqn. (1) can be integrated using the isentropic pressure-density relation to give

$$\frac{P_0}{P} = \left[1 + \frac{\gamma - 1}{2} M^2 \right]^{\gamma/\gamma-1}. \quad (5)$$

For small Mach numbers, this can be expanded using the binomial theorem together with the relation

$$\frac{1}{2} \rho u^2 = \frac{1}{2} \gamma M^2 p \quad (6)$$

to give

$$P_0 - p = \frac{1}{2} \rho u^2 \left[1 + \frac{M^2}{4} + \frac{2-\gamma}{24} M^4 + \dots \right] \quad (7)$$

which can be approximated by the incompressible Bernoulli equation up to Mach numbers of 0.2 with an error in $(P_0 - p)$ of less than 1%. Keeping the first two terms of the expansion allows the same accuracy to be maintained up to Mach 0.85 and the first three terms gives an accuracy of 0.2% up to Mach 1. Although eqn. (5) remains valid for isentropic flows at supersonic speeds, however, the introduction of a probe into the stream generates a normal shock in front of the probe thus obviating the further validity of this relation. We leave the discussion of the correct relation to be used under such conditions to the following section.

One way of presenting calibration results for compressible flow is suggested by the form of eqn. (5) as follows:

$$\frac{P_m}{P_B} = h(Re, M) \quad (8)$$

where $P_B = P_0$, the ideal impact pressure.

An alternative way, however, is to plot the

viscous correction to the impact pressure as in the case of incompressible flow; this is

$$C_\mu = \frac{P_m - P_0}{\frac{1}{2} \rho U^2} = f(Re, M). \quad (9)$$

It can be easily shown that this is related to the pressure coefficient in incompressible flow, C_p , as follows

$$C_\mu = C_p - \frac{P_0 - p}{\frac{1}{2} \rho u^2} = C_p - \left[1 + \frac{M^2}{4} + \frac{2-\gamma}{24} M^4 + \dots \right]. \quad (10)$$

A theoretical solution in the form of eqn. (9) has been reported by Lin and Schaaf⁽⁷⁷⁾ for flow over a semi-infinite cylinder having a hemispherical nose. This is in fact obtained as a more general solution to eqn. (4). It is

$$C_\mu = \frac{7.25 - 1.821 M^2}{Re + 0.455 \sqrt{Re}}. \quad (11)$$

It can be seen that both eqns. (10) and (11) indicate that the effect of compressibility is to decrease the calibration function at a given Reynolds number. The incompressible form of eqn. (11) has been seen to over-predict the calibration function for pitots of the same geometrical configuration. The same is seen to be still true for subsonic compressible flow from Fig. 6, where the source-shaped probe data of Sherman obtained in the range $0.1 < M < 0.7$ and $1 < Re < 400$ ⁽¹²²⁾ are plotted together with eqn. (11) evaluated at $M = 0.4$ and 0.8. It is evident that though the experimental data agree quite well with the trend predicted by theory, the former show no discernible Mach number dependence over the entire range reported whereas the latter display a significant Mach number influence on the results. Based on this set of results, it has been generally accepted that the effect of compressibility on the calibration function is negligible, see, for example, refs. 28 and 99. Until further evidences are forthcoming to indicate otherwise, we shall also accept this conclusion.

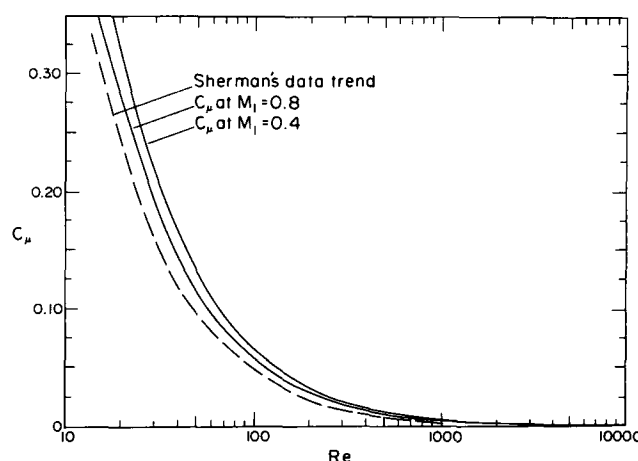


FIG. 6. Viscous correction for source-shaped and hemispherical nose pitots at high subsonic Mach numbers.

One point worthy of mention at this juncture is that Sherman's results may not lie entirely in the continuum regime. It can be easily shown using the flow regime criterion given in Section 1.8 that for slip flow to occur, the ratio M/Re for the probe should be greater than 0.0067. On this basis, the Reynolds numbers below which slip flow occurs are 104 and 15 at Mach numbers of 0.7 and 0.1 respectively. Assuming that the results at the lower Reynolds number range reported by Sherman were mainly obtained at the lowest Mach number tested, the data reported would have encroached into the slip flow regime. However, Sherman's results are not comprehensive enough for slip behaviour to be clearly identified though this might have accounted for part of the scatter in the results. We shall return to this topic in Section 1.8.

It has been often pointed out that data reduction in compressible flow is facilitated by taking the impact and static pressures separately. This convenience disappears if we want to incorporate the viscous correction to the measured impact pressure because both the velocity as well as the Mach number are now required, though measuring the pressures separately will allow the exact isentropic relation to be used and thus avoids the error caused by using the approximations.

Using eqn. (6), the various forms of pressure measurements and viscous correction factors can be related to the stream Mach number by the following equations:

(i) differential pressure measurement and using two-term approximation

$$\frac{P_m - p}{\frac{1}{2} \rho u^2} = \left(1 + \frac{M^2}{4}\right) + C_\mu; \quad (12)$$

(ii) separate impact and static pressure measurements

$$\frac{P_m}{p} = \left(1 + \frac{\gamma - 1}{2} M^2\right)^{\gamma/\gamma-1} + C_\mu \frac{1}{2} \gamma M^2 \quad (13a)$$

$$\frac{P_m}{p} = \left(1 + \frac{\gamma - 1}{2} M^2\right)^{\gamma/\gamma-1} h. \quad (13b)$$

In addition, it can easily be shown that the two forms of calibration functions for the impact tube in subsonic compressible flow are related as follows:

$$\frac{P_m}{P_B} = h = 1 + \left(1 + \frac{\gamma - 1}{2} M^2\right)^{-\gamma/\gamma-1} C_\mu \frac{1}{2} \gamma M^2. \quad (14)$$

1.2.3. Calibration in supersonic flow

When a pitot tube is inserted into a supersonic stream the air is decelerated in two stages. The first is a non-isentropic compression through a detached shock in front of the tube, and the second an isentropic compression after the shock to the mouth of the tube. Because of the increase in entropy at the shock, Bernoulli's isentropic equation can no longer apply; instead the Rayleigh

supersonic pitot formula now relates the theoretical stagnation pressure existing at the mouth of the pitot to the undisturbed stagnation pressure before the shock.

Since the flow aft of the shock is subsonic, the subsonic viscous correction discussed in the previous section should be applicable. As now the theoretical stagnation pressure aft of the shock is the Rayleigh pressure, P_R , the viscous correction factor can be written as

$$C_\mu = \frac{P_m - P_R}{\frac{1}{2} \rho u^2}. \quad (15)$$

Using eqn. (6) together with the appropriate Rankine-Hugoniot equations, this can be related to the measured to ideal pressure ratio as follows:

$$\frac{P_m}{P_R} = h = 1 + \left(\frac{\gamma + 1}{2} M^2\right)^{-\gamma/\gamma-1} \left(\frac{2\gamma}{\gamma + 1} M^2 - \frac{\gamma - 1}{\gamma + 1} \right)^{\gamma/\gamma-1} \frac{\gamma}{2} \frac{1 + \frac{\gamma - 1}{2} M^2}{\gamma M^2 - \frac{\gamma - 1}{2}} C_\mu. \quad (16)$$

In order that the Reynolds number can be evaluated for effecting the viscous correction, the velocity has to be known. It can be calculated from the following relation:

$$u_2 = \frac{M_2 \sqrt{(\gamma R T_0)}}{\sqrt{\frac{T_0}{T}}} = \frac{M_2 \sqrt{(\gamma R T_0)}}{\left(1 + \frac{\gamma - 1}{2} M^2\right)^{1/2}} \quad (17)$$

where M_2 is the Mach number aft of the shock. This is related to the free stream Mach number, M , as follows:

$$M_2 = \left\{ \frac{1 + \frac{\gamma - 1}{2} M^2}{\gamma M^2 - \frac{\gamma - 1}{2}} \right\}^{1/2}. \quad (18)$$

The advantage in using eqn. (17) lies in the fact that if no heat is being transferred between the body and the air stream, T_0 does not vary much across the boundary layer; and the velocity can be derived with the assumption that T_0 is constant and equal to its free stream value.⁽⁷⁾ If heat transfer occurs, this assumption is no longer valid, and the correct theoretical variations must be used. These, however, can be approximated by formulae given in ref. 89.

Experimental calibrations of the pitot tube at supersonic speeds had been reported by Kane and Maslach⁽⁶³⁾ for source-shaped pitots, by Sherman⁽¹²²⁾ for source-shaped and sharp-lipped probes, by Graves and Quiel⁽⁴⁴⁾ for probes having 10° internal chamfer and by Matthews⁽⁸⁷⁾ for flat-nosed (square-ended) impact probes. The tests of Kane and Maslach were conducted with the tubes submerged in flows remote from any solid boundaries. There were no velocity gradients normal to the tube axis. The operational Mach number ranged from 2.3 to 3.8. Their results are shown in Figs. 7 and 8. In Fig.

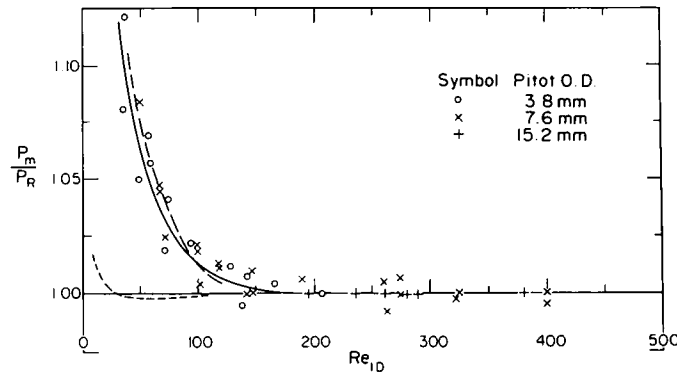


FIG. 7. Calibration function for source-shaped and hemispherical nose pitots at supersonic Mach numbers-variation with Re_{ID} . Legend: --- Sherman's source-shaped probe data trend, - - - Sherman's 10° internal chamfered probe data trend.

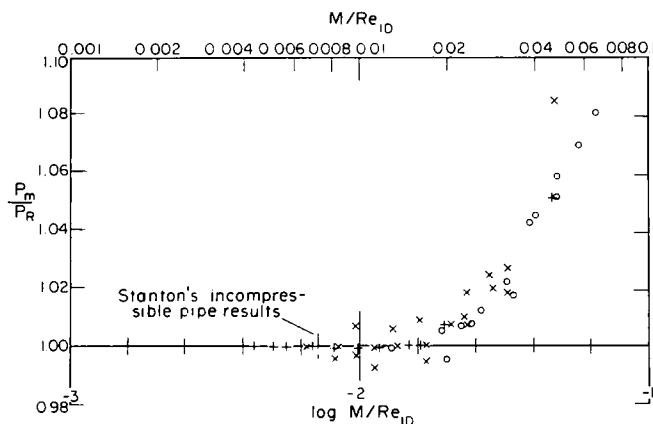


FIG. 8. Calibration function for source-shaped and hemispherical nose pitots at supersonic Mach numbers-variation with M/Re_{ID} and $\log M/Re_{ID}$.

7 the pressure ratio P_m/P_R is plotted against the undisturbed free-stream Reynolds number based on probe diameter, Re_D , as suggested by subsonic compressible flow considerations. It is seen that the viscous effect becomes important for Reynolds numbers smaller than 200. This is much lower than the corresponding limit found in subsonic and incompressible flows, since the value of 300 for the later case is based on the probe radius instead of diameter. Within the scatter of the data, the Mach number does not seem to influence the calibration factor. In Fig. 8 the same results have been plotted against M/Re_D , which is derived from molecular mean free path considerations. However, since the probe generates a bow shock in a supersonic stream such that it effectively senses only a subsonic stream, the use of Re_D as the correlation parameter does not seem justified. In fact, this may have resulted in the larger scatter in this figure. We shall postpone the discussion on the effect of slip to Section 1.8.1 later.

The results of Sherman for the source-shaped probe were obtained in the ranges $1.7 < M < 3.5$ and $15 < Re_D < 800$. These agree very well with the data reported by Kane and Maslach, see Fig. 7. A comparison of the source-shaped probe data of Sherman with eqn. (17) has been made in a later

figure, Fig. 27, from which it can be seen, contrary to the subsonic data, that fair agreement with the theoretical results of Lin and Schaaf exists. The main difference between experimental and theoretical results is that the former show no Mach number dependency over the entire range whereas the latter display appreciable influence.

Sherman's results for the sharp-lip probe, having a 10° internal chamfer, were obtained in the same Mach and Reynolds number ranges as for the source-shaped probe. Again, the viscous effect becomes important for $Re_D < 200$, based on the undisturbed free stream conditions. For $27 < Re_D < 200$, the measured impact pressure was less than the inviscid value, reaching a minimum of about 1% below. It becomes greater than the inviscid value for $Re_D < 27$. These results are shown in Fig. 9. In comparison, the results of Graves and Quiel for the same type of probe in the Mach number range of 5.3 to 5.6 as well as those of Matthews for the flat-nosed probe in the Mach number range of 5.4 to 5.7 are also shown. These two latter sets of results are in excellent agreement, showing the viscous effect to be important for $Re_D < 6000$ in the present Mach number range. This probably points to the same conclusion reached earlier for incompressible results, that the viscous characteristics for inter-

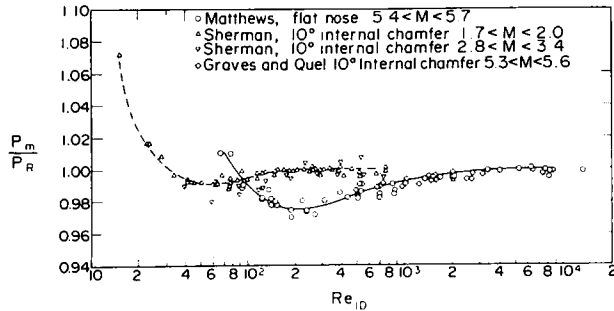


FIG. 9. Calibration function of internally chamfered pitots against Reynolds numbers (free stream).

nally chamfered and flat-nosed probes are identical. Thus, the marked difference between the results of Sherman and Matthews, or for that matter, Graves and Quiel, cannot be explained by the geometry of the probes. Therefore we have to seek an explanation elsewhere. It is well known that the normal shock in front of the probe causes a compression in the flow, which depends on the strength of the shock. One way to remove the effect of this compression is to plot the pressure ratio against the Reynolds number based on the flow conditions behind the shock, Re_{2D} . The impact pressure variations thus reduced are shown in Fig. 10. There is a significant improvement in the agreement between the two sets of results. However, a Mach number dependence is still present. A further improvement in the agreement can be obtained in the light of an analysis reported by Potter and Bailey.⁽¹⁰⁾ They

found that expressions for P_m/P_R derived from the Navier-Stokes equations with assumptions of a Hugoniot normal shock wave, Newtonian velocity gradient, no slip at the wall and constant density and viscosity in the shock layer suggest that the parameter $Re_2(\rho_2/\rho_\infty)^{1/2}$ is superior to Re_2 alone for correlating data on impact pressure in the continuum flow regime. Following this suggestion, the data shown in Fig. 10 have been recorrelated and the results given in Fig. 11. It is clearly evident that this parameter is capable of collapsing the Mach number effect of the two graphs into one, especially in the region where the measured impact pressure is greater than the inviscid value. Though in the region where the measured impact pressure is below the inviscid value, the trends of the two sets of data are clearly discernible, they are, however, within 2% of each other. Potter and Bailey, after

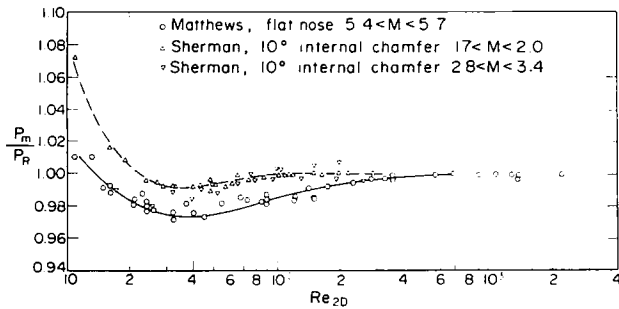


FIG. 10. Calibration function of internally chamfered pitots against Reynolds numbers (behind a normal shock).

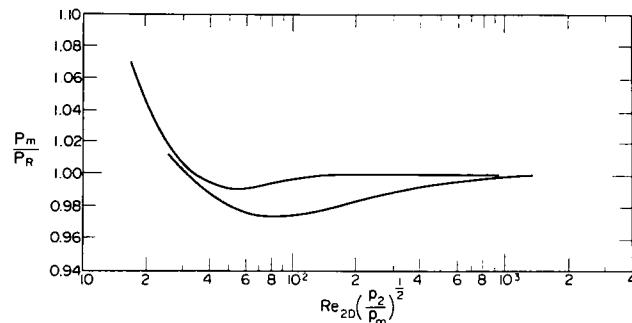


FIG. 11. Calibration function of internally chamfered pitots against Reynolds numbers (modified).

reviewing an extensive amount of data, reported that this parameter is capable of correlating all data for a given nose shape to within 3% of each other. The difference can be attributed to differences in the gas medium or wall cooling for the probe. Furthermore, they noted that the effect of nose shape is small when $Re_{2D}(\rho_1/\rho_s)^{1/2} \geq 200$.

Further discussion of supersonic data including those exhibiting effects of rarefaction is given in Section 1.8.2.

1.3. Impact Pressure Measurement in Incompressible Flow

1.3.1. Velocity or total pressure gradient effect

Impact and pitot-static tubes are generally calibrated in flows simulating a uniform flow field. But, in practice, they are often used for measurements in the neighbourhood of a solid surface, where a transverse velocity gradient exists. Thus, even a well-calibrated tube might not indicate the reading at the same location as the geometric centre of the orifice. Errors caused by the presence of a shear flow across the mouth of the pitot tube may be due to the following two effects:

- (i) the stagnation pressure is proportional to the square of the velocity and when this is integrated over the orifice, it will have a higher value than the stagnation pressure calculated from the square of the velocity at the geometric centre of the orifice; and
- (ii) the presence of the probe in a velocity gradient causes deflection of the stream lines toward the region of lower velocity. This deflection causes the probe to indicate an impact pressure in excess of that existing at the same location in the absence of the probe.

The existence of the second effect has been qualitatively demonstrated by smoke photographs. Both these effects are therefore seen to cause the probe to read high, which explains for the outward displacement of the effective from the geometric centre. Both of these, as will be seen later, diminish with probe size.

The combined effects of these two influences cannot be subjected to rigorous theoretical analysis, simply because the velocity gradient varies throughout the boundary layer and the corrections on the readings may have to be different at each location. Though a satisfactory theory is still lacking, theoretical predictions of an approximate nature would be very helpful in supplementing our experimental findings on the subject; because in spite of the fact that it is generally agreed that errors are being introduced by these effects, their correction remains the most controversial topic in the literature.

The first or the velocity head displacement effect can be obtained easily by integrating a velocity profile linearized in the neighbourhood of the nose; such profile can be represented by the expression

$$u = U \left(1 + \frac{\alpha z}{a} \right) \quad (19)$$

where U = magnitude of a velocity approaching centre of tube, a = radius of an infinitely thin-walled pitot, z = distance from centre of the tube, α = a shear parameter, represented by the maximum difference between the velocities at the edges of the orifice divided by twice the mean velocity. The result of this integration indicates that the effective displacement expressed as a percentage of the orifice diameter is given by

$$\frac{\delta}{2a} = 0.021. \quad (20)$$

On taking into account that the pitot has a wall of finite thickness, this becomes

$$\frac{\delta}{D} = 0.021 \frac{d}{D} \quad (21)$$

where d = diameter of impact orifice = $2a$ and D = external diameter of pitot.

It is therefore seen that the displacement due to the velocity head effect is only about 1% of the outer diameter for pitots of conventional designs. This, being much smaller than the observed magnitude, reported to be in the range of 10–16%, shows that the velocity head effect contributes at most a very small percentage towards the total displacement.

The second effect which causes the displacement of the effective centre from the geometric centre towards the region of higher velocity arises from the vorticity present in a sheared stream. Simple two-dimensional analyses as detailed in ref. 131, though inadequate to explain the magnitude of the displacement, have thrown considerable light on the two mechanisms involved: (i) a streamline on the left (or high-velocity side) of the geometric centre may avoid deflection to the left round the obstacle owing to the tendency of image vorticity to move it to the right, as exhibited by the cylinder in cross flow, the Rankine half-body or in fact any semi-infinite bodies ending in a parallel portion of external thickness $2a$, whatever the shape of the front portion and whether or not they include an internal cavity; (ii) a streamline on the left of the geometric centre of a semi-infinite thin-walled two-dimensional channel may enter the channel and be forced against the left inside wall because its normal tendency to come out again is cancelled by the downstream flow within the tube associated with the original vorticity. Thus, it is seen that both these mechanisms relate the displacement of the stagnation streamline to the vorticity present in the shear flow; and the magnitude of the displacement caused by this vorticity effect as predicted by simple two-dimensional theories for semi-infinite bodies can be approximated by the expression

$$\frac{\delta}{2a} = \frac{1}{4} \alpha. \quad (22)$$

For more realistic pitot shapes, such as thick-walled two-dimensional channels, both the above effects may occur to some extent. The resulting displacements, however, cannot be greater than that produced by the simpler shapes considered above, which amounts to a displacement of only about 8% even in the extreme case of $\alpha = \frac{1}{3}$ experienced in wake flows. This is still much below the experimentally observed values reported by many investigators.

Thus, one is forced to examine what further features in the three-dimensional flow past an actual pitot tube that could amplify the displacement of the effective centre by the vorticity effect. As is well known, the vorticity lines in two-dimensional flows are perpendicular to the plane of the flow so that they cannot be stretched. Hence, the vorticity carried by each vortex line remains constant. In particular, for a simple shear flow model comprising of a uniformly sheared section interposed between two inviscid streams, as was the case for all the two-dimensional investigations, the vorticity is everywhere constant in the sheared section. On the other hand, in three-dimensional flows, the vorticity does not remain constant as it approaches the front of the tube. As the vortex lines are stretched as they pass over the tube, the vorticity builds up to much higher values near the nose of the tube. A number of theoretical investigations have been partially successful in accounting for the effects of these local concentrations of vorticity at the nose of a three-dimensional obstacle.

Much of the theoretical work reported has been carried out for a sphere in a shear flow. This is because the main need is to take into account the vorticity amplification produced by the three-dimensional character of the flow; the sphere, while geometrically simple, exhibits this. Furthermore, a spherical-nosed pitot is a conceivable configuration. In what follows, we shall discuss the results of two of these investigations in further detail. The interested reader can refer to ref. 131 for further discussions.

Hall⁽⁴⁶⁾ has shown that, when the vorticity field alone is considered, the displacement of the stagnation streamline from its position at infinity for a sphere in uniform shear can be expressed as

$$\frac{\delta}{D} = 0.6200\alpha - 0.5786\alpha^3 + O(\alpha^5) \quad (23)$$

where D is the sphere diameter, Hall further suggested that the square-ended round pitot may be represented by a sphere of slightly larger diameter.

Lighthill's more exact theory⁽⁷⁵⁾ for flows with small shear gives

$$\frac{\delta}{D} = 0.45\alpha - C\alpha^3. \quad (24)$$

where C is probably greater than 1.35.

Both the results of Hall and Lighthill are plotted together with the experimental results reported by Davies⁽²¹⁾ in Fig. 12. A casual comparison shows that the magnitude of the theoretical predictions differ quite substantially, though they give similar trends in the variation of the ratio δ/D with the shear parameter. Before we compare these predictions with Davies' experimental data, we first turn to a summary of other major experimental findings.

Young and Maas⁽¹³⁹⁾ were the first to report on the displacement effect of the total pressure gradient. They observed this in a study of the wake close to a symmetrical airfoil. By plotting the observed widths of the wake at a given velocity against the external pitot diameters they obtained points lying approximately on a straight line. The correction being equal to half this slope. For several total pressures, they found that the slopes of these lines were the same. Their results showed that the distance δ between the geometric and the effective centres for a square-ended round pitot having inner to outer diameters in the ratio of 0.6 is given by about 18% of the outer diameter. More generally, they reported the following relation for pitots of the same family having other diameter ratios:

$$\frac{\delta}{D} = 0.131 + 0.083 \frac{d}{D}. \quad (25)$$

The range for which this result holds was reported to be

$$0.35 < \frac{d}{D} < 0.75. \quad (25a)$$

The fact that this correction is independent of the velocity gradient is rather surprising, because it

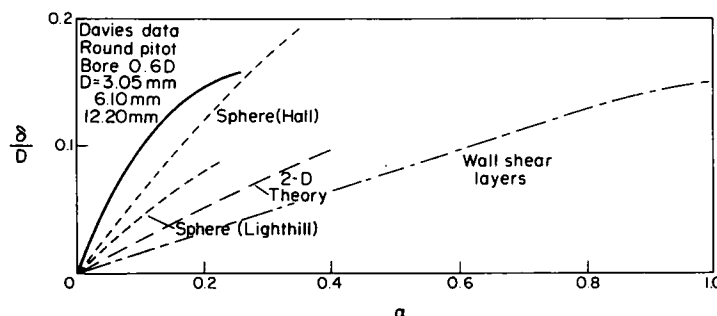


FIG. 12. Displacement corrections for square-ended round pitot (α computed using velocities at external radii of pitot).

implies a sharp discontinuity in the displacement correction as the velocity gradient approaches zero.

However, MacMillan,⁽³⁵⁾ also using square-ended round pitots having $d/D = 0.6$ in both turbulent pipe and boundary layer flows, obtained $\delta/D = 0.15$ for distances when the pitot is greater than $2D$ from the wall. Within a distance less than $2D$ from the wall, MacMillan found that another correction is necessary. This we shall discuss in subsection (b) later.

Similar experiments were carried out by Livesey⁽⁷⁹⁾ in a turbulent boundary layer artificially thickened by a wire cloth screen. For square-ended pitots having $d/D = 0.6$, he obtained a displacement error of $0.16D$, of the same order indicated by other investigators. For hemispherical-nosed probes having $d/D = 0.5$ he observed a smaller displacement, of magnitude $0.1D$. He further reported that for a sharp-lipped conical pitot of included angle 8° , no corrections were observed, both for geometrically similar probes, i.e. probes having the same d/D ratio and for probes of different d/D ratios. However, the influence of the conical angle has not been investigated.

Davies, having benefitted from the theoretical results discussed earlier, carried out more extensive investigations on the behaviour of the pitot tube in transverse shear aft of a symmetrical aerofoil.⁽²¹⁾ Using square-ended tubes having $d/D = 0.6$, which had been used by all previous investigators, he found a correlation between δ/D and the shear parameter, α , defined earlier. His results have been plotted in Fig. 12, together with the theoretical results of Hall, Lighthill as well as that obtained from the simplified two-dimensional analysis. It is seen that the maximum displacement

recorded by Davies agrees well with those of Young and Maas and of MacMillan. However, for values of $\alpha < 0.2$, the experimental results are of the same trend as predicted by the theoretical analyses, which are obtained for a sphere. But, the results indicate larger correction for a pitot than for a sphere of the same diameter, as Hall has suggested. This higher initial rate of rise for the pitot tube shaped body over the solution for the sphere can be attributed to the source-type flow which it generates far upstream.^(76,36) The contribution due to this source flow takes the form $\frac{1}{2}\alpha \log(s_c/a)$, where s_c is of the order of the width of the shear layer. Thus, the results of Davies seem at present to be the most plausible of all experimental results reported since they indicate that δ increases with the velocity gradient, and is zero, as it surely must be, when the velocity gradient is zero.

In addition, the investigation of Davies revealed further results which had not been reported previously. His results, shown in Fig. 13a, indicate that for a set of pitots of constant outer diameter but of varying bore no significant difference was observed in the velocity profiles obtained 50 mm downstream of the trailing edge of the airfoil even though the bore to diameter ratio was varied from 0.075 to 0.800. This implies that the displacement correction is governed solely by the external dimension of the pitot. To this effect, the results of Rechenberg⁽¹¹⁵⁾ and Patel⁽⁹⁶⁾ obtained with the pitot resting on the wall can also be quoted. Preston⁽¹⁰⁴⁾ has indicated that when placed in this manner, the pitot tube can be used for skin friction measurements, a topic which we shall deal with in detail in Section 5. Rechenberg and Patel's results showed that for a

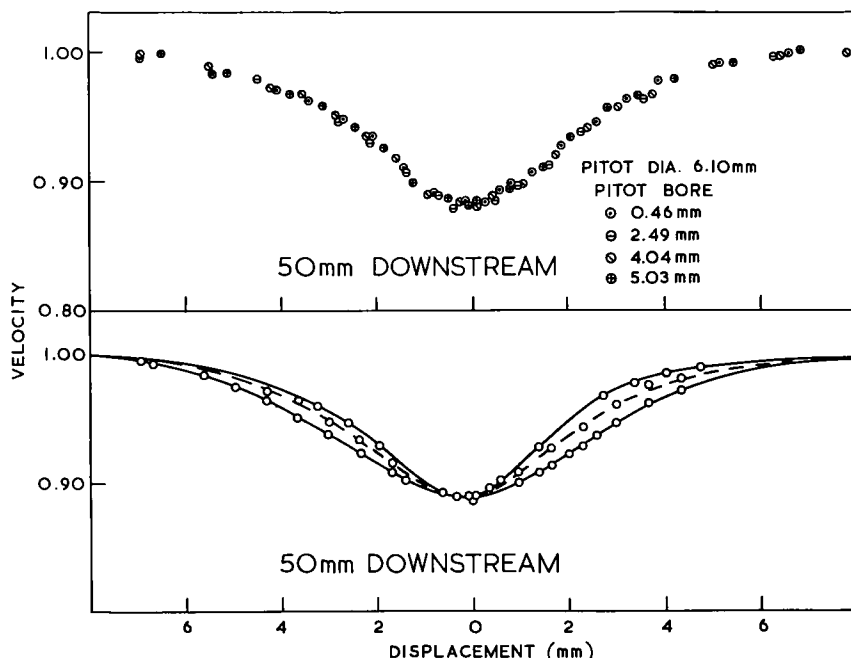


FIG. 13a. Comparison of wake profiles obtained 50 mm downstream of a symmetrical airfoil using constant-external-diameter and geometrically similar pitots.

round pitot with a symmetrical bore, the d/D ratio has a negligible effect on the calibration of the Preston tube. These results therefore support the above finding of Davies. In addition, Davies' measurements made 6.4 mm behind the trailing edge reveal that the velocity profiles obtained by geometrically similar pitots are substantially different from each other, as can be seen from Fig. 13b. The fact that these profiles do not coincide even at the centre of the wake, unlike those obtained 50 mm downstream, where the displacement error is supposedly zero by symmetry, implies that a total head correction also exists. Such anomaly in the profiles had also been observed by Young and Maas, but they did not discuss this in their paper. Using Young and Maas' technique to reduce his results, Davies obtained a displacement correction equal to $0.24D$ for results obtained in this traverse. Carrying his investigation one step further, Davies found that for traverse 4.8 mm closer to the trailing edge, a correction of $0.28D$ was obtained, whereas traverses an equal distance downstream gave a correction of $0.16D$ when reduced by Young and Maas' method. These results obviously indicate that some other factor besides the transverse velocity gradient is operating simultaneously. Davies attributed this to the behaviour of the pitot in an

oscillatory and hence yawed flow. It is all too evident that close to the trailing edge such oscillations are very violent while further downstream the fluctuations become much smaller. In such flows, the pitot will record a pressure lower than the mean total head due to its directional characteristics, which will be discussed in a later section. Davies further confirmed the existence of this velocity head error by obtaining another series of profiles using pitots of constant outer diameter but varying bore. Such series of profiles are also shown in Fig. 13b. As it has been demonstrated that the displacement error is essentially governed by the external dimension of the pitot and it is reasonable to assume that influence on the flow around the pitot also depends on the same dimension, the differences exhibited by the two series of profiles in Fig. 13b should be due to the total head error. The existence of this error can be used to account for the discrepancy between the previous data, which were reduced by Young and Maas's technique, and those of Davies. The presence of velocity head corrections at the centre and edges of the wake, where the velocity gradient is small, boosts the displacement corrections in the same direction as the vorticity error, so much so that they lie on the same straight line. In this respect, Davies made a distinct contribution towards the resolution of the paradox posed by the experimental data of past investigators and the theoretical predictions.

The results of all these investigations seem to show that the displacement errors due to vorticity reach different maximum asymptotic values for different nose geometries. An explanation for this can be sought in terms of the image vorticity: the square-ended tube presumably has a stronger image vorticity than the hemispherical nose tube and thus the displacement of the effective centre is larger in the former. This explanation seems to be further substantiated by Livesey's results for the sharp-lipped tube, for which the front portion approximates a thin-walled tube. The lack of displacement in this case can be interpreted by noting that (i) image effects would be much smaller for this shape and (ii) internal reversal flow as that occurring in the two-dimensional pitot could hardly take place since vortex lines cannot readily penetrate into a tube in the three-dimensional case.

(a) *Free shear layers.* Some general remarks can now be made on the behaviour of the displacement error in transverse shear. Wake profile measurements when reduced by Young and Maas' technique show a displacement correction which depends on the longitudinal location at which the profile is taken. Above a certain critical distance from the trailing edge of the object, this displacement correction is inversely proportional to the distance from the trailing edge, reaching perhaps a minimum asymptotic value (and there is no evidence to show that this value was reported by any of the investigators prior to Davies). From Davies' results, it

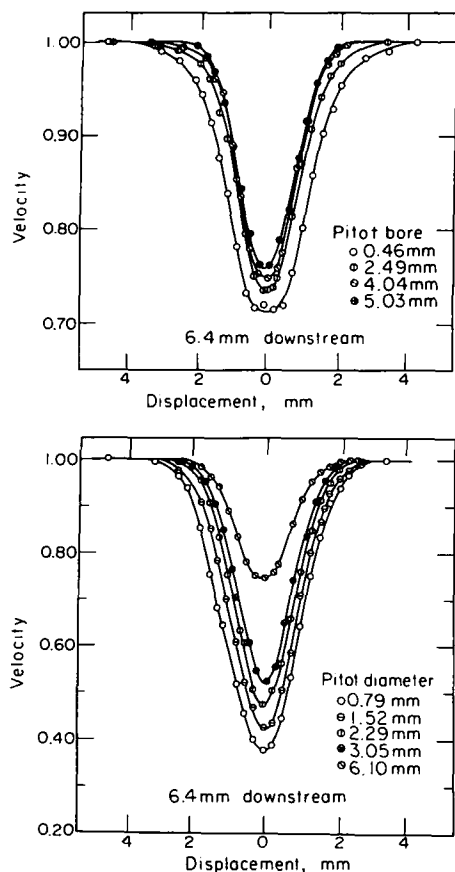


FIG. 13b. Comparison of wake profiles obtained 6.4 mm behind a symmetrical airfoil using constant-external-diameter and geometrically similar pitots.

seems that the lack of total head error at the centre-line of the wake profiles can be used as an indication that the asymptotic profile has been reached. After this asymptotic profile, the displacement correction alone is sufficient, whereas before this, a total head error due to yaw also exists.

For square-ended round pitots, which are small compared with the width of the transverse shear region, displacement corrections in two-dimensional uniform shear can be made with the aid of Fig. 12. Since it has been shown that the bore dimension does not affect the displacement correction, for a truly uniformly sheared region there is no ambiguity in computing the shear parameter—both the terminal velocities at the internal or external radii of the pitot can be used. For shear flows which are not uniform, Davies' investigation indicates that the external radius would be a better choice.

(b) *Wall shear layers.* In the presence of a wall, it is reasonable to expect that the results obtained in free shear layers will be modified to some extent. An effect of this kind would be anticipated from consideration of a forward-facing two-dimensional step in an irrotational flow. The streamlines near to the wall are displaced outwards as they approach the step. Thus, the presence of the wall tend to reduce the displacement of effective centre due to vorticity.

Boundary-layer profile measurements by MacMillan and Livesey reported earlier, however, indicated displacement corrections of the same order as those in free shear layers. MacMillan's results implies, in addition, a velocity or total head correction due to the proximity of the wall. This holds in the region $y/D < 2$, and is reported in the form of the variation of the correction $\Delta u/U$ with the distance from the wall, y/D . This correction function has been modified by Bryer and Pankhurst to the form incorporating a direct error on the pitot reading. This wall proximity error has been interpreted in terms of a negative displacement in accordance with the qualitative explanation given above. It is, in fact, more suggestive to view the combined effect of the vorticity and wall proximity displacements in the layer close to the wall as shown in Fig. 14, since the magnitude of the negative displacement cannot be expressed as a universal correlation of the other pertinent parameters, such as y/D or α .

It is rather unfortunate that the results of Davies, which help to clear up the confusion in free shear flows, paradoxically enough, throw considerable

doubt onto the past results for wall shear layers. In the same experimental investigation quoted earlier, Davies obtained six boundary layer traverses, near the trailing edge of a flat plate of length 0.91 m and at zero incidence, using geometrically similar pitots having outer diameters varying from 0.8 to 12.2 mm. His results indicated no appreciable displacement or velocity-head error even when the pitot was touching the wall, although the largest pitot was almost 16 times that of the smallest.

On the contrary, the experiments of Patel made in connection with the Preston tube which we had cited earlier seem to demonstrate beyond any doubt the existence of displacement correction for pitot tubes in wall shear layers. In this paper, Patel has also demonstrated how this displacement correction can be deduced using both the universal $u^+ - y^+$ profile for turbulent boundary layer or fully developed turbulent pipe flows and his calibration curves. It should be pointed out that this technique presumes the $u^+ - y^+$ profile to be comparatively free of this displacement error. Patel has obtained for this purpose a $u^+ - y^+$ profile using the flattened pitot, for which if similar correction procedure holds (a topic we shall deal with later in this section), the error will be an order of magnitude smaller than that for round pitots. For the sublayer where it can be easily shown that the shear parameter for a pitot resting on the wall is unity, Patel obtained a displacement correction of $0.15D$, the same as that reported by MacMillan and equal to the maximum value in Davies' data. For the region having a linear-logarithmic velocity profile, it can be easily shown that the displacement is only $0.0795D$. These results substantiate those of Davies for the free shear layer. However, we now have to seek an explanation on why the displacement should be constant in the log-linear region. It can be shown that when the centre-line of the pitot starts to sense this velocity profile, the shear parameter can be approximated (using $A \approx B$, which is close to Patel's values of $A = 5.5$ and $B = 5.45$) by the expression

$$\alpha = \frac{1 + \log D^+}{2[1 + \log(D^+/2)]}. \quad (26)$$

In the range $150 < D^+ < 1000$, which embraces the usual range of validity of the log-linear profile, we have $\alpha = 0.556$ for $D^+ = 150$ and $\alpha = 0.542$ for $D^+ = 1000$; which shows that the variation of α in this region of the turbulent wall layer is rather insignificant. It logically follows that the variation of the displacement correction in this region is negligible. This result serves to demonstrate the compatibility among Patel's calibration curves for the Preston tube, the velocity profile measurements in wall shear layers having small longitudinal pressure gradients and the trend for the variation of the effective displacement with α established earlier.

In recapitulation, it can be said that present evidence seems to indicate that the displacement is

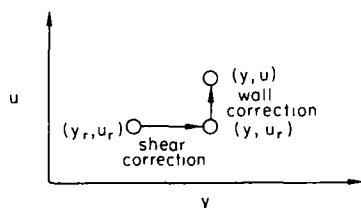


FIG. 14. Effect of wall shear layer on pitot reading.

a function of the local properties in the flow field such as u , $\partial u / \partial y$, and D rather than of global properties such as R_p , u^* , μ , ρ and y as suggested by MacMillan. Furthermore, this is found to be solely determined by the external dimension and not influenced to any significant extent by the bore dimension. At the present, displacement correction in wall shear layer measurements can be performed using the corresponding curve shown in Fig. 12, which has been constructed from the two points computed from Patel's results together with the origin.

The wall proximity correction of MacMillan, which has not been observed by other investigators, may turn out to be a result of the functional relation inherent to his choice of global-dependent variables. However, further investigation on this is necessary before a final conclusion can be reached.

(c) *Pitots having non-circular cross-sections.* Results of the above investigations, which are carried out for pitots having circular cross-sections and of square-ended nose, have been applied generally to tubes having other nose shapes and/or cross-sections due to the lack of specific data regarding these configurations. This procedure is not to be recommended.

Only for the case of flattened pitots were some experimental results available. Livesey⁽⁷⁸⁾ stated, without presenting the supporting experimental evidence, that for incompressible flow, the displacement error is a function of the solidity of the cross-section and the aspect ratio of the probe tip. He recommends a displacement correction of $0.15 < \delta/H < 0.18$. He further points out that there is no consistent indication of a displacement error in compressible sub- or supersonic flows. More recently, a series of experimental results on five near geometrically similar flattened pitots having $h/H \approx 0.6$, $h/w \approx 0.52$ and $H/W \approx 0.65$ has been

reported by Quarmby and Das.⁽¹⁰⁶⁾ Their results, reduced using MacMillan's technique, showed a displacement of $0.19H$ and the resulting velocity correction curve is found to be similar to that of MacMillan for round pitots if this is plotted with $\Delta u/U$ against y/W . However, in view of our discussion in the earlier sections, the continual validity of these results is rather doubtful.

1.3.2. Yaw and pitch effects

When the flow direction is not parallel to the axis of the pitot tube, errors occur in the total head readings. Flow misalignment can also arise even though the tube is correctly aligned with the mean flow if the impact tube is used for measurements in highly turbulent flows such as that close to the trailing edge in wake flow. As the pitot tube has a stem, the error due to pitch (angular deviations in the plane containing both head and stem) is generally different from that due to yaw (angular deviations about the axis of the stem).

Pitch or yaw characteristics for pitots having a wide variety of nose shapes have been reported over a broad spectrum of flow velocities, including incompressible, subsonic, transonic and supersonic flows.^(40-43, 88)

For the incompressible case, typical characteristics for several commonly used nose configurations are shown in comparison with the Kiel probe (Section 1.6) in Fig. 15. For the purpose of comparing the yaw insensitive range of the various pitots, the critical angle has been defined as the angle of yaw at which the total pressure error reaches a value of 1% of the dynamic pressure measured at zero yaw. These angles are given beside the probes shown in Fig. 15. Critical angles of other designs tested by Gracey *et al.* and Winternitz have been given in Bryer and Pankhurst.

Total head errors due to misalignment have been found to depend on the d/D ratio. Yaw characteris-

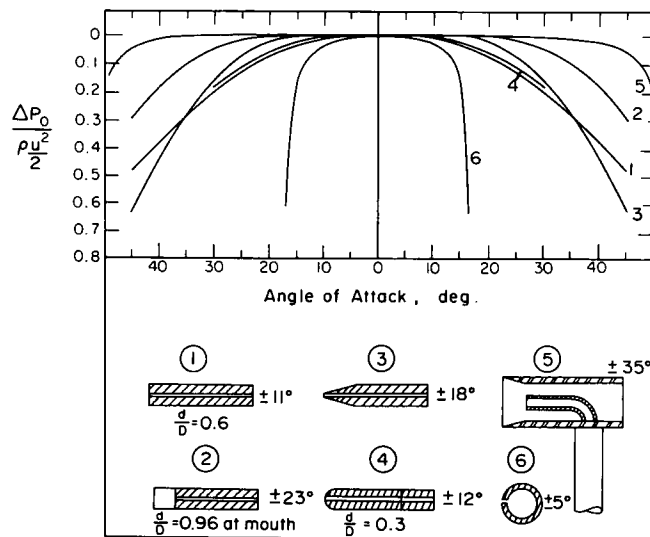


FIG. 15. Yaw characteristics for various pitot-head shapes.

tics illustrating this influence, reported by Davies⁽²¹⁾ for square-ended and Huston⁽⁶⁰⁾ for hemispherical pitots, have also been given in Bryer and Pankhurst. That the total head error varies with the d/D ratio of the probe seems very plausible, since the distortion in the pressure distribution caused by the yawed flow can be minimized by averaging over a large orifice than a small one. This trend may also be exhibited by conical pitots, though no experimental data are available. In this connection, configuration 2 in Fig. 15 may be considered to be a pitot of a large d/D ratio. To this effect, Davies⁽²¹⁾ has reported that the traverse in wake flow obtained by a pitot of external diameter 6.10 mm and bore diameter 2.49 mm is essentially the same as that measured by the same pitot fitted with a plug to reduce its bore to 0.46 mm when the plug was pushed back more than 1.27 mm into the head tube. This indicates that the pitot behaves as if it were unplugged when the ratio of the recess depth to the orifice diameter is greater than 0.51. Configuration 2 therefore provides a means of extending the yaw insensitive range of the square-ended pitot without undermining its rigidity.

Davies further reported that the error in the total head reading due to pitch and yaw increases as the size of the pitot is reduced. This observation seems to have been collaborated by the findings of Merriam and Spaulding⁽⁸⁸⁾ for hemispherical pitots. The reduction in the error is roughly proportional to the diameter of the tube. Davies attributed this to the stabilization on the flow due to the extra shear stresses introduced when the flow direction departs from that of the pitot. Thus, pitch and yaw corrections cannot be made from characteristics obtained for geometrically similar pitots alone, the actual dimension of the pitot have also to be taken into account.

For the case of flattened pitots, Bradshaw and Goodman⁽⁹⁾ have reported that they are very sensitive to pitch unless great care has been taken to make the forward face exactly plane.

1.3.3. Turbulence effects

Turbulence may affect the readings of the pitot tube in two ways. Firstly, the r.m.s. value of the fluctuating velocity component may directly affect the calibration of the pitot tube. However, this is generally believed to be small and of secondary importance. Of primary importance is the direct effect of the turbulent velocity components on the total-head and static orifices. Goldstein⁽³⁹⁾ has investigated the turbulence effect theoretically. He neglected other possible factors such as frequency, damping, resonance and lag in the leads. Subject to these limitations, the correction of turbulence errors further depends on the assumption of whether the pitot tube responds to all the turbulent velocity components or just the longitudinal component, i.e. of the so-called cosine square response type.

For the more general case, the impact pressure

measured by the pitot tube in incompressible flow can be written as

$$\begin{aligned} P_m &= p + \frac{1}{2}\rho \bar{V}^2 \\ &= pt\frac{1}{2}\rho(u^2 + v^2 + w^2 + \bar{u}^2 + \bar{v}^2 + \bar{w}^2) \\ &= p + \frac{1}{2}\rho q^2 + \frac{1}{2}\rho \bar{q}^2. \end{aligned} \quad (27)$$

This obviously requires the resultant mean velocity not to make too large a pitch or yaw angle with the axis of the pitot tube. When the tube is assumed to be aligned with the flow direction, eqn. (27) becomes

$$P_m = p + \frac{1}{2}\rho u^2 + \frac{1}{2}\rho \bar{q}^2. \quad (28)$$

For cosine square response, we simply replace the total turbulent energy term, \bar{q}^2 , by the longitudinal component, \bar{u}^2 .

For the usual turbulence intensity encountered in pipe and wind-tunnel flows, the turbulence error is small, e.g. for a turbulence intensity of 20%, which is too high for practical situations, the impact pressure reads high by only 2% if the static pressure is assumed to be correctly measured. However, for higher degrees of turbulence it is possible for turbulence errors to reach appreciable magnitude in terms of the dynamic pressure, as now the angle of attack at the probe tip may vary over such a wide range that the probe could have instead of just the turbulence error also errors due to both pitch and yaw. In this case, the error is exceedingly difficult to correct.

In general, the turbulence intensity required for correction have to be obtained independently from measurements for the operating flow situation.

Since the turbulent velocity components can be considered to produce a time distribution of pitched and yawed incident flows at the impact orifice it follows from Section 1.3.2 that a proper choice of the head-tip geometry can alleviate the turbulence errors to a certain extent. The influence of the head-tip geometry on the readings of the impact tube has been reported by Walsche and Garner.⁽¹³⁵⁾ They have included the following types of impact tubes in their study: a Conrad probe (Section 4.3.2), a five-tube probe (Section 4.4.3) an axial probe, a Kiel probe (Section 1.6) and a rectangular pitot. The static pressure was measured by means of a disc static probe. The calibrations obtained when these probes were subjected to several types of angular and linear oscillations in steady flow, with and without a superimposed steady yaw angle, were used to correlate the turbulence in the wave of an airfoil. The amplitude of the angular oscillations was varied up to 15°, corresponding to an equivalent turbulence level of 44%. Hot wire measurements in the test region showed intensities of approximately 35%. Their conclusions are as follows:

1. In fluctuating flow, the measured value of pressure will give the time-averaged value only if the fluctuations are in the flow direction. When velocity fluctuations occur, the

- measured value of pressure will be less than the time-averaged value.
2. The Kiel probe gives the most accurate total head reading. In a highly turbulent wake, typical discrepancies between this and other probes amounted to 7% of the free-stream dynamic pressure.
 3. When the mean angle of flow is required together with the total and static pressures from one set of readings, the five-tube probe is preferred to the axial probe.
 4. A comprehensive assessment of the usefulness of these probes in a fluctuating flow would require more extensive data on the effects of Reynolds number and mode, frequency and amplitude of oscillations. More fundamental studies of internal and external flows are needed to explain the behaviour of any probe.
 5. It is confirmed that in steady flow the Conrad probe will give accurate results within a boundary layer if the pitch angle of local flow direction does not exceed 6°.

1.3.4. Pressure variation over the impact area

Goldman *et al.*⁽³⁸⁾ integrated the potential pressure distribution for a cylinder

$$\Delta P = \frac{\rho U^2}{2} (1 - 4 \sin^2 \theta)$$

over the pitot mouth and assumed that this averaged pressure to be the true pressure sensed by the impact tube. As the potential pressure distribution remains valid for values of θ up to 60° in viscous fluids, the pressure correction thus obtained can be expected to hold over values of r/R or $d/D = 0.866$, which covers most common impact tube designs.

Their method, assuming no static pressure errors, gives the equation

$$\Delta P_{av} = \frac{\rho U^2}{2} \left\{ 1 - \left(\frac{d}{D} \right)^2 \right\} \quad (29)$$

which is to be used instead of Bernoulli's equation.

By incorporating the turbulence correction in the impact pressure, the velocity can be written as

$$U = \left\{ \frac{2\Delta P_{av}}{\rho \left[1 - \left(\frac{d}{D} \right)^2 \right]} - \overline{u'^2} \right\}^{1/2}. \quad (30)$$

Goldman *et al.* has claimed that this error could be as high as 12%. They have reported that raw data obtained by them using a pitot having $d/D = 0.454$ read 10% low compared to Deissler's hot wire measurements. Application of their correction boosted the results to read 3% high. This was then removed by incorporating the turbulence correction.

Though there is little doubt that such error does exist, the large correction implied by the above equation is rather questionable. A large impact

orifice at the pitot mouth definitely alters the geometrical configuration of the nose so much that it is no more justifiable to assume the potential pressure distribution to apply. For actual pitot configurations, the distribution for the sphere rather than the cylinder should be more realistic. Furthermore, the large error as claimed would be too conspicuous to evade so many investigators. In fact, the data reported by Davies⁽²¹⁾ in wake flow and by Patel⁽⁹⁶⁾ in turbulent pipe flow clearly indicate that the d/D ratio has only a negligible effect on the total head reading.

1.3.5. Blockage and interference effects

The following results have been reported with regard to these effects:

- (i) In the absence of transverse velocity gradient in the direction of the stem, downstream geometry has no measurable effect on the pitot reading, even with the stem at the mouth of the probe.⁽⁹³⁾
- (ii) Wind tunnel tests conducted in the range of Mach numbers from 1.9 to 3.7 show no significant interference effects at any spacing of two neighbouring cylindrical pitots, even when they are touching each other.⁽⁷¹⁾
- (iii) On the basis of boundary-layer measurements, O'Donnell⁽⁹²⁾ recommended that interference effects become significant when $D/\lambda > 0.22$, where λ is the boundary-layer thickness.
- (iv) When the dimension of the pitot becomes too large compared to a critical dimension of the channel in which measurements are to be made, the reduction in the flow area may cause a venturi effect large enough to influence the measurement recorded by the probe.⁽⁵⁷⁾

1.4. Impact Pressure Measurement in Subsonic Compressible Flow

It is not at present clear whether the pitot tube in subsonic compressible flow is subjected to the influences of all the factors reported for incompressible flow.

As regards the velocity gradient effect, Livesey⁽⁷⁸⁾ has pointed out that there is no consistent indication of a displacement error in subsonic flow.

The only effect that has come under close study is that of yaw, mainly because of interests related to yawmeters. It has been found that in general the marked insensitivity of the pitot to misalignment in incompressible flow is retained up to supersonic speeds. Results for the hemispherical nose pitot in subsonic flow had been reported by Walchner.⁽¹³⁴⁾ These are shown in Fig. 16. It is seen that within the range of Reynolds numbers for which the calibration function is unity, the total head tube at zero yaw is capable of registering the true impact pressure from the lower limit depending on the sensitiv-

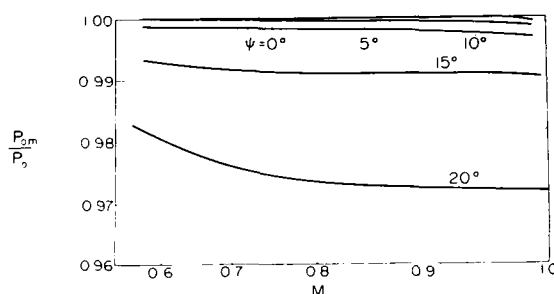


FIG. 16. Effect of compressibility on the readings of a yawed pitot (hemispherical head).

ity of the manometers right up to the upper limit of about Mach 0.95, and up to a yaw angle of 15° compressibility and yaw effects together reduce the total head reading of the probe by less than 1% up to almost Mach 1. However, the d/D ratio of the probe is not given.

An alternative form of displaying the same results is to plot the stagnation pressure error against the yaw angle for each Mach number. Results in this form had been reported by Rogers and Berry⁽¹⁶⁾ and are shown in Fig. 17. From this figure, it is seen that the critical angle of the probe is reduced as the Mach number increases. In this connection, the results of Gracey *et al.* given in Bryer and Pankhurst cover only the low-speed subsonic range and are valid for incompressible flow only. No comprehensive data seem to exist covering the high subsonic-speed range. Thus, the effect of Mach number on the critical angle of each probe cannot be established. An exception being the Kiel probe, which we shall discuss more fully in Section 1.6.3.

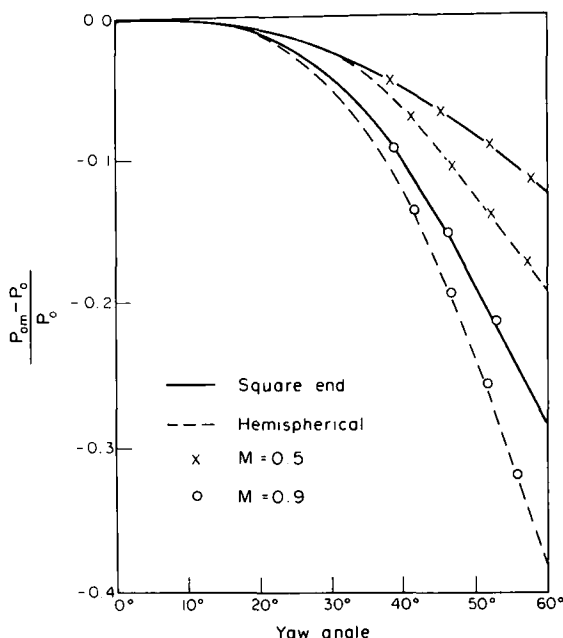


FIG. 17. Effect of compressibility on the readings of a yawed pitot-alternative presentation (square-ended and hemispherical heads).

1.5. Impact Pressure Measurement in Supersonic Flow

Results reported by Davies with round pitots in the laminar boundary layer on a 20° cone at a distance of 960 mm from the apex indicate that the velocity profiles may be subjected to three effects. These are illustrated in Fig. 18.

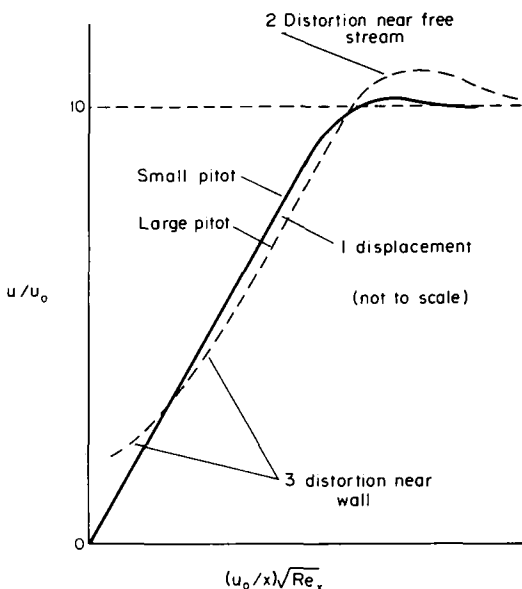


FIG. 18. Effects on the velocity profile due to insertion of a pitot tube in a supersonic laminar boundary layer.

1.5.1. Displacement of the main body of the profile

This is caused by the velocity gradient effect. However, contrary to incompressible flow results, the displacement observed by Davies⁽²⁰⁾ for a laminar boundary layer on a cone at $M = 2.45$, is in the direction towards the region of lower velocity. In this connection, Bradfield *et al.*⁽⁸⁾ reported the result of a single check on this effect, made in the course of their investigation on the effects of leading-edge bluntness at $M = 3.05$. Two flattened pitots of heights 0.064 mm and 0.203 mm were used in a boundary layer about 1.3 mm thick. No displacement on the main body of the velocity profile had been noted.

Since boundary-layer measurements in supersonic flow requires the use of very small probes, this effect if present may be difficult to detect. However, the variations in the displacement and momentum thicknesses reported by Davies by integrating the assumed profiles could not be explained solely by the two effects which we are to discuss below, so that the displacement of the main body of the profile (though small) must be considered to have some influence on the measured profiles. In this respect, it may be noted that Blue and Low⁽⁷⁾ also observed a variation of the momentum thickness. However, their results provide no additional information on the displacement effect, since they did not report the measured profiles,

which were obtained by using flattened pitots of $0.20 < h/H < 0.72$ and $2.5 < W/H < 16.6$ in the laminar boundary layer on a flat plate at $2 < M < 3$.

The present situation has been aptly summed up by Livesey,⁽⁷⁸⁾ who pointed out that there is no consistent indication of a displacement error in supersonic measurements.

1.5.2. Peaking near the outer edge of the boundary layer

This effect is common to all three investigations mentioned earlier. It has been found that the peak increases in height and extent as the pitot size is increased. This may be due to interference effects. On the basis of the data reported by Davies as well as Blue and Low, Monaghan⁽⁹⁰⁾ recommended that the ratio of the diameter to boundary-layer thickness should be kept below 0.1 and 0.2 in order that errors in the integral thicknesses (displacement and momentum) be within 2% and 4%, respectively.

1.5.3. The distortion of the profile near the wall

This is also observed by all the three investigations mentioned above. It is essentially the result of the Reynolds number effect as can be seen from the fact that this distortion increases as the tube size is decreased. This is because a decrease in probe size lowers the operational Reynolds number which in turn causes the probe to read higher, as can be observed from the calibration results reported in Section 1.2.3.

1.5.4. The effect of pitot shape and end finish

The data examined in the previous sections were obtained with

(a) circular pitots in the laminar boundary layer on a cone,⁽²⁰⁾

(b) flattened pitots in the laminar boundary layer on a flat plate.⁽⁷⁾

The agreement among the results was good. However, it has been found that additional distortions of the profiles near the wall may occur if flattened pitots are used to measure boundary layers on slender bodies of revolution. This could be due to the fact that the mouth of the flattened tube does not follow the cone surface and hence

may not receive similar filaments of flow across its width. In view of this, it would be advisable to use tubes of circular cross-sections in such instances.

The effect of taper and end finish on pitot measurements has been investigated by Cooke.⁽¹⁷⁾ Results show that the taper has a negligible effect, but end finish is important. Thus, small pitots should be first examined under a microscope before they are used for measurements.

1.5.5. Yaw and pitch effects

The effect of yaw on pitots in supersonic flow has been studied by Gracey *et al.* for probes having different nose configurations.^(41, 42) It has been found that at $M = 1.62$ the yaw-insensitive range for unshielded pitots are slightly increased. However, this trend is reversed for shielded probes. Critical angles of several designs tested by Gracey *et al.* are given in Bryer and Pankhurst together with the incompressible values. Since the critical angles are functions of Mach numbers at subsonic speeds, it is expected that the same is true at supersonic speeds. However, as in the subsonic case, no comprehensive data are available to indicate the trend of the variations.

It should be pointed out that the symmetrical yaw characteristics in supersonic flow reported by most investigators were obtained with the pitot situated in a uniform free stream remote from any asymmetric influences: as only under such conditions can the readings remain symmetrical about the neutral position of zero yaw. In situations in which asymmetry is introduced into the flow, such as in a wall shear layer, the resulting characteristics obtained no longer remain symmetrical, as can be seen from characteristics in Fig. 19 reported by Rajasooria and Brundin.⁽¹¹²⁾ What aggravates the situation further is that now these characteristics do not peak at the position of zero yaw and the peak reading does not correspond to the theoretical impact pressure.

1.6. Impact Pressure Measurement in Highly Turbulent Flows: the Kiel Probe

As seen from Fig. 15 the Kiel probe is a total-pressure tube having a much wider yaw insensitive

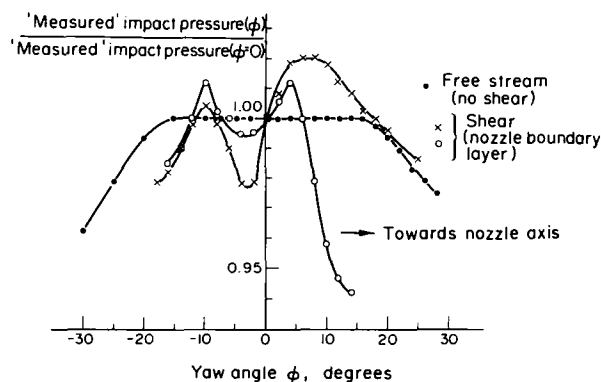


FIG. 19. Comparison of supersonic yaw characteristics in uniform and sheared flows.

range than pitots of more conventional design. As such it is ideally suited for total head measurements in situations where the exact flow direction is unknown or varying with operating conditions. For the standard Kiel probe shown in Fig. 15, the yaw insensitive range is up to about 35° . This range, however, can be increased to 45° or more by small variations on the design. Figure 20 shows the dimensions of the standard Kiel probe as well as its best modification. Both of these forms are rather difficult to manufacture in house. A variation of these forms, using a cylinder extending right across the external shield, can be made much more readily. However, the yaw insensitive range of this instrument is only 28° —a far cry from its parental forms, and actually not much better than probe 2 of Fig. 15.

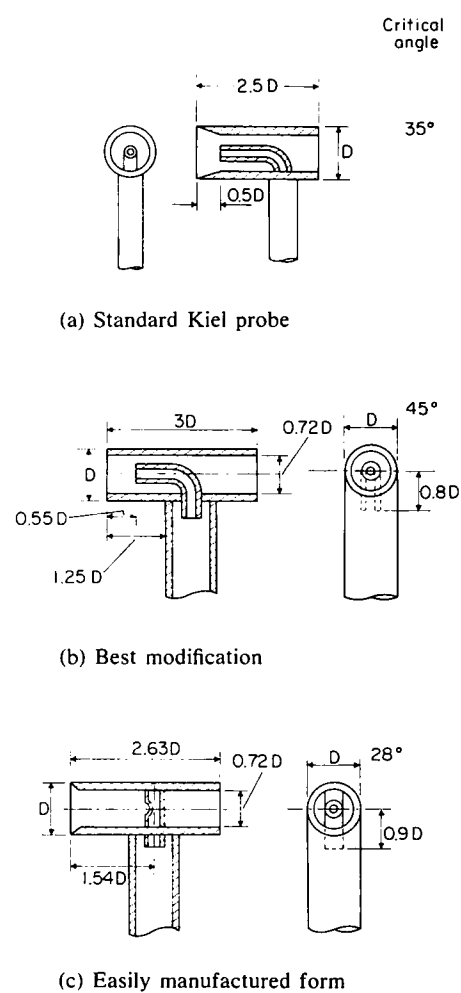


FIG. 20. Three versions of the Kiel probe.

Both the standard as well as the best modified Kiel probes have been produced commercially in miniature forms having shield diameter of 3.2 mm. Such instruments are well suited for use in turbomachine investigations, where small probes having a wide directional insensitivity range are desirable.

1.6.1. Velocity gradient effect

Corrections due to velocity gradients are small as in all total head probes. However, in steep total pressure gradients, as very close to solid boundaries or in "troughs" behind guide vanes, a shift in the effective centre of the probe occurs so the total pressure measured corresponds to the streamline $0.5d$ away from the geometrical centre of the head in the direction of higher total pressure. This is shown in Fig. 21. However, in view of our discussion in Section 1.3.1, it is recommended only with reservation.

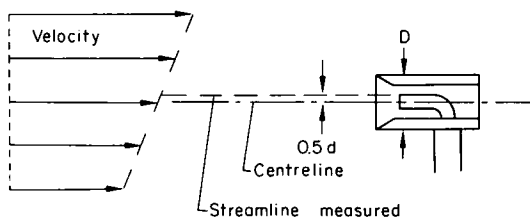


FIG. 21. Displacement correction for Kiel probe.

1.6.2. Turbulence effects

Since the Kiel probe is insensitive to yaw over a wide range of attack angles, turbulence errors should in general be corrigible by means of Goldstein's formula given by eqn. (27). However, very high turbulence intensity may reduce this yaw insensitive range.

1.6.3. Mach number effect

Gracey *et al.*⁽⁴³⁾ had reported that the yaw insensitivity range of the Kiel probe decreases with increasing Mach number. A typical characteristic for this effect for the modified Kiel probe is shown in Fig. 22, from which it is seen that the critical angle is reduced above a certain Mach number. This as well as the rate of decrease of the insensitive range are expected to depend on the particular design of the probe.

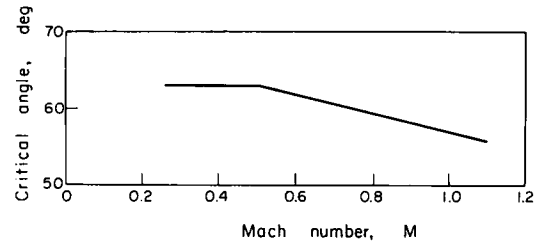


FIG. 22. Effect of Mach number on the critical angle of a modified Kiel probe.

1.7. Impact Pressure Measurement in Multiphase Fluids

The presence of liquid or solid particles in a gas stream will cause a total pressure probe to indicate a pressure between the stagnation pressure of the gas and that of the mixture. The magnitude of the difference between these two pressures depends on

the mass of the dispersed phase present in each unit volume of the gas and upon whether the particles enter or bypass the probe. Small particles tend to follow the gas flow, thus bypassing the probe, while larger particles have a greater tendency to enter the probe. If liquid droplets are carried in a gas stream, they may be partially or completely evaporated by the rising pressure and temperature due to stagnating effects at the probe.^(99, 127)

Taylor⁽¹²⁷⁾ further observed that if condensation takes place when a condensable vapour exists in the fluid, the velocity and temperature downstream from the condensation region will differ from corresponding properties in the undisturbed fluid. Care must be used in the interpretation of measurements obtained under such conditions. Pearcey⁽⁹⁹⁾ made experimental studies in wind tunnels with water vapour in air in a Mach number range of 0.5 to 0.8. He found that condensation caused a loss in total head which depend on saturation phenomena. These observations suggest that the gas should be dried whenever possible to obviate the effect of condensation on the pressure measurements.

Modified impact tubes may be used to determine impact pressures in two-phase fluid streams. Examples are gas-velocity measurements when liquid or fine solid particles are involved in the stream. Difficulties arise because of plugging and reading changes due to the influence of the momentum exchange between gas and particles upstream and within the instrument. The tendency to plug can be reduced by venting the tube at the rear through a nozzle having an area of about 5% of the inlet area. Dussourd and Shapiro⁽²⁴⁾ have, theoretically and experimentally, studied the momentum exchange effects on pressure in a uniform stream for a deceleration probe with static taps located in the inside wall of the probe head. Good correlation of theory and experiments was obtained in the overpressure recorded with the tube.

In supersonic flows, Hansen and Nothwang⁽⁴⁷⁾ observed that both the total pressure and the Mach number obtained from the ratio of total pressures before and after the shock are virtually independent of the presence of condensation.

1.8. Impact Pressure Measurement in Rarefied Gas Flows

Flow of gases can exhibit a phenomenon very different from flow of liquids at very low Reynolds numbers. This is because for a liquid the variation in the Reynolds number is essentially brought about by velocity changes, whereas for gases, a substantial variation in the Reynolds number can also be brought about by variations in its density or pressure. Thus, for a gas, a low Reynolds number flow may occur under conditions of low density. When the density of a gas falls sufficiently low, the gas exhibits what has been termed "rarefied phenomena", due to the fact that now the molecu-

lar mean free path, λ , of the gas is comparable to some significant dimension, L , of the surroundings. The gas then does not behave entirely as a continuous medium but also exhibits characteristics of its coarse molecular structure. On this basis, we define a rarefied gas flow to be a flow in which the Knudsen number, i.e. the ratio λ/L , becomes sufficiently large.

A criterion for demarcating the occurrence of rarefied phenomena has been derived solely on the basis of measured viscosity data.⁽¹³⁾ This is

Continuum behaviour

$$\frac{\lambda}{L} < 0.01, \quad (31a)$$

Slip behaviour

$$0.01 < \frac{\lambda}{L} < \frac{1}{2} \left[\frac{\mu}{400} - 1 \right], \quad (31b)$$

Free molecule behaviour

$$\frac{\lambda}{L} > \frac{1}{2} \left[\frac{\mu}{400} - 1 \right], \quad (31c)$$

where μ is the nominal dynamic viscosity (in poise) of the gas under atmospheric pressure.

The above criterion can be expressed in the more familiar form involving the Mach and Reynolds numbers by means of the relation

$$\frac{\lambda}{L} = \left(\frac{\pi \gamma}{2} \right)^{1/2} \frac{M}{Re_L} \quad (32)$$

where γ = specific heat ratio of the gas.

Thus, it can be concluded that rarefaction and viscous effects represent two aspects of the same physical phenomenon; and it follows that viscous effects should persist right through all the rarefied flow regimes. In this connection, Tsien⁽¹³³⁾ has indicated that at low pressures, the viscous effect can become important even at high velocities.

1.8.1. Slip flow

Theoretical solution for the viscous correction in slip flow has been developed by Lin and Schaaf⁽⁷⁷⁾ for an impact tube with hemispherical nose at subsonic speeds having its longitudinal axis parallel to the direction of flow by matching an inviscid compressible free stream to an incompressible boundary layer in the neighbourhood of the stagnation point. This is

$$C_\mu = \frac{2}{Re} \times \frac{(29/8 - 31/34 M^2)(1 + 1.317\lambda)}{1 + \frac{0.455 - 0.816\lambda}{\sqrt{Re}}} \quad (33)$$

where

$$\lambda = 1.997 \left(\frac{1 - 0.252M^2}{1 + \frac{0.455}{\sqrt{Re}}} \right)^{1/2} \frac{M}{\sqrt{Re}} \quad (34)$$

V = free stream velocity of gas, M = free stream Mach number, $Re = \rho V R / \mu$, R = radius of nose of impact tube.

This expression reduces to the correction for continuum flow if λ is set equal to zero. Both the incompressible and compressible continuum limits

have been discussed earlier in this chapter, see Sections 1.2.1 and 1.2.2. Subsonic results predicted by this solution at Mach 0.4 and 0.8 for both continuum and slip flows are shown in Fig. 23, from which it is seen that the characteristics display similar trends and the effect of slip on the viscous flow about an impact tube is to increase the viscous correction to the Bernoulli impact pressure.

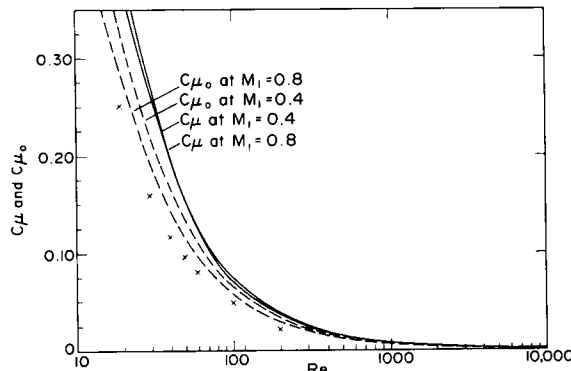


FIG. 23. Viscous corrections with and without slip (C_μ and C_{μ_0}) for hemispherical-nosed pitot at subsonic Mach numbers. Crosses denote Sherman's data trend shown in Fig. 6.

Experimental calibration results of the impact tube at both subsonic and supersonic speeds in a low density gas stream had been reported by Enkenhus⁽²⁸⁾ and Pollard.⁽¹⁰⁰⁾ The subsonic results have been presented in terms of the viscous correction versus Re_D plots. These are reproduced in Figs. 24 and 25. The form in which these results are displayed undoubtedly simplifies comparison with existing theory. Enkenhus' data, shown in Fig. 24, were obtained with sharp-lip pitots having $L/r = 50$ and a 10° externally chamfered mouth from traverses in the subsonic part of the boundary layer of a Mach 2 nozzle. The size of the pitots ranged from 0.36 to 9.53 mm o.d. and having d/D from 0.428 to 0.921. The Mach and Reynolds number

ranges of the tests were $0.42 < M < 0.95$ and $0.077 < Re_D < 11.1$, respectively. The results of Pollard, shown in Fig. 25, were obtained in orifice discharges using geometrically similar square-ended pitots ranging from 0.409 to 9.507 mm in diameter and having $d/D = 0.55$ and $L/d = 25$. The Mach and Reynolds number ranges were $0.25 < M < 1.04$ and $0.2 < Re_D < 30$, respectively. For comparison, the subsonic data of Sherman⁽¹²²⁾ and the incompressible data of Hurd *et al.*⁽⁵⁹⁾ have been reproduced by Enkenhus; while the subsonic results of Sherman for the 10° internally chamfered probe as well as the incompressible data of MacMillan⁽⁸³⁾ have been reproduced by Pollard. It should be pointed out that Enkenhus had misinterpreted the data of Hurd *et al.*, which were based on Re_R rather than Re_D , as assumed by Enkenhus. This error has been rectified in the present figure.

Since the Mach number has been shown to have no effect on the continuum calibration results, see Section 1.2.2, the effect of slip on pitot calibrations is clearly displayed in Figs. 24 and 25. Before slip occurs, the calibration function would undoubtedly be the same as that for continuum flow. After slip has occurred, the calibration function fans out into a family of an infinite number of curves, each of which is valid for one particular Mach number only. Using the flow regime criterion given earlier, it can easily be shown that slip flow would occur at Reynolds numbers ranging from 150 to 15, corresponding to operating Mach numbers of unity and 0.1, respectively. This implies that the effect of slip becomes more intense as the Mach number increases. A casual inspection of these figures reveals that the trend required by the flow regime criterion is exactly the same as that displayed by the experimental data. However, the demarcating Reynolds numbers predicted by this criterion seem somewhat too high compared with experimental data. On this basis, it is recommended that the slip limit Knudsen number can be raised to around 0.03 or 0.04, which

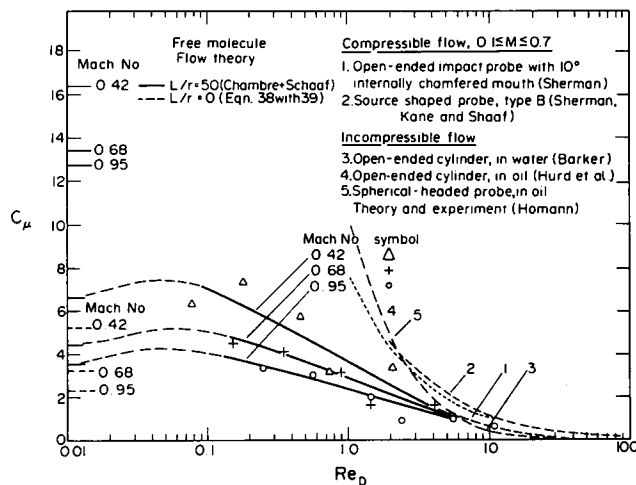


FIG. 24. Viscous corrections for open-ended impact tubes in subsonic flow (from very small to very large Reynolds numbers).

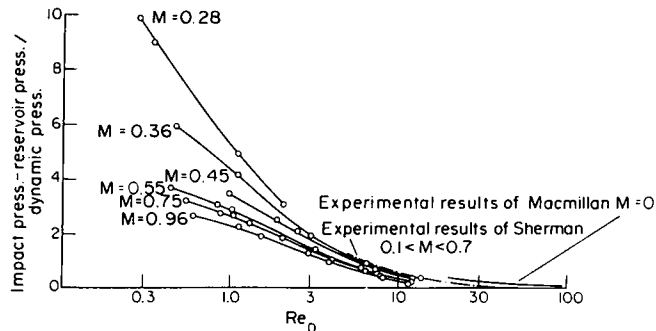


FIG. 25. Viscous correction for square-ended pitots in subsonic flow (data of Pollard for the low Reynolds number range).

corresponds to a demarcating Reynolds number at Mach one of 50 or 37, respectively. These later values seem more probable, as an extrapolation of Pollard's results would indicate. Another point worthy of mention at this juncture is that although both sets of data were obtained under very different conditions, they are not just in qualitative, but also to some extent in good quantitative agreement, as a casual check at $Re_D = 1$ would reveal, though the data of Enkenhus possess a substantial scatter in this connection. It is obvious that, as in continuum flow, the theoretical results of Lin and Schaaf do not agree with the experimental data. The effect of slip predicted by theory is of an opposite trend to that exhibited by experimental data. In addition, the theoretical results at low and high Mach numbers exhibited a cross-over at $Re_R = 40$ which is not substantiated by experimental data. Such has been the chief difficulty in obtaining theoretical solutions, since usually the actual situation has to be excessively simplified to enable an analysis to be made. As in the case of incompressible results, the viscous correction for the impact pressure is expected to be a function of probe shape too, though this is not evident from the results obtained with square-ended and internally chamfered probes by Pollard and Enkenhus respectively. The reader is referred to Section 1.2.3 for more discussion on this.

An alternative way of presenting the results is to plot the ratio of measured to theoretical impact

pressures against Reynolds number. This plot has also been given by Pollard, and is given in Fig. 26. The same trend as shown in Fig. 25, that the correction gets larger as Mach number increases, is again observed here.

Both Enkenhus and Pollard had also indicated the free molecule limits in their plots. It is obvious that none of their data come close to free molecule flow. The free molecule limits quoted by Enkenhus were obtained from the analysis of Chambre and Schaaf.⁽¹¹⁾ Limits for both the orifice probe (i.e. an impact tube of negligible length) and an impact tube having $L/r = 50$ were given. It is seen that the theoretical results of Chambre and Schaaf do not agree with Enkenhus' data. The free molecule limits quoted by Pollard were calculated for a temperature recovery factor of 0.95 using the method reported by Rothe and de Leeuw.⁽¹⁷⁾ Pollard's data are seen to be approaching these limiting values. In the light of these, the author has made rough estimations of the free molecule limits using values reported by Harris and Patterson,⁽⁴⁹⁾ who first set up the relevant equation for free molecule flow through a circular tube when the tube and gas are in relative motion and provided a series solution for the case of long tubes and low speeds. The results of Rothe and de Leeuw represent merely a more extensive documentation of results obtained from these equations by means of numerical analysis for tubes of arbitrary length and at arbit-

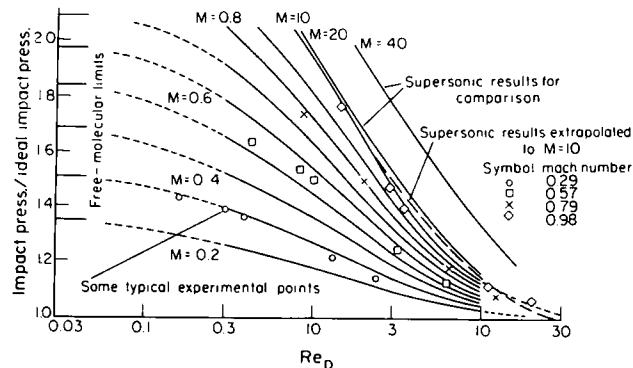


FIG. 26. Measured to ideal impact pressure ratio for square-ended pitots in subsonic low Reynolds number flow (alternative presentation of Pollard's data displayed in Fig. 35).

rary speed ratios. Like those reported by Enkenhus, these limits are calculated by assuming full temperature recovery, i.e. with $T_2 = T_0$. They have also been shown in Fig. 24 in comparison to those obtained by Chambre and Schaaf. The agreement between the experimental data of Enkenhus and these new limits is very fair indeed.

Next, we shall review the supersonic results.

These have been reported in a wider variety of forms, due to the combination arising from the use of a new abscissa parameter, $Re_2(\rho_2/\rho_\infty)^{1/2}$, first suggested by Potter and Bailey.⁽¹⁰²⁾ As has been seen in Section 1.2.3, this parameter is superior to Re_2 alone for correlating data on impact pressure in the continuum flow regime.

In addition to their subsonic results, both Enkenhus and Pollard had also reported results in supersonic flow. Besides, there are many other investigations carried out only under supersonic conditions. In what follows, we shall briefly summarize the essence of each of these investigations and then proceed to compare the effectiveness of the various correlating parameters used.

The results of Enkenhus, shown in Fig. 27, were performed over a supersonic Mach number range of $1.23 < M < 1.99$ for probes of various diameters having either externally or internally chamfered mouths and $L/r = 50$ in the supersonic part of the boundary layer of a Mach 2 nozzle. The Reynolds number, based on the free stream parameters and probe diameter, ranges from 0.36 to 40.9 for externally chamfered probes and from 2.1 to 24.5 for internally chamfered probes. Enkenhus had also included in his plot for comparison the theoretical supersonic results incorporating the viscous correction of Lin and Schaaf for both slip and no-slip cases. Also shown in the figure are the supersonic data of Sherman⁽¹²²⁾ for the source-shaped probe and also for probes having a 10° internal chamfer. All of Sherman's data were obtained over the ranges $1.7 < M < 3$ and $5 < Re_D < 800$. Data for the 10° internally chamfered probe, which were obtained essentially over the same Mach number range as Enkenhus' data are seen to merge well into

the latter's results for probes having similar geometry, while those for the source-shaped probe are in fair agreement with Lin and Schaaf's prediction at $M = 1.2$ for the no-slip case. As in all other comparisons made with theory so far, the experimental data show no Mach number dependence, contrary to the predictions of theory.

It is not completely clear at what conditions the Knudsen number should be evaluated under supersonic conditions. Considering Sherman's results for the chamfered probe, more detailed results of which has been given earlier in Figs. 9 and 10, the use of free stream conditions gives the highest operating Knudsen number of 0.15, showing some of the data to lie deeply in the slip regime. However, using conditions behind the shock gives a value of 0.086 indicating much less rarefaction effect being experienced by these data. Since the presence of the probe in a supersonic stream generates a bow shock in front of it such that the probe effectively senses only a subsonic stream, the use of the latter conditions, therefore, appears more plausible.

Independent of whichever condition is used, the supersonic data of Enkenhus are seen to have penetrated deeply into the slip regime. Since these data are taken over a rather limited Mach number range, the Mach number effect, which is clearly exhibited in Figs. 9 and 10 has not been strongly displayed.

The supersonic data of Pollard were obtained for uncooled square-ended impact tubes in a flow of air expanded from room temperature to the conditions $1.4 < M < 4.1$ and $0.2 < Re_{2D} < 60$ by means of either contour nozzles for high Reynolds number flows or orifices for low Reynolds number flows. The static pressure of the flow ranges from 10 to 70 microns of Hg. The flows were reported to be blockage free even with the largest pitots. As for the subsonic results, a family of geometrically similar pitots ranging from 0.409 to 9.507 mm in diameter and having $d/D = 0.55$ and $L/d = 25$ were used.

Results were presented using both $Re_{2D}(\rho_2/\rho_\infty)^{1/2}$

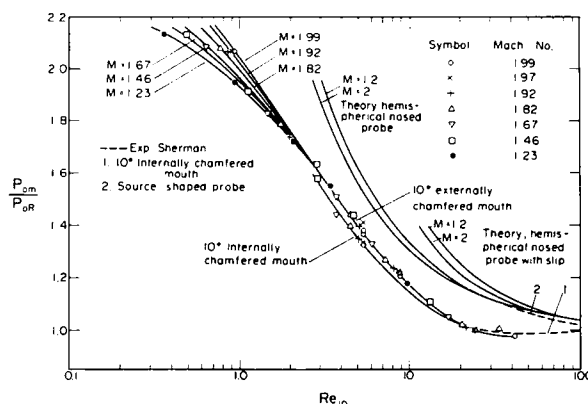


FIG. 27. Measured to ideal impact pressure ratio for square-ended pitots in supersonic low Reynolds number flow (data of Enkenhus).

and M_2/Re_{2D} as abscissa. P_m/P_R was used as ordinate throughout. These plots are shown in Figs. 28 and 29. From these figures, it can be observed that the data are well correlated on both plots, although these parameter are derived from entirely different concepts. Figure 29 clearly indicates the fanning of the calibration curve to approach the free molecule limits. Though this rarefaction effect has not been graphically displayed in Fig. 28, it is apparent from Pollard's text that such phenomenon occurs: "The correlation holds up to values of $Re_{2D}(\rho_2/\rho_\infty)^{1/2} \approx 2$ (or $M_2/Re_{2D} \approx 0.6$). Around this value a Mach number dependence becomes apparent and the individual curves begin to approach the appropriate free molecular limits." Pollard had also included in Fig. 28 the mean of the AEDC results reported by Potter and Bailey⁽¹⁰²⁾ for comparison. These results were obtained in a wind-tunnel where the flow was established from expansion through a contoured nozzle to $3.9 < M < 6.0$. It is evident that the agreement between the two sets of results is excellent.

The data reported by Chang and Fenn⁽¹²⁾ were obtained with probes having outside diameters of 3.15, 4.75 and 6.33 mm in free jets formed by expansion of nitrogen, argon and argon-helium mixtures through simple converging nozzles having

diameters of 0.81, 2.41 and 3.31 mm. The bow ends of the probes were hemispherical in shape having 0.83 mm wall with stagnation orifices ranging from 0.51 to 2.54 mm in diameter. Free stream Mach numbers ranged from 2.8 to 23. The Reynolds number range tested was $2 < Re_{2D} < 2000$. The results, shown in Fig. 30, were in the form of viscous correction versus Re_{2D} . There appears to be considerable scatter among the data of Chang and Fenn, probably due to the difference in atomicity of the gas media used in the experiments as well as the effect of Mach number. In addition to their own data, results reported by other investigators have also been included for comparison. However, it is believed that in reducing these data to the form shown in Fig. 30, Chang and Fenn have used the mean Mach numbers for each set of data reported. Otherwise the Mach number effect caused by the factor $(\rho_2/\rho_\infty)^{1/2}$ would have become evident even among the same set of data, i.e. for each set of data which was obtained over a wide Mach number range, the Mach number effect would have been noticeable, as we have seen earlier in Fig. 10. That such would have been the case is illustrated by the "scatter" among the different sets of data shown in this figure, since each of these has a different mean Mach number value.

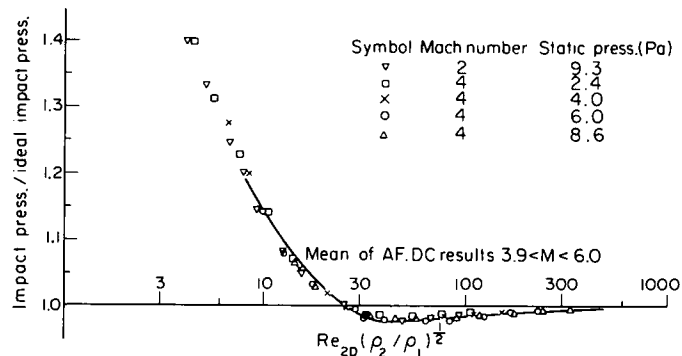


FIG. 28. Measured to ideal impact pressure ratio for square-ended pitots in supersonic low Reynolds number flow (data of Pollard).

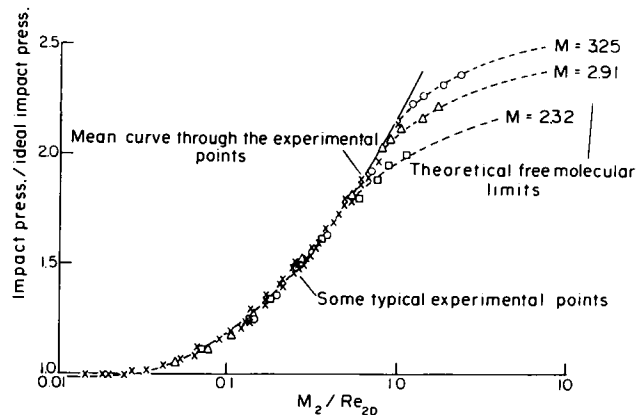


FIG. 29. Measured to ideal impact pressure ratio for square-ended pitots in supersonic low Reynolds number flow (alternative presentation of Pollard's data as function of Knudsen number).

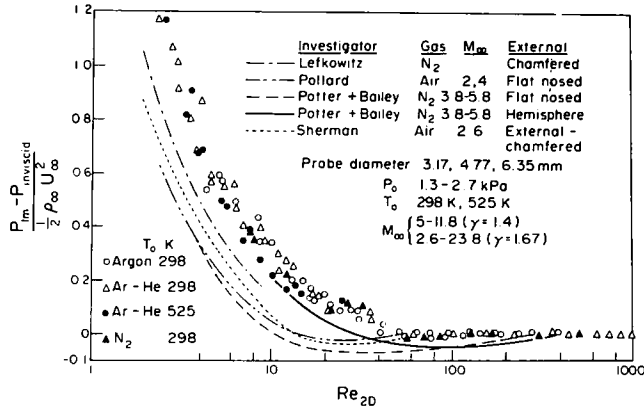


FIG. 30. Viscous correction for various types of impact tubes in supersonic and hypersonic flow (data reported by Chang & Fenn).

Figure 31 shows pitot characteristics, reported by Ashkenas and Sherman,⁽³⁾ in the form of P_m/P_R versus Re_{2D} for Mach numbers ranging from 2 to 7. These results were obtained by means of 10° externally chamfered pitots having $d/D = 0.8$ and $L/D = 50$ in a free jet. Except for measurements obtained at Mach 7, the characteristics overlap each other well and portray a trend similar to that reported by Enkenhus and Pollard. A casual check indicates that this characteristic intersects the abscissa at a value of Re_{2D} of 10, though data at Mach 2 seems to intersect the abscissa at a higher value. Although the trend for the Mach 2 data is similar to that of the general trend, it is believed to be of lower accuracy than other data obtained at higher Mach numbers. The reason being that while the Mach 2 data indicate a minimum point as the other data, this minimum does not decrease below unity and such trend has never been observed by other investigators who had reported that the characteristic either tends asymptotically to unity or shows a minimum which is within a few percent below unity. Hence, more quantitative significance should be attached to the point of intersection indicated by data at Mach 3 and 4. Using this value, the results reported by Ashkenas and Sherman have been reduced to the form having $Re_{2D}(\rho_2/\rho_\infty)^{1/2}$ as the abscissa parameter. This new characteristic is also

shown in Fig. 31. A causal comparison of Figs. 28 and 31 shows good agreement between the results of Pollard and the portion of the present characteristic for which the ratio P_m/P_R is less than 1.4. On this basis, it can be said that the claim made by Potter and Bailey that the parameter $Re_2(\rho_2/\rho_\infty)^{1/2}$ is superior to Re_2 alone for correlating impact pressure data has been substantiated. In addition, the results of Ashkenas and Sherman also show the effect of high rarefaction on the impact pressure characteristic. Under such conditions, the calibration function deviates from the general data trend and starts to approach the appropriate free molecule limit. This is just another succinct illustration of the fact that nature abhors a singularity.

Another point of interest is whether the pressure ratio should decrease below unity. This has generated much debate in incompressible calibration results. From the data reviewed so far, it is seen that for most data obtained in high speed flows, the pressure ratio first decreases below unity over a certain range of (modified) Reynolds numbers, and later rises above it as the (modified) Reynolds number decreases. Potter and Bailey⁽¹⁰²⁾ has reported that this phenomenon occurs for both cooled and insulated probe surfaces, with cooling seeming to slightly reduce the magnitude of the decrease, and for both monatomic and diatomic

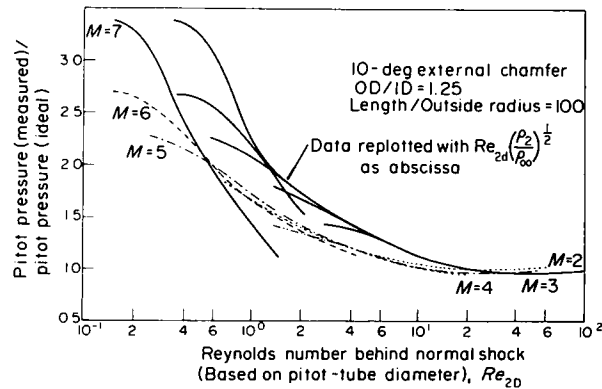


FIG. 31. Measured to ideal impact pressure ratio for externally chamfered pitots in supersonic low Reynolds number flow (data of Ashkenas and Sherman).⁽³⁾

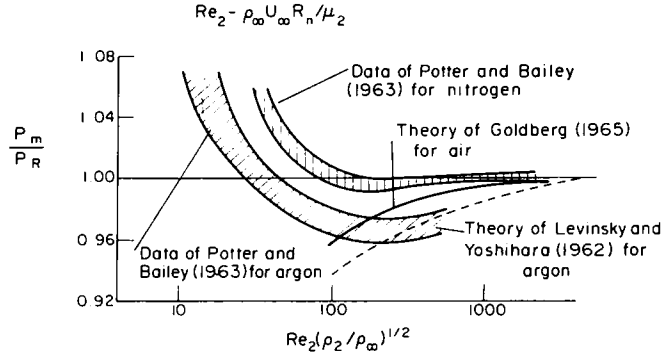


FIG. 32. Variation of measured to ideal impact pressure ratio with Reynolds number for hemispherical-nosed pitots; comparison between theory and experimental data with $T_w = 0.1$ to $0.2 T_\infty$ and $4.4 \leq M_\infty \leq 9.2$.

gases, the former attains a lower minima. This observation has been shown to be in perfect order with theory. Analyses based on the Navier-Stokes equations as described by Probstein and Kemp⁽¹⁰⁵⁾ leads to the prediction of reduced pressure in the stagnation region when effects behind the bow shock are taken into account. This theory has later been refined by Levinsky and Yoshihara⁽⁷⁴⁾ and Goldberg⁽³⁷⁾ as well as many others. The results for argon and air reported by the above-mentioned named references respectively have been given in Fig. 32. Satisfactory qualitative agreement exists between theory and corresponding experimental data of Potter and Bailey.⁽¹⁰²⁾ One notable difference between theoretical and experimental results is that the former decreases progressively as Reynolds number decreases while the latter reverses its trend at intermediate Reynolds numbers and then starts to rise again. This trend of rising impact pressure can be predicted, on the other hand, by a simple analysis based on the Navier-Stokes equations and Rankine-Hugoniot shock. This illustrates the inadequacy of present theories, since they can at best provide only piecewise information on the entire picture. It has been suggested that this decrease in the pressure ratio below unity is associated with the effects of shock-weakening, since analysis based on a Rankine-Hugoniot shock fails to predict, while

analysis based on transport effects behind the shock predicts, its occurrence.

Though Potter and Bailey have reported that there is no more than approximately 3% difference in the pressure ratio due to differences in gas media or wall cooling for a given nose shape at a given value of $Re_{2D}(\rho_2/\rho_\infty)^{1/2}$, the calibration results, like their incompressible counterparts, show a strong dependence on the nose configuration of the probe, with hemispherical nose probes experiencing the effect of rarefaction at higher values of Reynolds numbers than flat-nosed or square-ended probes in both monatomic and diatomic gases. However, Potter and Bailey have also demonstrated that this nose effect can be correlated by using either the shock stand-off distance, Δ , i.e. the inviscid shock layer thickness (including the shock), or the shock radius of curvature as the characteristic length for computing the Reynolds number. Figure 33 shows the results for three types of nose configurations collapsing into a single plot, to same experimental scatter as other results reported by Potter and Bailey, when Re_2 is based on Δ .

1.8.2. Free molecule flow

The results in the previous section indicate that under sufficiently rarefied conditions free molecule flow can develop both around and within the pitot

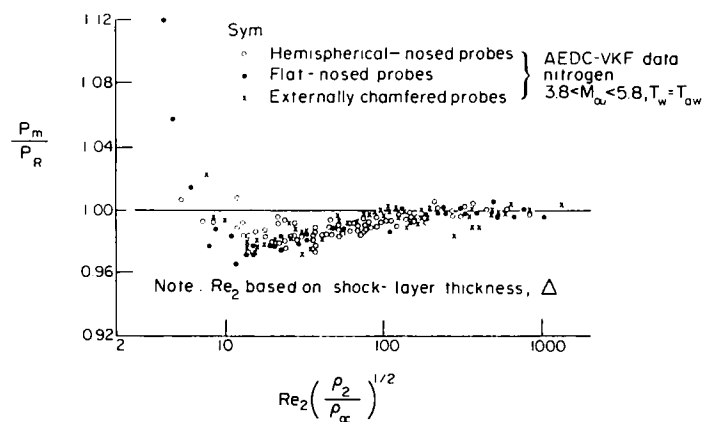


FIG. 33. Generalized impact pressure ratio characteristics for pitots in supersonic flow.

tube. This regime corresponds to that of extreme rarefaction and the flow situation is again amenable to theoretical analysis. The basic assumption is that intermolecular collisions can be neglected. Consequently, it is valid to neglect the effect of the re-emitted particles on the incident stream. Hence, the incident flow is entirely undisturbed by the presence of the body, even in supersonic streams; and no shock wave is expected to form in the vicinity of the object. Additional assumptions are that the random molecular motion of the exterior gas is Maxwellian, implying that the flow is isentropic; that the molecular reflection process at the tube wall is diffuse; and that outgassing from the interior surface of the probe is absent.

Under such conditions, it can be shown, using kinetic theory and the perfect gas law, that the pressure of the gauge volume to the free stream static pressure is given by, see, for example, Chambre and Schaaf⁽¹¹⁾ and Harris and Patterson,⁽⁴⁹⁾

$$\frac{p_2}{p_1} = \sqrt{\frac{T_2}{T_1}} \chi(S) \frac{W\left(S, \frac{L}{r}\right)}{W\left(0, \frac{L}{r}\right)} \quad (35)$$

where

$$\chi(S) = e^{-S^2} + S \sqrt{\pi} \{1 + \operatorname{erf} S\} \quad (36)$$

and $W\left(S, \frac{L}{r}\right)$ = the probability that a molecule having speed ratio S entering one end of the tube will reach the other end without returning to its source.

The subscripts 1 and 2 denote free stream and gauge volume conditions respectively, and the speed ratio S is defined as the ratio of the bulk velocity to the most probable molecular speed, $C_m = \sqrt{(2RT)}$.

The pressure in the gauge, where the bulk velocity and hence S is zero corresponds, therefore, to the impact pressure of the flow. The probability $W(0, L/r)$, i.e. the probability that a molecule leaving the gauge will re-enter the free stream, is called the Clausing factor, since it was first calculated by Clausing⁽¹⁴⁾ in his study of the problem of free molecule flow through short tubes. Simple approximations of the Clausing factor are

$$W\left(0, \frac{L}{r}\right) = \begin{cases} \frac{1}{1 + 0.5 \frac{L}{r}} & 0 \leq \frac{L}{r} \leq 1.5 \\ \frac{1 + 0.4 \frac{L}{r}}{1 + 0.95 \frac{L}{r} + 0.15 \left(\frac{L}{r}\right)^2} & \frac{L}{r} > 1.5 \end{cases} \quad (37)$$

The probability $W(S, L/r)$ for arbitrary S was first calculated by Chambre and Schaaf. However, we have seen in the previous section that experimental results do not agree with their theory. The problem of calculating this probability was first correctly formulated by Harris and Patterson, who

also presented a series solution for the case of molecules having low speeds in long tubes. A complete solution, however, has been given later by Pond⁽¹⁰⁾ and independently by Rothe and de Leeuw⁽¹⁷⁾ by means of numerical methods. The results of Pond, which had been given as $W(S, L/r)$ against S and which is directly applicable to eqn. (35), is shown in Fig. 34. The results of Rothe and de Leeuw were in the form displaying the fractional deviation of the impact tube pressures from the orifice probe pressure as a function of tube geometry and speed ratio. This is shown in Fig. 35.

The orifice probe is a special case for which the length of the impact tube tends to zero. Under such

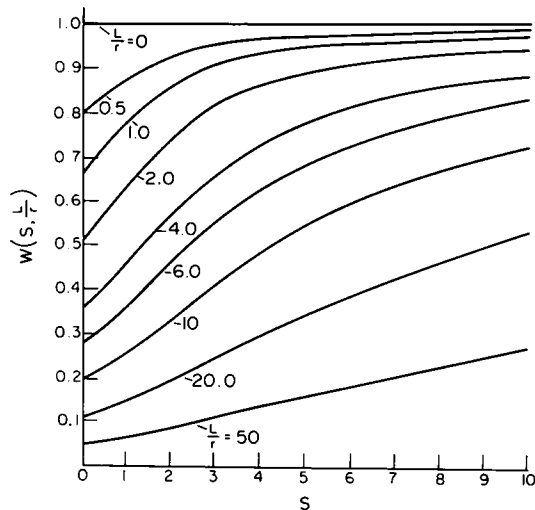


FIG. 34. The probability $W(S, L/r)$ as functions of S and L/r .

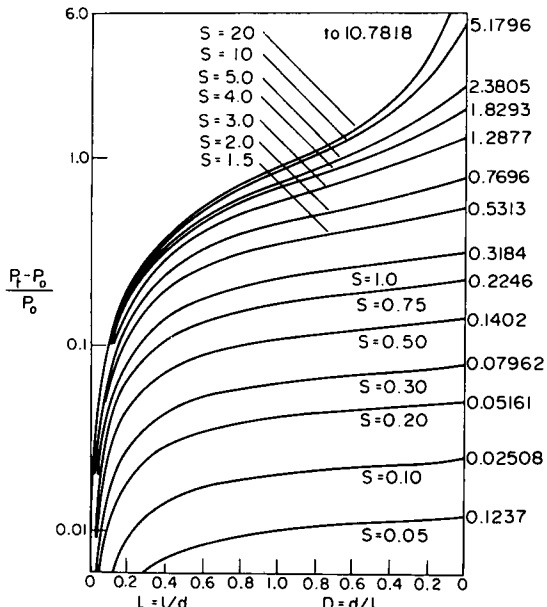


FIG. 35. Fractional deviation of impact pressure from gauge pressure as functions of tube geometry and speed ratio.

conditions, the probability that a molecule striking the opening from either direction will cross it is unity; thus

$$W(S, 0) = W(0, 0) = 1$$

which result is also evident from the graphs of Pond in Fig. 34. Thus, for the orifice probe

$$\frac{P_2}{P_1} = \sqrt{\frac{T_2}{T_1}} \{e^{-S^2} + S\sqrt{\pi}(1 + \operatorname{erf} S)\}. \quad (38)$$

Equation (35) has been derived for a probe having a sting support. For conventional L-shaped pitots, it can be shown that the same expression applies; only that the effective length of the probe is now the length from the open end to the junction with the stem.⁽²⁸⁾

In most cases, the temperature in the gauge volume will correspond to the ambient temperature which, if the gas is not preheated, will be the same as the gas stagnation temperature, T_0 . When the flow is adiabatic, the stagnation and stream static temperatures are related by the relation

$$\frac{T_0}{T_1} = 1 + \frac{\gamma - 1}{2} M^2 = 1 + \frac{\gamma - 1}{\gamma} S^2 \quad (39)$$

whence the impact tube reading becomes a function of the speed ratio and L/r only. The case of the orifice probe is particularly simple, being a function of the speed ratio only.

As for the case of slip flow, the proper choice of parameters for evaluating the Knudsen number is important. For instance, even the Knudsen number range reported by Enkenhus was between 0.072 and 18, based on the outer probe diameter of the square-ended impact tube and free stream conditions, only a few of the data obtained by Enkenhus at the low Reynolds number domain have been found to approach the free molecule limit rather closely.⁽⁴⁹⁾ This is because even though the Knudsen number based on free stream conditions and probe diameter may be fairly large, equals to 3.2 at Mach 2 for the 0.35 mm o.d. probe, the Knudsen number of the internal flow in the probe can still remain quite small, equals 0.057 based on the mean free path in the gauge volume and probe length. From the above consideration, it appears unlikely for square-ended impact tubes to encroach into the free molecule regime even under extremely rarefied free-stream conditions.

In addition to disposing of the geometry dependence of the conventional pitot, the orifice probe confers the advantage that the criterion of a large Knudsen number evaluated on the basis of the mean free path of the external flow and probe diameter implies also that the mean free path inside the probe is large compared to the diameter of the orifice. Enkenhus had reported that such probes are capable of operating much closer to the free molecule regime. He was also able to correlate his data in the range $0 < M < 2$ spanning the continuum and free molecule regimes by the following empirical formula:

$$\frac{P - P_c}{P_{FM} - P_c} = \frac{B K n^{1.2}}{1 + B K n^{1.2}} \quad (40)$$

where

$$B = 1.1 \{1 + (M - 1.25)^2\} \quad (41)$$

and $P = P_m/p$, the measured impact to free stream static pressure ratio, P_c = theoretical impact to static pressure ratio in continuum flow, P_{FM} = theoretical impact to static pressure ratio in free molecule flow, given by eqn. (38).

The correlation of experimental data with this formula is shown in Fig. 36. The functional form of this formula should be predictable theoretically by slip flow solution close to the continuum limit and by near-free molecule-flow solution close to the free molecule limit. However, no theoretical solutions are at present available for comparison.

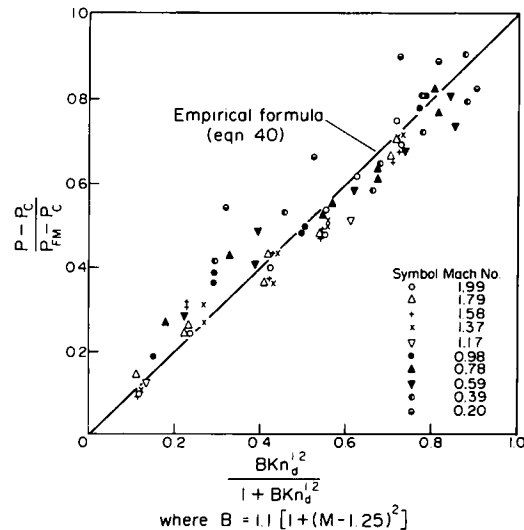


FIG. 36. Enkenhus' correlation of impact pressure measured by an orifice probe as a function of Knudsen number (based on probe diameter).

1.8.3. Relaxation effects in rarefied gas flows

Under high-temperature conditions, relaxation effects occurred due to the time necessary to excite the vibrational mode of the gas molecules. This vibrational "heat capacity" lag during and after the compression of the gas at the stagnation point of the impact tube would affect the total pressure reading. The time interval in which the compression of the gas occurs is essentially determined by a characteristic dimension of the impact tube and the free stream velocity. If this time interval is comparable to or shorter than the time required for the gas to maintain an equilibrium partition of energy, the process will be accompanied by an increase in entropy with a corresponding drop in impact pressure. Since the relaxation time necessary to excite the vibrational energy is inversely proportional to the static pressure level of the gas, the effect becomes significant in low-density gas streams with

fully excited vibrational energy levels. For more details of this topic, the reader is referred to the article by Kantrowitz.⁽⁶⁴⁾

1.8.4. Effect of yaw

Both Pollard⁽¹⁰⁰⁾ and Rajasooria and Brundin⁽¹¹²⁾ had investigated the effect of yaw on the impact tube in rarefied streams. Their results indicate that the yaw characteristic of a uniform stream in slip flow is essentially similar to that in continuum flows. In sheared flows, however, yaw correction becomes very difficult, since it now depends on the local flow conditions.

On the other hand, when fully developed free molecule flow occurs, the phenomenon is amenable to analytical treatment. The case of the orifice probe has been given by Patterson,⁽⁹⁸⁾ who showed that the pressure measured by the orifice probe rotated so that the radial plane containing the orifice makes an angle α with a uniform free stream is given by

$$\frac{p_2(\alpha)}{p_1} = \left(1 + \frac{\gamma - 1}{\gamma} S^2\right)^{1/2} \{e^{-(S \cos \alpha)^2} + \sqrt{\pi} S \cos \alpha [1 + \operatorname{erf}(S \cos \alpha)]\}. \quad (42)$$

A significant feature of this relation is that when the orifice is at an angle of attack to the flow, the probe registers a pressure which corresponds to the component of the speed ratio normal to the orifice area.

Enkenhus had reported data obtained from the axial rotation of orifice probe in free molecule flow at Mach numbers of 0.13, 0.45, 0.66 and 0.86. These are shown compared with the above relation in Figs. 37 a-d. The agreement is seen to be excellent.

In addition, Patterson has also investigated the behaviour of the yawed orifice probe in a non-isentropic sheared stream. The result is given by

$$\begin{aligned} \frac{p_2(\alpha)}{p_1} = & \left(1 + \frac{\gamma - 1}{\gamma} S^2\right)^{1/2} \\ & \times \left[\left(1 + \frac{1}{5} S \sin \alpha \cos \alpha \frac{\lambda}{p} \sqrt{\frac{2}{RT}} \frac{\partial T}{\partial y}\right) e^{-(S \cos \alpha)^2} \right. \\ & \left. + \sqrt{\pi} S \cos \alpha [1 + \operatorname{erf}(S \cos \alpha)] \right] \end{aligned} \quad (43)$$

where the minus sign is for $0^\circ \leq \alpha \leq 90^\circ$ and the plus sign for $90^\circ \leq \alpha \leq 180^\circ$, and λ , μ refer to the thermal conductivity and dynamic viscosity respectively. It is seen that this equation differs from eqn. (42) due to the additional terms involving the gradients $\partial u / \partial y$ and $\partial T / \partial y$. These terms are zero for $\alpha = 0^\circ$, 90° and 180° , so that when the probe is facing forward, rearward and sideways, it behaves as it were situated in a uniform stream.

It has been noted that both these equations can be applied to measure the speed ratio of the flow,

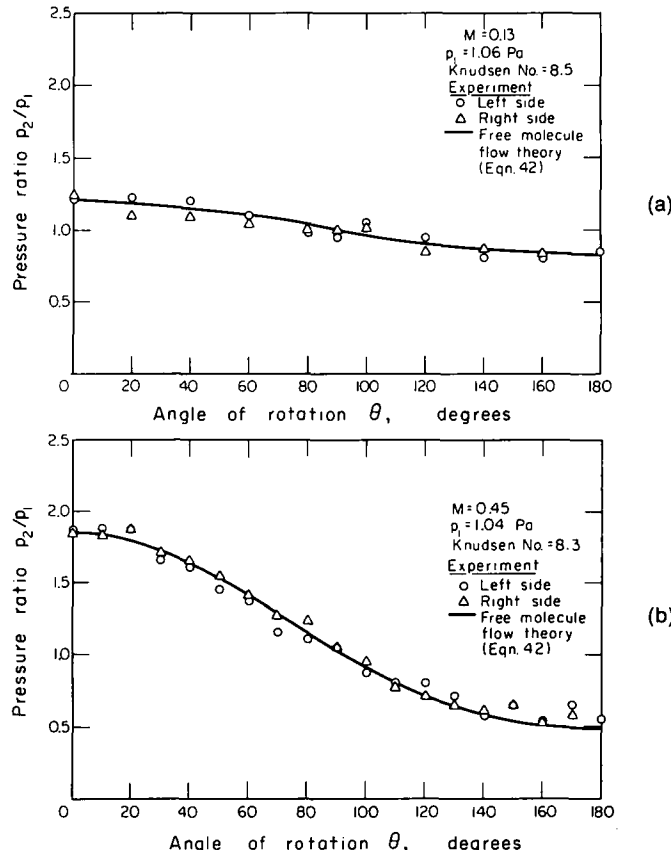


FIG. 37. Effect of yaw on the orifice probe reading in free molecule flow at various Mach numbers.

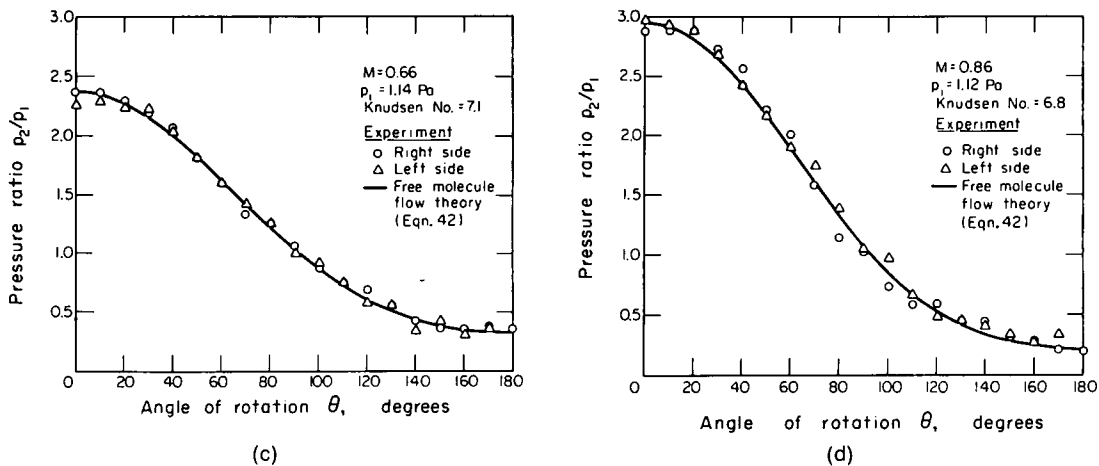


FIG. 37. (continued).

since it can be easily shown that

$$S = \frac{p_2(0) - p_2(\pi)}{2\sqrt{\pi} \times p_2\left(\frac{\pi}{2}\right)}. \quad (44)$$

The case for an arbitrary-length impact tube in a uniform free molecule stream at an angle of attack had been presented by Hughes and de Leeuw.⁽⁵⁸⁾ Unfortunately, the simple dependence of the orifice probe on α does not remain valid. It was shown that the solution to this problem can be expressed in the form

$$\frac{p_2}{p_1} \sqrt{\frac{T_1}{T_2}} = R(S, D, \alpha) \quad (45)$$

where $D = d/L$. However, to avoid the difficulty in interpreting the probe "pressure ratio", $R(S, D, \alpha)$,

the results have been reported in the form of reduced pressure ratio defined by

$$\frac{p_2}{p_{2,\text{orifice}}} = \frac{R(S, D, \alpha)}{\chi(S \cos \alpha)} = \Psi(S, D, \alpha). \quad (46)$$

Calculations for Ψ had been made for angles of attack up to 90° , for speed ratios from zero to infinity, and tube geometry ranging from an orifice to an infinitely long tube. Since there are three parameters involved, results have been presented in three different forms: in Fig. 38 as a function of non-dimensional probe diameter, D , with S as the parameter for given values of α ; in Fig. 39 as a function of speed ratio with α as parameter for fixed values of D ; and in Fig. 40 as a function of the angle of attack with S as parameter for various values of D .

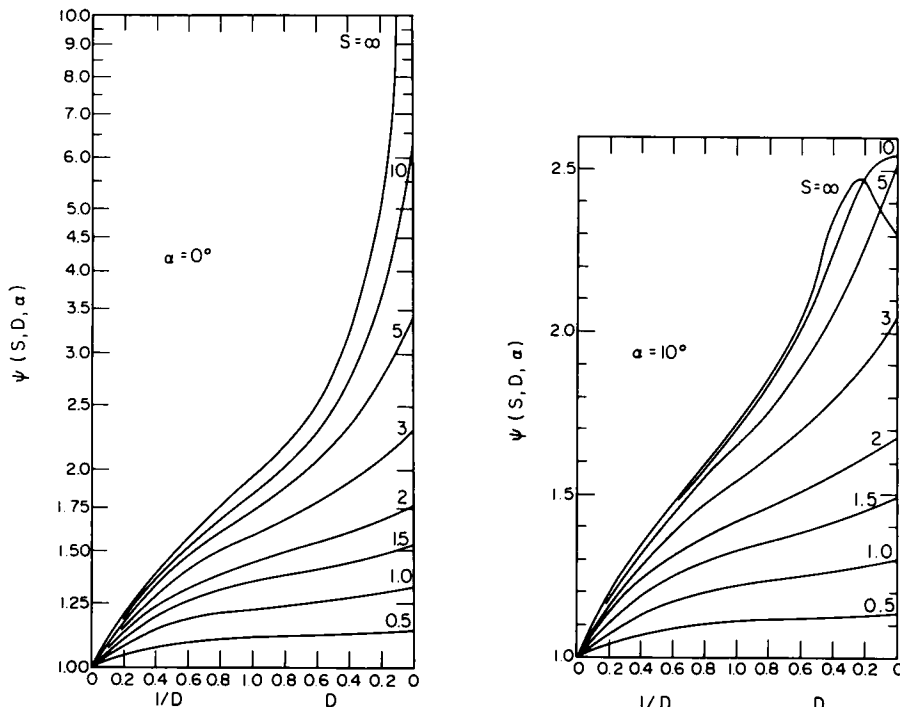


FIG. 38. Reduced pressure ratio as a function of non-dimensional probe diameter.

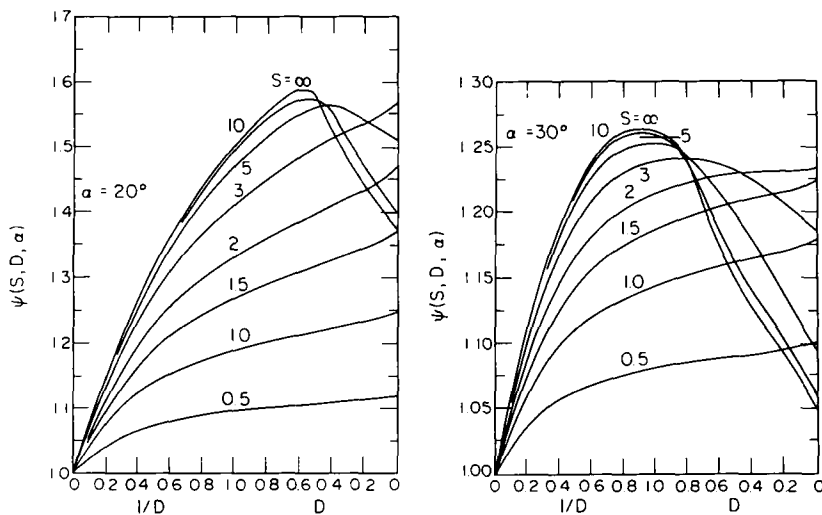


FIG. 38. (continued).

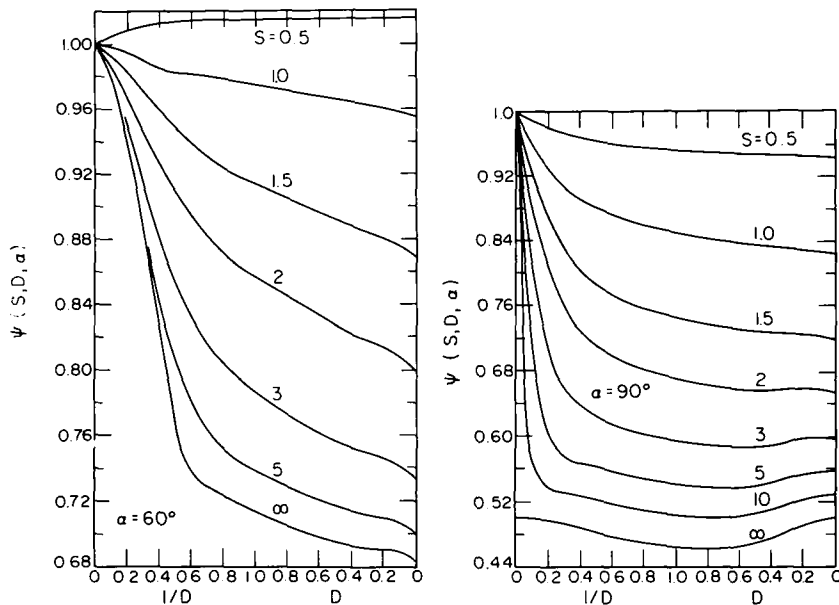


FIG. 38. (continued).

1.8.5. Effect of velocity gradient

Pollard⁽¹⁰⁰⁾ had reported the effect of total pressure gradient on impact pressure readings in low density free shear flows. A displacement of the effective centre of pressure towards the region of higher velocity has been observed in both sub- and supersonic flows.

In subsonic streams, this equals $0.18D$, a constant value independent of both the velocity or total pressure gradient and Mach number.

In low supersonic streams, the displacement appears to be Mach number dependent. However, the Mach number effect decreases at higher speeds, approaching an asymptotic value which can be represented by the following expression

$$\frac{\delta}{D} = 0.18 \left(1 - \frac{0.34}{\Delta} \right) + 2.88 \times 10^{-3} \frac{1}{\Delta} \frac{dP_0}{dr} \quad (47)$$

where dP_0/dr is the radial pressure gradient in Pa/mm and Δ the non-dimensional shock wave stand-off distance.

These results, of course, are subjected to the same criticisms as those of Young and Maas.⁽¹³⁹⁾ The reader is referred to Section 1.3.1 for a fuller discussion on this topic.

In fully developed free molecule flows, the effect of shear has no effect on the reading of the orifice probe, as is evident from eqn. (43), provided that the probe is facing forward, rearward or sideways.

1.8.6. Effect of orifice size

Potter *et al.*⁽¹⁰³⁾ had observed that both cold and adiabatic walled, flat-nosed impact tubes in supersonic argon or nitrogen streams experience an effect whereby the pressure measured with a probe of fixed external dimension varies with the radius of

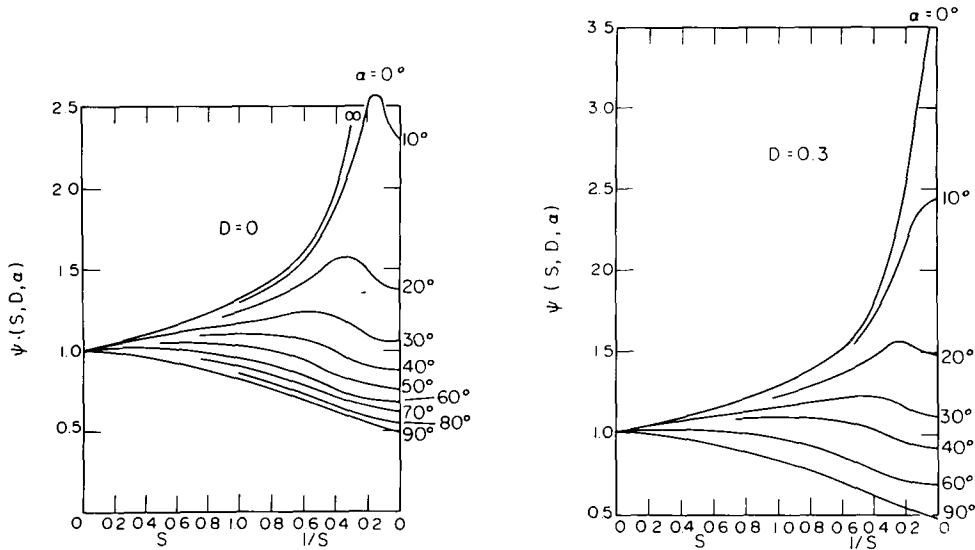


FIG. 39. Reduced pressure ratio as a function of speed ratio.

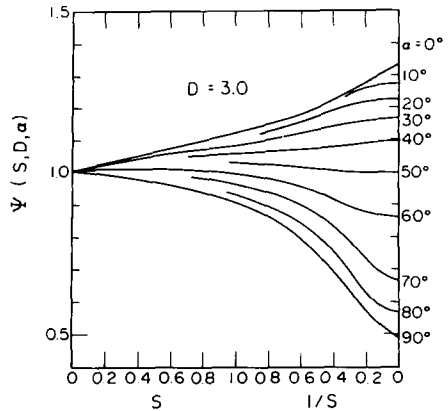


FIG. 39. (continued).

its pressure sensing orifice, when this becomes small enough to cause very low Reynolds numbers. This effect is plainly evident from Fig. 41, which shows that the ratio of measured to reservoir stagnation pressures begins to deviate from unity when

$$Kn_{2,r} \approx 0.4 \quad (48)$$

where $Kn_{2,r}$ is based on conditions behind the normal shock and the orifice radius. Alternatively, this criterion may be expressed as

$$Re_{2,r} \left(\frac{\rho_2}{\rho_\infty} \right)^{1/2} \leq 5 \quad (49)$$

$$\text{or} \quad Re_{2,r} \leq 2. \quad (50)$$

Since the pressure at the surface of a probe and in the measuring device are equal only if equilibrium exists in the neighbourhood of the orifice and

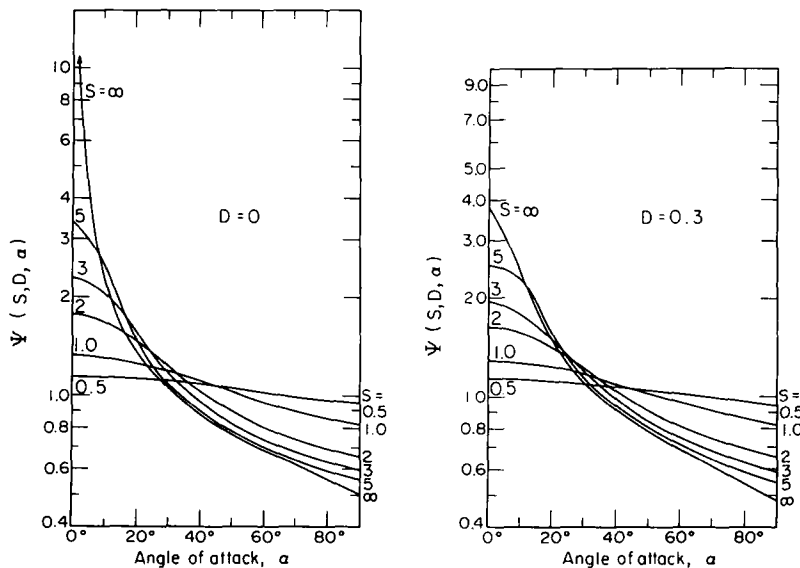


FIG. 40. Reduced pressure ratio as a function of angle of attack.

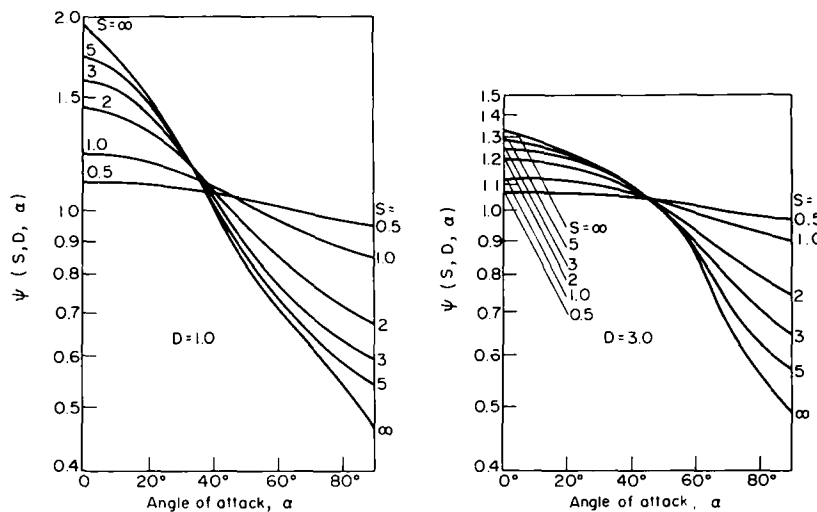


FIG. 40. (continued).

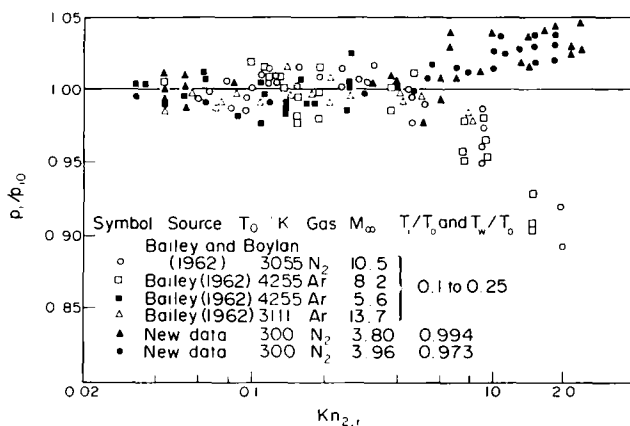


FIG. 41. Measured to reservoir impact pressure ratio as a function of Knudsen number based on orifice radius showing the influence of orifice size on the readings of both cold- and adiabatic-walled square-ended probes.

the most obvious departure from equilibrium under operating conditions is the presence of heat transfer in the case of a cold wall probe, the observed orifice effect has been attributed thereto. An analysis of this effect corresponding to the free molecule limit for the orifice probe has been presented in.⁽¹⁰³⁾ This is then extended by experimental means to predict the influence of heat transfer to

lower Knudsen numbers (smallest reported value being $Kn = 0.0455$) and arbitrary probe length up to a L/d ratio of 7.4. The combined theoretical and experimental results for both argon and nitrogen (the atomicity being accounted for by the specific heat ratio, γ) have been reproduced in Fig. 42. The curve for $d/\lambda_{c,i} = 0$ corresponds to the theoretical free molecule limit. Both this mean free path as

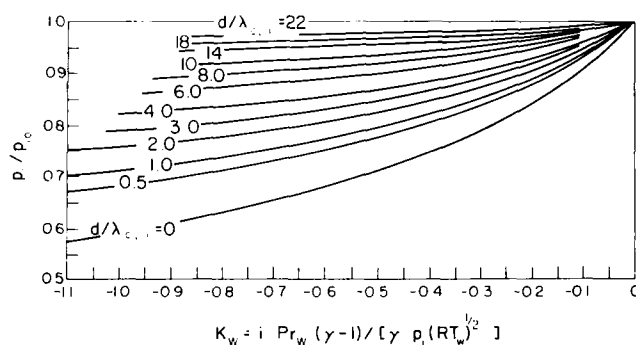


FIG. 42. Semi-empirical correlation of orifice influence on cold-walled square-ended probes.

well as the abscissa parameter have been evaluated in terms of P_i and T_c ; the indicated or measured pressure and the cold wall temperature rather than the true stagnation pressure.

With Fig. 42 it is possible to predict the variation of P_i/P_{i0} with orifice size for cold-walled impact probes. Several examples are shown in Figs. 43 and 44. Generally, the agreement between experimental and predicted results is good, in regard to both the initial departure of P_i/P_{i0} from unity as well as its subsequent variation at lower $d/\lambda_{c,i}$.

The above results predict zero orifice influence for adiabatic probes. This contradicts the experimental data shown in Fig. 41, which indicates that an orifice effect also exists when $\dot{q} \approx 0$, although it now causes $P_i/P_{i0} > 1$, a trend opposite to that displayed by cooled-probe data. This effect may be explained on the basis of a rarefaction phenomenon. Referring to eqn. (42), if continuum flow exists at the nose of the probe, it might be assumed that immediately upstream of the orifice $S \rightarrow 0$, $P_i \rightarrow P_{i0}$ and $T_1 \rightarrow T_w$ so that

$$\frac{P_i}{P_{i0}} \approx \left(\frac{T_2}{T_w} \right)^{1/2}. \quad (51)$$

On the other hand, with a velocity slip at the entrance of the impact tube, an effective speed ratio

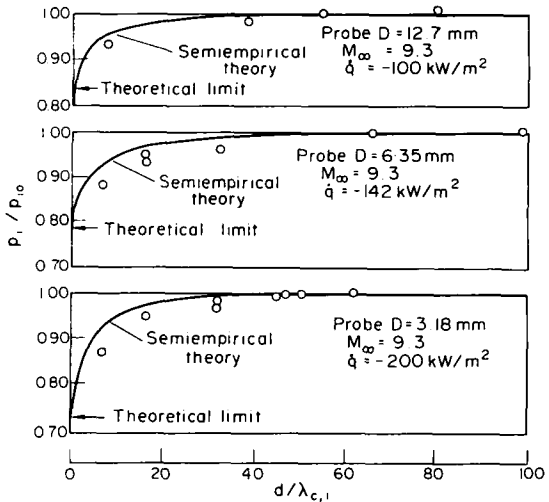


FIG. 44. Comparison of predicted and measured orifice effect on cooled, flat-nosed impact-pressure probes in nitrogen ($T_0 = 3060^\circ\text{K}$, $T_w/T_0 \approx 0.19$).

persists at the probe orifice. Under such conditions, eqn. (42) indicates that $P_i/P_{i0} > 1$ since $S > 0$, even if $T_2 = T_1$. This provides a qualitative explanation of the observed phenomenon. However, a quantitative prediction of the effect can only be achieved by means of a rigorous analysis based on slip flow in

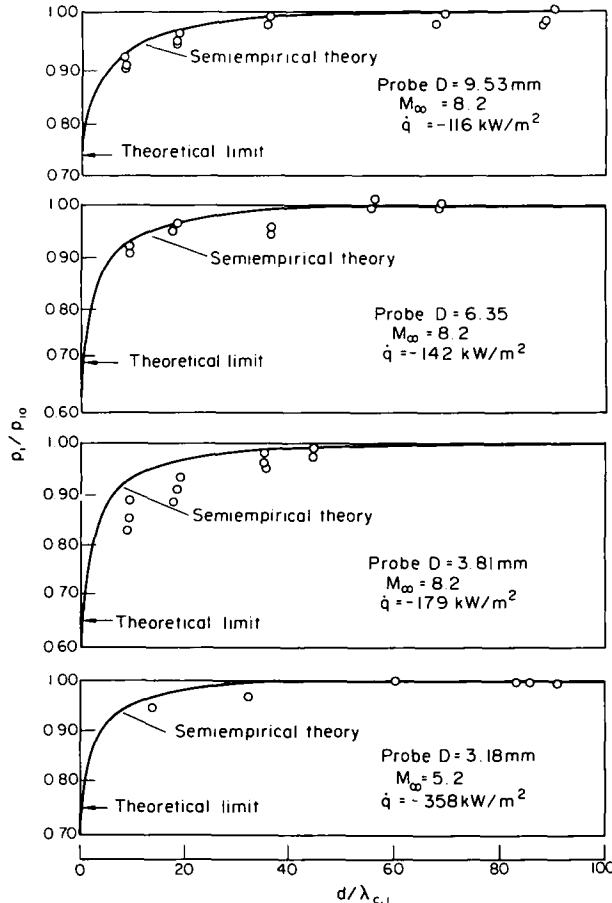


FIG. 43. Comparison of predicted and measured orifice effect on cooled, flat-nosed impact-pressure probes in argon ($T_0 = 4200^\circ\text{K}$, $T_w/T_0 \approx 0.19$).

the probe. At lower pressures when free molecule flow can be attained, eqn. (42) will probably be sufficient for predicting the observed pressure rise.

With regard to the use of eqn. (42) for predicting the free molecule limit for the orifice probe, Enkenhus⁽²⁸⁾ has reported that the hole acts as an orifice only if $L/r < 0.3$. Otherwise, it behaves as a short tube and causes a higher impact pressure to be measured.

1.8.7. Effect of thermal transpiration

If the mean free path is large compared with tube diameter, a pressure drop exists across a tube if the ends are at different temperatures. The magnitude of this thermal transpiration effect in free molecule flow has been given by Kennard⁽⁶¹⁾ as

$$\frac{p_2}{p_1} = \left(\frac{T_2}{T_1} \right)^{1/2} \quad \text{or} \quad \frac{\Delta p}{\bar{p}} = \frac{1}{2} \frac{\Delta T}{\bar{T}} \quad (52)$$

where the subscripts 1 and 2 refer to conditions at the two ends of the tube, and the bar denotes mean values in the tube. In slip flow, this effect is

$$\Delta p = \frac{24 \bar{\mu}^2 R \Delta T}{\bar{p} d^2 \left(1 + 8 \frac{\lambda}{d} \right)} \quad (53)$$

which can be rearranged as

$$\frac{\Delta p}{\Delta T} d = \frac{C_1}{\bar{p} d (1 + C_2 \bar{p} d)} = f(\bar{p} d) \quad (54)$$

where C_1 and C_2 are numerical constants.

A chart for the calculation of the thermal transpiration pressure drop across tubes in slip and free molecule flows is given in Fig. 45.

1.8.8. Effect of outgassing on pressure readings and time response in free molecule flow

Outgassing is the evolution of absorbed gases from a surface placed under vacuum. The outgassing rate depends on the type of surface, its cleanliness and its previous history. Harris⁽⁴⁸⁾ has shown that for probe and gauge geometries likely to be encountered in practice, the outgassing pressure drop and time response are

$$\Delta p = \frac{Q' A}{V} t_L, \quad (55)$$

$$t_L = \frac{3}{4} (2\pi RT)^{-1/2} V \left\{ \frac{L_1}{r_1^3} + \frac{8}{3r_0^2} \right\} \quad (56)$$

where Q' = throughput of gas per unit area due to outgassing, $= p \times \text{volume of gas/sec/unit area}$, A = internal surface area of gauge, V = gauge volume, L_1 = length of probe, r_1 = internal radius of probe, r_0 = orifice radius.

These relations show that the outgassing pressure drop is directly proportional to the time response. In order to ensure a fast response time and also to reduce the outgassing pressure errors, it is therefore necessary to keep the gauge volume and hence

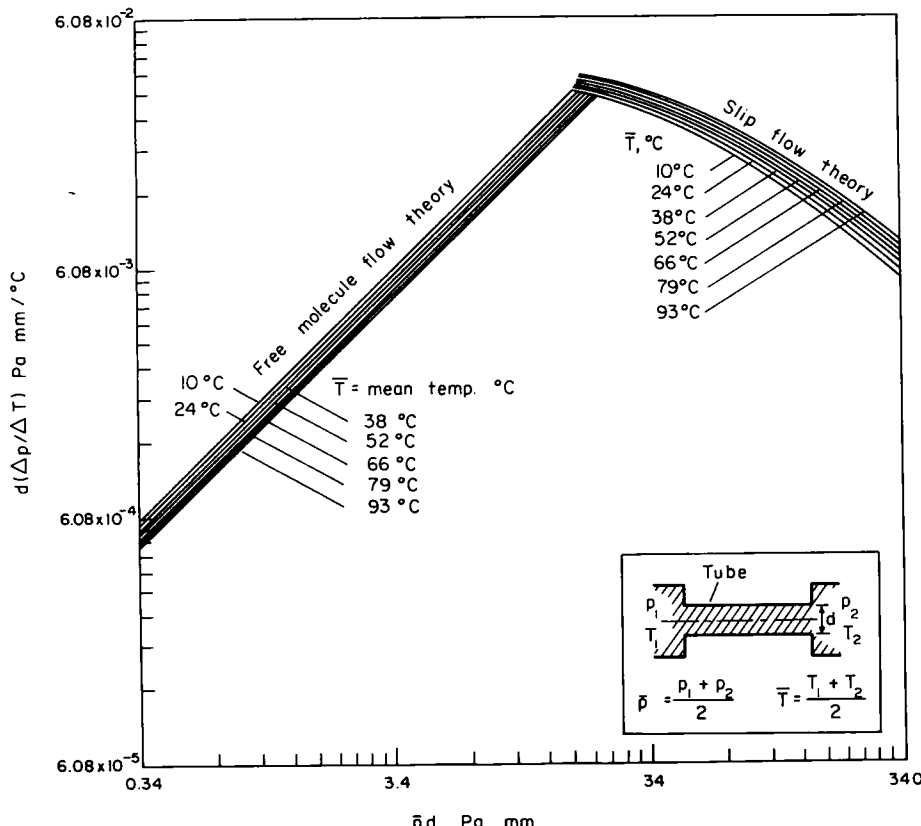


FIG. 45. Chart for the calculation of the pressure drop across a tube due to thermal transpiration in slip and free molecule flow.

internal area small. However, in certain instances, such as when using orifice probes, appreciable outgassing pressure drops are unavoidable even when using a U-tube directly connected to the gauge. The effects of outgassing on pressure readings for this case has been studied in detail by Enkenhus.⁽²⁹⁾ With a given flow condition, readings were taken first with the flow on, and then with the flow off and the tunnel at high vacuum. The difference between these readings was found to be independent of how well the probe was outgassed, indicating that the same outgassing error is present when the flow is on as when the tunnel is under vacuum. Thus, the pressure reading may be corrected for outgassing by subtracting the outgassing pressure drop measured under vacuum from the total pressure reading.

This observation is of significant importance in low-density impact pressure measurements since it eliminates from consideration the previous history of the outgassed probe. The base pressure of the probe can now be obtained after the measurement by shutting off the flow and bringing the tunnel to high vacuum. Results reported by Enkenhus indicate that this base pressure can be attained much faster for probes that had previously been outgassed for a longer time.

Roughly speaking, the outgassing rate of a surface is proportional to the square root of its absolute temperature. Thus, a marked decrease in outgassing pressure drop can be obtained if the line leading to the pressure gauge is refrigerated. To avoid thermal transpiration effects, the refrigerated portion should be centrally located so that both ends of the line can be maintained at the same temperature. For the same reason, a liquid cold trap connected into the line leading to the pressure gauge will greatly increase the response time due to additional volume, while the outgassing pressure drop is hardly affected.

1.9. Impact Pressure Measurement in Confined Situations

The conventional L-shaped pitot is not suited for investigations in confined regions, such as in turbomachinery. More compact designs for such applications consist of tubes closed at one end placed transverse to the flow and having pressure taps located some distance from the close end, while the open end of the tube is connected to the manometer. These probes can be of any cross-sectional shape, but the circular one is the most common and has been more extensively tested. Depending on the number of orifices present, these cantilever probes can be used for measuring impact, static and dynamic pressures as well as for determining the direction of velocity in two or three dimensions.

1.9.1. The pitot cylinder

Standard probe configuration consists of a

cylindrical tube having caps of hemispherical, square-ended or ellipsoidal shapes with one, two or three holes in a transverse plane located at a suitable distance from the tip.

The total pressure measured with pitot cylinders appears to have constant coefficients for $Re_D > 4000$. This result holds for hemispherical, square-ended and ellipsoidal heads with holes 0.5 tube diameter or more from the tip. However, unless the orifice is more than 5 tube diameters from the tip, effects due to the flow around the end cause the total head at the orifice to be lower than that at the same point in the free stream, i.e. the calibration factor is less than unity. This ranges from about 0.97 when the tube is one tube diameter from the tip to about 0.99, at 4 tube diameters.⁽¹³⁷⁾

Theoretical calibration result for cross flow over an infinite cylinder has been reported by Homann.⁽⁵⁵⁾ This is

$$C_p = 1 + \frac{4}{Re + 0.457\sqrt{Re}} \quad (57)$$

where Re is based on the external radius of the cylinder. Equation (57) may be used to define the calibration of the pitot cylinder for $Re_D < 4000$ or $Re < 2000$ for designs with pressure taps 5 tube diameters from the tip. However, there are no experimental data available to check its accuracy.

When the flow is not normal to the axis of the cylinder, the coefficient is lower than for the normal position. For the same pitch angle, the reading is lower when the tip is pointing downstream than when pointing upstream within inclinations of $\pm 20^\circ$. Often, the flow direction will be known approximately, and it is therefore possible to align the probe with sufficient accuracy by rotating it, first about its axis until the pressures at the side holes are equal and then about a perpendicular axis passing through the impact orifice until the total head reading is a maximum.

Livesey⁽⁷⁹⁾ has carried out extensive tests on the one-hole, hemispherical-tip pitot cylinder at low Mach numbers. His results suggest the following comprehensive design and error correction informations:

1. The ratio of the stagnation hole diameter, d , to the probe diameter should be less than $\frac{1}{8}$.
2. The distance of the stagnation hole from the end of the probe should be greater than $2D$, where D = probe diameter.
3. The angle of inclination of the probe to the direction of flow should not be more than 5° from normal.
4. The stagnation hole itself should not be shallow but preferably several hole diameters in depth, e.g. a depth of $4d$ was used by Livesey.
5. In traversing flows with transverse total pressure gradients the correction to be applied to the traverse due to the displacement of effective centre of the hole is $\delta/D = 0.09$. Displacement is towards the higher total pressure side.

It should be noted that Livesey used a d/D ratio of 0.12 throughout his tests, whether or not this displacement is dependent on d/D is not known.

6. This type of probe should not be used for boundary-layer measurements at distances smaller than $0.2D$ from the wall. This is because the horseshoe vortex formed at the wall around the probe may now interfere with the readings of the probe.

Pitot cylinders are very sensitive to yaw, as can be seen from Fig. 15. The yaw-insensitive range, however, can be considerably extended by modifications of the orifice geometry—the reader is referred to Bryer and Pankhurst for further details and also for effects of total pressure gradients normal to the probe axis.

1.9.2. The pitot wedge

This consists of a triangular prismatic tube closed by a square-ended cap at one end. The stagnation pressure tap is fitted on the leading edge. It is superior to the pitot cylinder in both impact and static pressure measurements. This is because the impact pressure measured by the wedge should be less sensitive to yaw than that of the pitot cylinder, since the yaw characteristic of this instrument is probably similar to that of a conical impact tube. Furthermore, the critical Mach number at which shocks first appear on the wedge is higher than that for the cylinder so that compressibility effects are also smaller. The critical Mach number is a function of the wedge angle.

More details on the pitot wedge as well as its many modified forms can be found in Bryer and Pankhurst.

2. STATIC PRESSURE MEASUREMENT

2.1. Introduction

The static tube and the wall piezometer, or "pressure tapping" are the two most commonly used methods for obtaining the static pressure of a fluid.

A variety of static pressure tubes has come into use. Of these, the L-shaped round static tube with an arbitrary nose configuration and having static pressure orifices around the circumference of the body is most common. This is perhaps because of the ease with which it can be coupled together with the pitot tube to form the pitot-static combination, which is compact as well as easily installed. However, the pitot-static tube requires a concentric configuration which has a minimum size limit of about 0.8 mm diameter for a reasonable response time. Thus, for measurements closer to the wall, a hypodermic or flattened impact tube referred to a wall piezometer or a separate static probe provides the only alternative.

Bryer and Pankhurst have given brief descriptions on many other types of static probes that have come into use; including the static cylinder, static wedge and disc static probes which will be discussed in this chapter in greater detail. In addition, we shall also describe the knife-edge type briefly.

2.2. The Wall Piezometer

Generally speaking, the wall piezometer suffers from less limitations than other static probes, its main disadvantage is that, if for some reasons, the pressure is not constant across the flow domain, the wall piezometer will not be measuring the same pressure existing at the tip of the pitot tube.

2.2.1. Stem and tip blockage effects

(a) *Stem blockage.* When a pitot tube is used in a pipe and the static pressure determined by means of a wall piezometer, the pressure distribution about the pitot stem may affect the piezometer reading. Hubbard⁽⁵⁷⁾ has investigated this stem effect on the pressure or resulting velocity measurement in a 305 mm-diameter pipe. Various distances of piezometer ahead of the pitot stem were considered, as well as different positions around the pipe circumference. For all the tests reported, the stem extends to the middle of the pipe. His results are shown in Fig. 46. The contour values in the figure indicate the relative error in terms of the mean velocity. To convert these values into error in velocity measurement, it is necessary to multiply the contour values in Fig. 46 by the factor $2d/\pi D_p$, where d and D_p are the stem and pipe diameters respectively. As an example, suppose that a pitot having a stem 25 mm in diameter is to be used in a 305 mm pipe, what would be the effect of the rod if a wall piezometer is situated 90° and 38 mm upstream of the stem axis? Reference to Fig. 46 shows that the relative error is 0.36, hence the error in the mean velocity is $0.36(2/12\pi) = 0.019$ or 1.9%. An inspection of Fig. 46 shows that if the pipe-wall piezometer were situated 45° from the plane of the

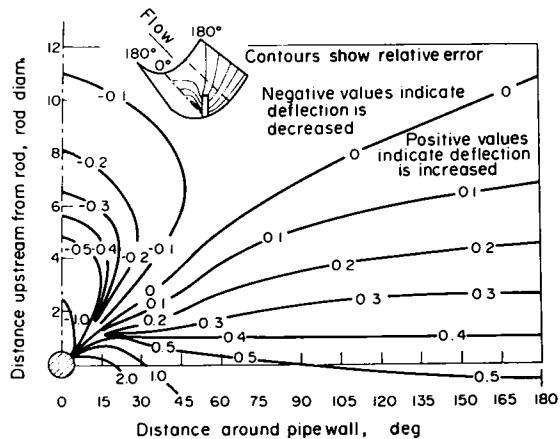


FIG. 46. Effect of stem of impact tube on wall piezometer reading in a 300 mm diameter pipe.

stem axis, it should be placed $3.7d$ ahead of the stem centreline to obtain a static pressure reading of zero error. At 90° , the distance becomes $7d$, etc. Errors for other positions can be similarly read off.

These results will be modified for cases when the stem does not extend right up to the centre-line of the pipe. Noting that the factor $2d/\pi D_p$ represents the blockage area in the flow, these results may still be applied to give an estimation of the error for these cases as well as for other combinations of stem and pipe diameters, if the conversion factor is modified accordingly. In actual fact, these results seem to be restricted to an impact tube of the cantilever type, since the dummy tube used in simulating the impact tube does not have a nose tube; and there is no *a priori* reason to indicate that the combined effects due to stem and tip could be obtained by superposing the results in (a) and (b) of this section.

(b) *Tip blockage.* When the nose tube of a pitot extends into the plane of a wall piezometer fixed in a pipe, the pressure read by the piezometer tends to be low due to the reduced cross-section of flow. For the case of a tip projected area of 0.47% of the pipe area and located at the pipe centre-line, Hubbard⁽⁵⁷⁾ found the pressure reduction to correspond to the "venturi effect" obtained by using an effective area equal to pipe area less tip area when the tip was 5 or more tip diameters ahead of the plane of the piezometer—i.e. the error in the velocity head is exactly 0.94%. The complete result for this test, showing the variation of this error with the distance between the piezometer and the tip, is given in Fig. 47.

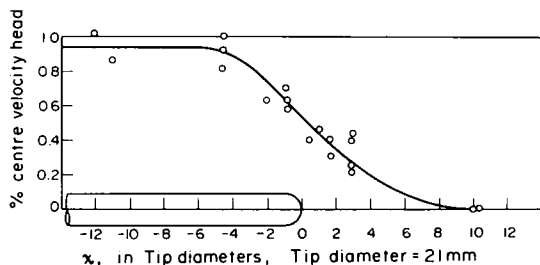


FIG. 47. Effect of tip of impact tube on wall piezometer readings in a 300 mm pipe: notice that the venturi effect causes the piezometer to read low but the resultant velocity head to be high.

Another investigation on the effect of probe tip on wall piezometer readings has been reported by Pollard⁽¹⁰⁰⁾ in conjunction with supersonic low density continuum flow. Data for a transverse traverse were obtained in a Mach 4 nozzle with the mouth of the impact tube located right above the static tap. Wall static pressure variations for different size impact tubes with the distance of the impact tube above the wall piezometer are shown in Fig. 48. These results have been corrected for shear displacement using eqn. (47). The wall piezometer readings are seen to be reinforced by the presence

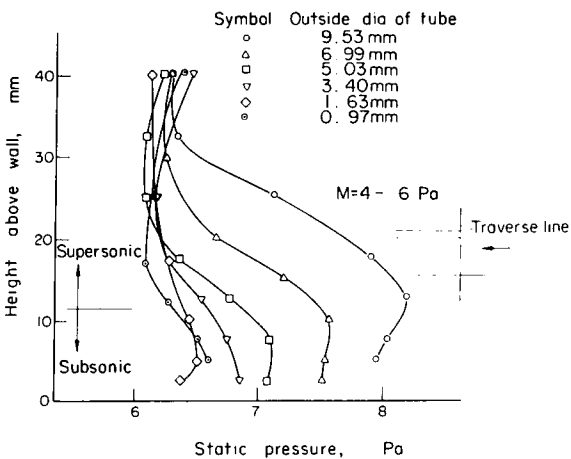


FIG. 48. Wall static pressure variation for impact tubes of various sizes as a function of their height above the wall at a supersonic free-stream Mach number.

of the impact tube, the larger the tube, the higher the reading. This trend is contrary to that exhibited by the low-speed pipe-flow data obtained by Hubbard. However, none of the tubes seem to record the true static pressure. Results for an axial traverse were shown in Fig. 49. These were obtained at Mach 2 with a 9.53 mm impact tube

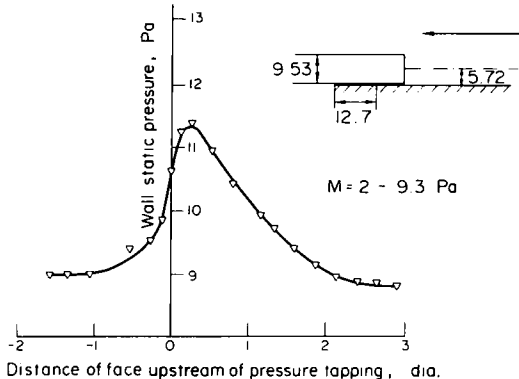


FIG. 49. Wall static pressure variation at a supersonic free-stream Mach number showing effect of tip blockage.

situated 5.72 mm above the nozzle wall. Again, it is seen that the wall tap reads high with the impact tube immediately above it. Also, the impact tube nose has to be situated more than either one tube diameter behind or three tube diameters in front of the wall tap for the reading to be consistent; though these two readings are not themselves identical.

2.2.2. Effect of orifice size and configuration

(a) *Orifice size.* The presence of a hole in the retaining wall is expected to influence the static pressure reading to some extent. This is because any finite hole is bound to produce some curvature in the neighbouring streamlines due to removal of the constraining boundary. The extent of the affected region must obviously depend on the size of the hole. Ray⁽¹¹³⁾ has reported that the thickness

of this layer varies between $d/10$ and $d/40$; the magnitude of this thickness diminishes with the size of the hole. As shown theoretically by Thom and Apelt⁽¹³⁰⁾ and observed experimentally by Ray, the neighbouring streamlines dip into the hole producing a centrifugal force field which raises the tap pressure above the free stream value. The magnitude of this pressure excess depends on the flow velocity and the geometry of the hole. In other instances in which separation of the flow from the leading edge of the hole occurs, the local tap pressure falls below the static pressure. However, more quantitative information on the influence of the orifice size and geometry on the measured static pressure has to be obtained by experimental means.

Many experiments have been conducted to investigate the effect of orifice size and geometry on the measured static pressure; and it is very difficult for us to identify which of these were conducted specifically for the static tube and which for the wall piezometer. A useful criterion appears to be the ratio of the hole thickness, l , to the hole diameter, d . For wall piezometers, this ratio is generally larger than unity, while for a static probe, it may be much smaller than unity.

In the previous chapter, we have seen that the calibration of an impact tube depends on the geometry of the impact orifice. We have, therefore, no reason to believe that the static hole geometry would not influence the static pressure measured. The discussion on this will be postponed to subsection (b) of this section. In this connection, it should be noted that even for circular static orifices having their axes perpendicular to the local streamline, variation in their geometry still occurs in the manner in which they are connected to the manometer tubing. At least three types of wall fittings have been reported. These are shown in Fig. 50. They

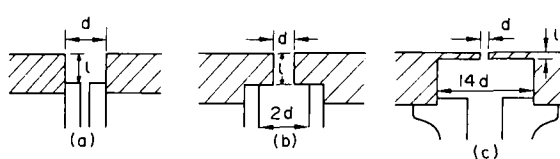


FIG. 50. Three versions of wall fittings reported for the wall piezometer: (a) used by Allen and Hooper,⁽²⁾ (b) used by Shaw,⁽¹²¹⁾ (c) used by Livesey *et al.*⁽⁸⁰⁾

can be classified by the size of the adaptor section at the back of the orifice. For type (a) the ratio $D_c/d = 1$, type (b) has a value of 2 and type (c) 14, where D_c represents the diameter of the cavity at the back of the orifice.

In fact, the static hole error problem is so very complex that it has not been the subject of any rigorous analytical investigation. However, attempts on dimensional analysis have been made to bring out the salient dimensionless groupings for the situation thus improving the presentation of the experimental results. Taking all relevant parame-

ters into consideration, the static pressure error for a finite size hole can be written as

$$\frac{\Delta p}{\tau_0} = f \left\{ \frac{d}{\nu}, \sqrt{\frac{\tau_0}{\rho}}, \frac{l}{d}, \frac{D_c}{d}, \frac{D}{d} \right\}. \quad (58)$$

The last dimensionless group, D/d , represents the ratio of the significant dimension of the channel on which the orifice(s) is (are) drilled to the orifice diameter. It is only of importance for wall piezometers since static probes are usually designed with fixed dimensions so that this group ceases to be an effective independent variable.

As it is impossible to experiment with holes of very small dimensions, some guide to the behaviour of the error as the hole Reynolds number, as the first dimensionless group inside the functional parentheses has been called, tends to zero is not only helpful, but also indispensable since the reference hole itself is subject to error and the readings have thus to be corrected to the actual static pressure at zero hole diameter. Two procedures have been reported for this correction. The one used by most investigators is based on the intuitive expectation that the true static pressure should be registered as the hole diameter tends to zero. However, this does not indicate the manner with which this limit is approached, so that the data reduced for the $\Delta p/\tau_0$ vs. Re^+ plot has to be further supplemented by the same condition again in the following form: $\Delta p/\tau_0 \rightarrow 0$ as $Re^+ \rightarrow 0$. The second procedure, put forward by Livesey *et al.*⁽⁸⁰⁾ is based on the assumption that the static hole error Δp is proportional to the mean dynamic pressure in the undisturbed flow between the surface and a point at a distance y proportional to d from it. Upon non-dimensionalizing with the pertinent parameters, τ_0 for pressure and ν/u^+ for length, this becomes

$$\frac{\Delta p}{\tau_0} = \frac{K}{kd^+} \int_0^{kd^+} u^{+2} dy^+. \quad (59)$$

This relation has been reported to portray the behaviour of the static pressure error with hole Reynolds numbers to some extent; however, both the coordinates of the graph need to be scaled empirically.

Having anticipated the functional relationship between static hole error and other relevant parameters and been forewarned against the difficulty in extrapolating for the absolute error, we shall now summarize the results of the various experimental investigations on this topic and then proceed to draw some general conclusions regarding static hole design.

The first investigation on static hole errors was carried out by Fuhrmann in 1912.⁽³⁴⁾ He employed an axisymmetric model of very thin walls and divided internally into three compartments. A 0.8 mm-diameter hole located in the wall of the centre compartment served as reference while two test holes located diametrically opposite in the front

compartment were varied in size from 0.12 mm to 1.0 mm diameter. The depth of the orifices was not reported. The model was tested in a wind tunnel in which the air velocity was maintained at 9.8 m/sec. He reported that negative errors were observed for sharp-edged holes. The magnitude of the error increases rapidly with increased hole size up to 0.4 mm diameter; thereafter it becomes nearly constant, as shown in Fig. 51.

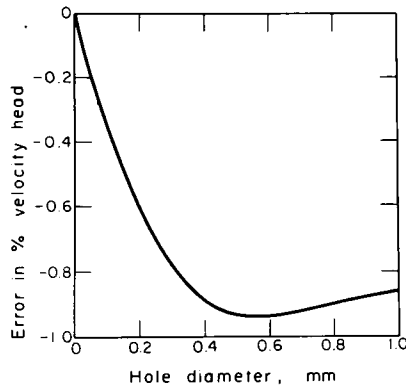


FIG. 51. Effect of hole size on wall static pressure (data of Fuhrmann).

Allen and Hooper⁽²⁾ conducted their investigation in a 305 mm-diameter pipe using piezometers of the type shown in Fig. 50a. The experiments were carried out with water flowing at velocities from 1.0 to 1.9 m/sec. For holes varying in diameter from 1.59 to 21.43 mm they reported that a truly square-edged hole without burrs, absolutely flush with the inside pipe wall, having $l/d > 2$ gives the actual

static pressure if there are no fluid swirls or crossflow.

Myadzu⁽⁹¹⁾ carried out tests in a square channel with water flowing at velocities up to 4.3 m/sec. Static holes tested had diameters ranging from 0.1 to 4 mm. The absolute error was obtained by graphical extrapolation. Results indicated a positive error which increases linearly with hole size but independent of velocity. The depth of the hole was found to be significant; the error is constant for $l/d > 2$, but decreases for smaller ratios until below a ratio of about 0.4 the error becomes negative.

In Rayle's investigation,⁽¹¹⁴⁾ orifice plugs having $l/d > 2$ were inserted into the wall of a 25 mm-diameter honed tube. This tube was situated downstream of a nozzle. In the course of the experiment, the orifices were varied in diameter from 0.13 to 3.18 mm. Also varied was the distance of the test section from the nozzle. Both air at mean velocities from 120 to 270 m/sec and water at velocities from 6.7 to 9.5 m/sec were employed to observe the effects of compressibility. Positive errors were recorded and these were found to increase with increase in hole diameter; with increase in Mach number and with reduction of distance between the nozzle and the test section. The effect of the first two factors on the static pressure error is shown in Fig. 52. Rayle had not, however, analysed the effect of the third parameter on the static pressure error.

Ray⁽¹¹³⁾ experimented with a rectangular section, measuring 71 by 41 mm. The static pressure taps were located in the longer side. The diameter of the holes was varied from 1 to 10 mm, and the l/d ratio from 0.1 to 1.75. The diameter of the connection to

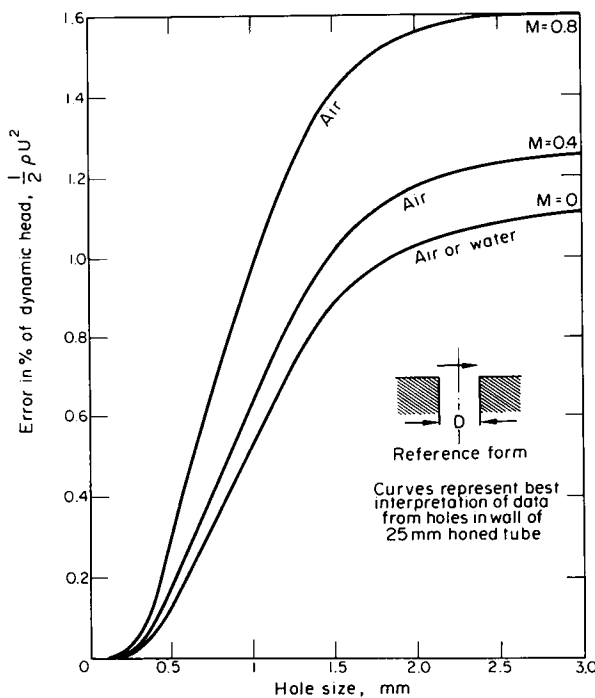


FIG. 52. Effect of hole size and Mach number on the static pressure error registered by a square-edged hole (data of Rayle).

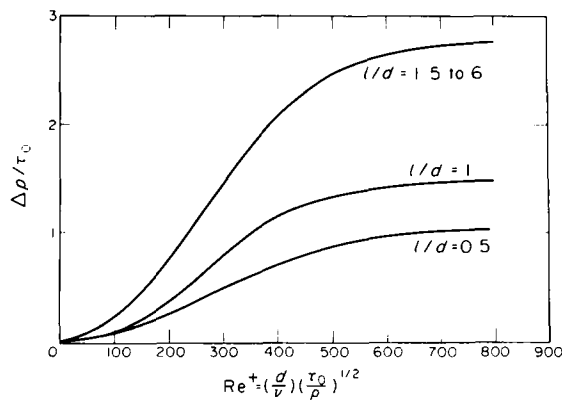


FIG. 53. Wall piezometer errors for incompressible turbulent flow (data of Shaw).

the manometer was also varied, being smaller than the hole diameter for most of the tests. His results can be represented by the following relation over the Reynolds number range tested:

$$\frac{\Delta p}{\tau_0} = f \left(\frac{l}{d} \right) \sqrt{Re^+} \quad 1.7 < Re^+ < 31.6 \quad (60)$$

where $f = 0.25$ for $l/d = 1.75$
 $= 0.54$ for $l/d = 0.1$.

Equation (60) shows the error to be positive and increases with increase in hole Reynolds number and with reduction of the l/d ratio. However, Ray also reported negative errors when the l/d ratio is very small and the enlargement behind the hole considerable.

Shaw⁽¹²¹⁾ carried out a series of extensive tests in a 50 mm internal diameter pipe. Square-edged static pressure holes having l/d between 0.5 and 6 and fitted normal to the pipe wall were used. Hole diameters were varied from 0.64 to 4.45 mm and the manometer connection was of that shown in Fig.

50b. The results were expressed in the form derived from dimensional analysis as was in the case of Ray. However, no simple functional relationship was found and they are presented graphically in Fig. 53. The main features of the results are as follows: positive errors are recorded for hole Reynolds numbers up to 800, i.e. over the entire range tested. The error increases with increase of l/d ratio up to a value of 1.5; thereafter it ceases to influence the static hole error any more. For any l/d ratio, the variation of the static hole error with hole Reynolds number is similar. The error is zero at zero hole Reynolds number; increases with increase in hole Reynolds number over the whole Reynolds number range, reaching an asymptotic value at a value of the Reynolds number somewhat greater than 800. The maximum asymptotic error for the various l/d ratios tested are:

$$\begin{aligned} l/d = 1.5 & \quad \left(\frac{\Delta p}{\tau_0} \right)_{\max} = 2.75 \\ l/d = 1 & \quad = 1.5 \\ l/d = 0.5 & \quad = 1.05 \end{aligned}$$

A set of experiments almost identical to Shaw's was reported by Livesey *et al.*⁽⁸⁰⁾ using a pipe of 63.5 mm internal diameter and orifices of the type shown in Fig. 50c. Their results, shown in Fig. 54, are in broad agreement with previous data and confirm that a positive error is obtained for deep static holes whereas shallow holes with large cavities behind them can also give rise to negative errors. However, their results differ in finer detail from previous investigations. In particular, for their type of deep static holes the error varies almost linearly with hole Reynolds number for $Re^+ > 150$, and its magnitude is smaller than that obtained by other investigators in the range $Re^+ \leq 1000$, see Fig. 55 which compares the results of Shaw, Rayle (results reduced by Shaw) and Ray with those of

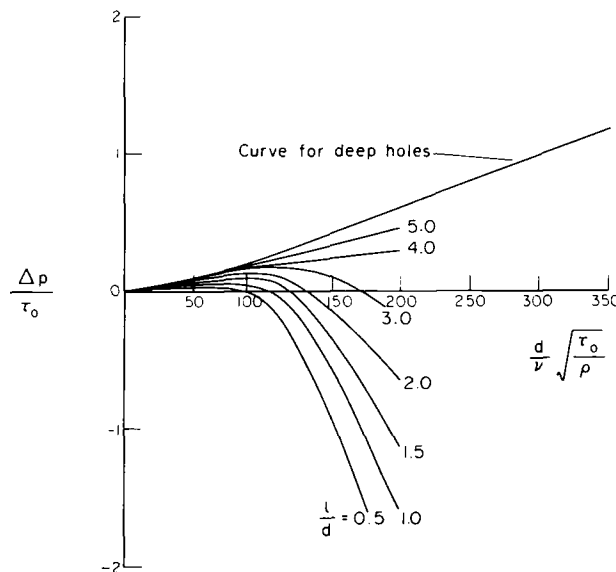


FIG. 54. Wall piezometer errors for incompressible turbulent flow (data of Livesey *et al.*)⁽⁸⁰⁾

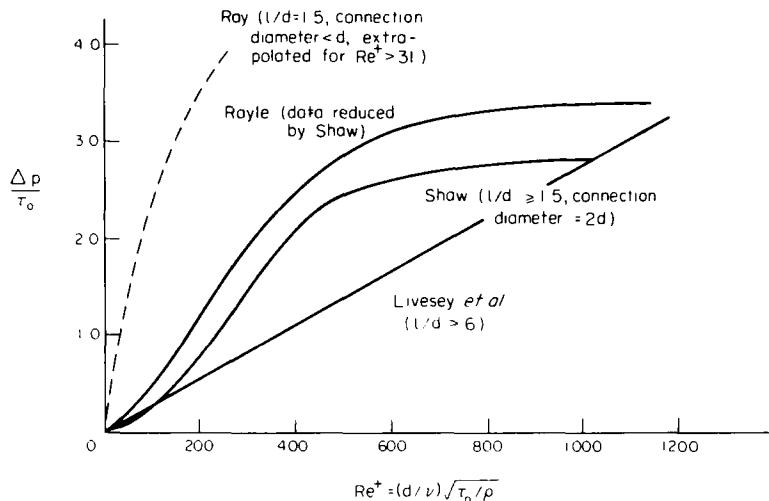


FIG. 55. Comparison of wall piezometer errors for incompressible flow reported by several investigators.

Livesey *et al.*; but overtakes them for $Re^* \geq 1000$, since it does not seem to tend to any asymptotic value.

It is not an easy matter to carry out a comparative study of all the above-reported results, since some of them do not contain the necessary information for a comparison to be made. For example, though the error curve reported by Rayle for the incompressible case looks similar to those given by Shaw on similar plots, we do not know whether the l/d ratio of the orifice plugs used by Rayle to obtain this curve is in fact constant. Assuming this, then Rayle's observation that Δp increases as the distance between the test section and the nozzle decreases is rather noteworthy; as this shows the required tendency in the variation of Δp with respect to the local shear if turbulent flow can be maintained for all these locations of the test section. We shall return to this later.

The unconventional shape of Fuhrmann's curve may be due to inconsistencies in the l/d ratio of the orifices. It is very likely that the wall of the model remained constant throughout his investigation. He could not, therefore, keep this ratio at a fixed value; and we have seen from the work of other investigators that for thin static holes the influence of this ratio is very significant.

Though Allen and Hooper reported no systematic errors, actually their results checked mutually to only within 0.7% of the dynamic head, a not too insignificant amount when compared to errors reported by other investigators. Furthermore, their results seem to be complicated by secondary flow effects. They, in fact, observed a difference of 0.5% in the readings of two identical piezometers installed diametrically opposite each other. When the pipe was rotated around by 180° , the error between the corresponding positions was then reduced to 0.1%.

It is rather unfortunate when Myadzu has not

reported his results in the form of static pressure error variation with respect to the l/d ratio. His observation that this error becomes constant for $l/d > 2$ is in good agreement with Shaw's results. However, his observation of a linear increase in the error with hole diameter favours the results of Livesey *et al.*; and the independence of the error on flow velocity disagrees entirely with both the data of Shaw and Livesey *et al.*

The results of Rayle appeared to have been influenced by the results of Myadzu since he averaged his incompressible flow results to obtain a unique curve for Mach zero. Furthermore, he has not analysed his data in terms of the hole Reynolds number even though his measurements would enable him to carry out such an analysis. We have seen earlier that the trend of his data is consistent with that of later investigators. Shaw had reduced part of Rayle's data to the form required by dimensional analysis (for the case when the static holes were located 27 diameters downstream of the nozzle). The form of the graph is similar to that of Shaw for deep static holes but gives higher error. In obtaining this curve, Shaw has assumed that fully developed turbulent flow has been attained. However, if the flow were not yet fully developed, which is more likely for the short entrance length, then the wall shear would be higher and better agreement would ensue.

Starting with Ray, the experimental results were correlated on the basis derived from dimensional analysis. The results of Ray are in broad agreement with other investigations, and his observation that negative error can be recorded if l/d is very small and the enlargement behind the orifice considerable has since been substantiated by Livesey *et al.* However, the manner in which Ray's curve tends to zero as the Reynolds number tends to zero is in complete disagreement with the data of Rayle, Shaw and Livesey *et al.*

Both the results of Shaw and Livesey *et al.* for deep static holes show that the error is positive and increases with hole Reynolds number. However, they differ in finer details as can be seen from Fig. 55. Livesey *et al.* attributed the difference to the different extrapolation techniques used. However, the present author has reduced the deep static hole data of Livesey *et al.* using Shaw's procedure and found the error curve to be identical to that reported by the authors. Thus, the only logical conclusion is that the wall fitting has a noticeable influence on the behaviour of the static hole.

No detailed investigation has been reported on the effect of the last dimensionless group in the functional notation of eqn. (58). Ower⁽⁹⁴⁾ suggested that the size of the static holes is not of great importance, provided that they are not too large; a maximum diameter of about 1.3 mm in a 9.5 mm pipe (i.e. $D/d = 7.5$) has been quoted. Shaw recommended slightly smaller static holes having $D/d = 10$.

(b) *Orifice configuration.* The results of Shaw show that the maximum static pressure error is about 2.75% of the dynamic head (based on errors for deep static holes and a maximum possible c_f of 0.01 in turbulent flow). For practical cases, the hole Reynolds number can be kept at a minimum by keeping d small so that the actual error is much smaller than this value. In addition, the error can be reduced by using small l/d ratios. The results of Livesey *et al.* indicate that for certain l/d ratios, the error incurred is rather insignificant. These results, however, have been obtained for the perfect static hole, i.e. one having square-edged orifices drilled perpendicularly to the plane of tangency of the flow surface, free from burrs and small compared to the radius of curvature of the surface. Since the construction of static holes involves the drilling of very small holes for which burrs are not uncommon especially in careless or unskilled hands, it is important to know, therefore, the effect of burrs or other equivalent edge imperfections on the static hole error. This information has also been provided by Shaw for deep static holes (having $l/d = 4$) over a range of hole Reynolds numbers up to 300. Results indicate that the error due to a drill burr projecting into the main stream at the downstream edge is approximately equal to the error due to hole size for a burr height, h , of 0.01 mm (i.e. for $h/d = 1/127$), and is approximately seven times the error due to hole size for a burr height of 0.05 mm (i.e. for $h/d = 1/31.7$).

The large error due to burrs naturally lead to investigations on various forms which enable the burrs to be removed. The first of such investigations was conducted by Allen and Hooper, who reported that a slight curvature on the hole edge (having radius of curvature about $\frac{1}{2}d$) does not affect the static hole reading, while a large curvature gives positive error. Later, Rayle experimented with a large variety of edge forms for

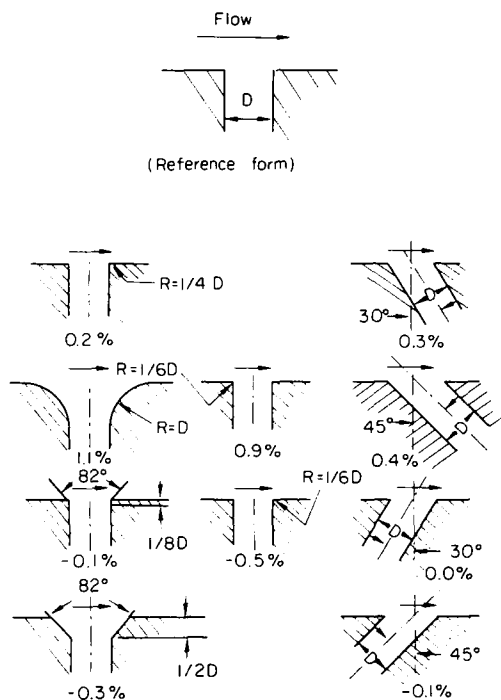


FIG. 56. Effect of orifice configuration on static pressure measurements: error shown as percentage of dynamic pressure.

the 0.81 mm and 1.17 mm diameter orifices. Results of these tests are shown in Fig. 56, which gives the difference between the static pressure measured by each orifice configuration and that of a sharp-edged one of the same diameter and drilled perpendicular to the test section.

Up to this point, we have considered static holes of circular shape. The influence of elongation of the orifice on the static pressure reading has been investigated at the Douglas Aircraft Company. Results from tests at supersonic speeds, shown in Fig. 57, indicate that the errors are Mach number dependent. The dynamic head errors are generally within $\pm 1\%$ of that obtained from a static probe having eighteen equally spaced circumferential orifices.

(c) *Conclusions.* The main conclusions drawn from the above-mentioned investigations are as follows:

- (i) For deep square-edged holes, the depth of the hole is unimportant. However, the critical l/d ratio for defining deep static holes seems to be influenced by the type of wall fitting used.
- (ii) Deep static holes always register a pressure greater than the true static pressure, i.e. they have positive errors.
- (iii) For shallow static holes, the error depends on both the hole depth and the dimension of the space behind the hole. The error decreases as the hole depth is decreased. Evidence indicates that this hole depth effect is reduced as the expansion ratio is increased and for holes having a contraction

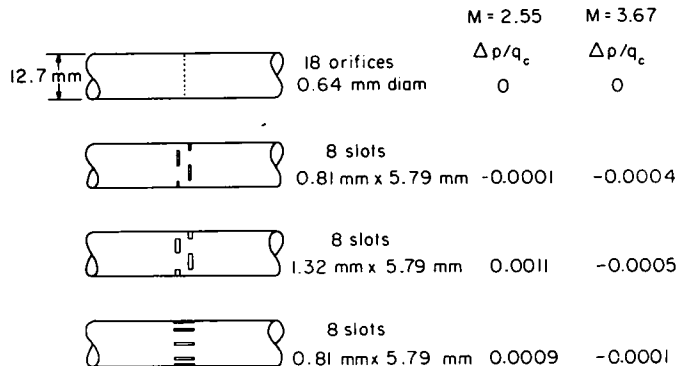


FIG. 57. Effect of elongation of orifices on static pressure measurements at supersonic speeds.

the hole depth effect is in the opposite direction.

- (iv) For shallow static holes having large cavity behind the orifice the error can become negative above a certain hole Reynolds number.
- (v) Burrs cause large errors in the static pressure readings. Their effect obviously depends on their shape and position around the hole. For burrs at the downstream edge of the hole the error is positive.
- (vi) Evidence indicates that specks of dirt collected at the edge of the hole have a similar effect on the static pressure reading as that of burrs.
- (vii) The effect of the edge shape of the hole is important and it has been found that holes with radiused edge have positive errors, while holes with chamfered edge have negative errors of smaller absolute magnitude than their radiused counterpart.

2.3. The Static Tube

The static tube consists essentially of a cylindrical tube placed parallel to the flow and having static pressure orifices located on its body. A variety of nose configurations have come into use; in fact, this is of much wider selection than the impact tube. This is because many of these configurations have been proposed to overcome the effects of compressibility in the transonic region.

As for the case of the impact tube, a large number of factors have been found to influence the readings of the static tube. These are discussed below.

2.3.1. Reynolds number effect

Schulze *et al.*⁽¹²⁰⁾ carried out tests on static tubes of diameters 1.52 mm, 3.18 mm and 6.35 mm over a Reynolds number range (based on the probe diameter) of 3000 to 53,000 and orifice depth to orifice diameter ratio from 0.04 to 0.33. Their results show no appreciable change in the static pressure indication. However, the viscous effect at lower Reynolds numbers is yet unknown, and evidence at high speeds indicates that this is by no means negligible.

In hypersonic flow, Lees⁽⁷²⁾ has indicated that the deceleration of the gas as it penetrates the viscous layer over a solid surface generates high temperatures in this region. As a result, the hypersonic laminar boundary layer can be 10 to 100 times thicker than the incompressible one at the same Reynolds number. Thus, at high speeds, even small changes in the flow direction result in large pressure changes. Corrections due to pressure changes induced by the boundary layer growth is therefore necessary for any body used as a static pressure probe. The geometry of the nose configuration used most often for static pressure measurements in high speed flows is conical in shape. Two variations of this probe have been used. The form known as the cone-cylinder has the static orifices situated on the body of the probe some distance aft of the base of the conical head. The other has static orifices located on the conical nose of the probe. In this form, the probe has an analytical advantage over the former configuration because the pressure distribution at the orifice can be related theoretically to the free stream static pressure. This will be referred to as the static cone.

The effect of viscosity on the cone-cylinder has been reported by Wilson⁽¹³⁶⁾ and Matthews.⁽⁸⁷⁾ The configuration investigated by Wilson had an apex angle of 15° with static holes some 13 tube diameters aft of the conical base. At Mach 4.13, 4.67 and 6.39, the probe diameter and static hole diameter have no effect on the static pressure readings for $Re_D > 3500$. There appeared to be a trend, however, for the static pressure to increase at Reynolds numbers below this value.

Matthews had investigated the viscous effect on three nose angles (5°, 10° and 20°) at a nominal Mach number of 5.8 and Reynolds number of 7600/mm or 16,000 based on the probe diameter and free stream conditions. The results are shown in Fig. 58, which reveals that the apex angle has a strong influence on the position at which correct static pressure can be read and that the static pressures measured tend to an asymptotic value of about 7.5% above the free stream value at a distance of 45 tube diameters behind the base of the cone.

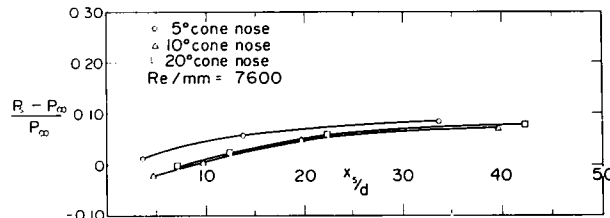


FIG. 58. Pressure distribution along body of conical static tubes for various apex angles.

For the static cone configuration, it has been found that the static pressures measured begins to depart from values predicted by the Taylor-Maccoll theory⁽¹²⁸⁾ at relatively high Reynolds numbers ($Re_D \approx 10^4$), due to the fact that boundary-layer growth increases the effective cone angle rather rapidly.

Talbot⁽¹²⁶⁾ first investigated the effect of viscosity on static cones of the form shown in Fig. 59 in rarefied gas streams over a Mach number range of

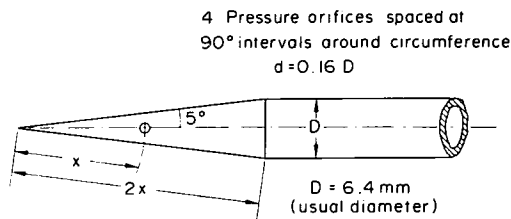


FIG. 59. Geometry of static cones in common use.

$3.69 < M < 4.13$ and a Reynolds number range of $36 < Re/\text{mm} < 138$. His data indicated that the viscous effect increases linearly with increasing orifice diameter and also increases almost as $1/\sqrt{Re_x}$, where x is the distance from the vertex to the pressure tap. Thus, in general, the static pressure coefficient for the static cone is of the form

$$C_p = \frac{p_2 - p_{2,\text{ideal}}}{p_{2,\text{ideal}}} = \frac{f(M, \theta)}{\sqrt{Re_x}} \quad (61)$$

where p_2 represents the static pressure on the surface of the cone and θ the semi-vertex angle.

The pressure correction data reported by several investigators for geometrically similar static cones have been correlated by Enkenhus on the basis of eqn. (61). His results are shown in Fig. 60.

2.3.2. Effect of nose

The magnitude of the pressure sensed at the static holes of a static tube in a steady, locally uniform stream is a function of the shape of the nose and the distance from the nose to the plane of the static holes. This can be easily seen from the theoretical pressure distributions on two axisymmetric bodies shown in Fig. 61. It is obvious that close to the nose, the pressure is strongly influenced; however, with increasing distance, the pressure returns to the free-stream value. This return is seen to occur further downstream for the supersonic probe. These theoretical trends have been

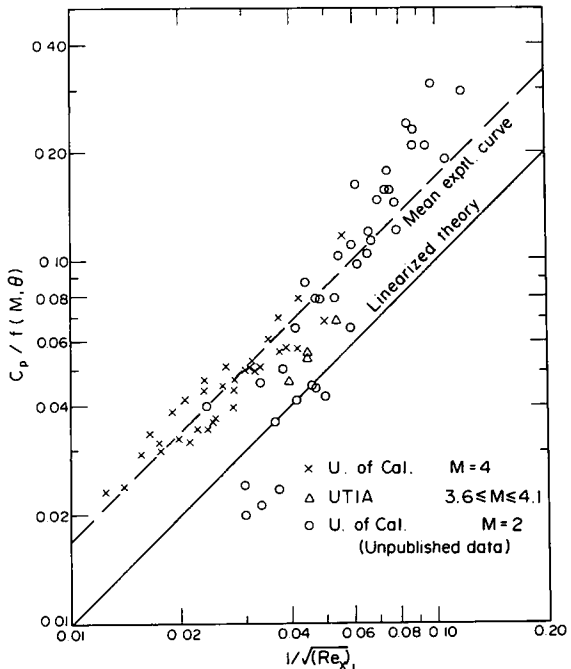


FIG. 60. Pressure coefficient for geometrically similar static cones.

confirmed experimentally: Lock *et al.*⁽⁸¹⁾ reported that subsonic tests at Mach 0.3 to 0.95 for tubes having hemispherical, orgival and truncated orgival noses showed that when the orifices were located 6 or more tube diameters behind the end of the nose section, the static pressure errors of the three tubes were in close agreement. Likewise, Holder *et al.*⁽⁵⁴⁾ reported that supersonic tests at Mach 1.61 for tubes having square-ended, hemispherical, 30° conical, short and long orgival noses showed that for orifice locations at least 10 tube diameters rearward of the nose section, the measured pressure were substantially independent of the shape of the nose. However, later evidence indicates that the location of the static holes varies with Mach number: Hahn⁽⁴⁵⁾ has reported that for the square-ended tube, 28 times the tube diameter is needed at Mach 2 and 22 times at Mach 2.5 and 3.0. Because of this Mach number dependence, improved supersonic designs having static pressure taps situated on the slant surface of the cone or wedge have come into use. In this respect, the cone is better disposed for static pressure measurements since its readings can be related to the true free stream value by theoretical means.

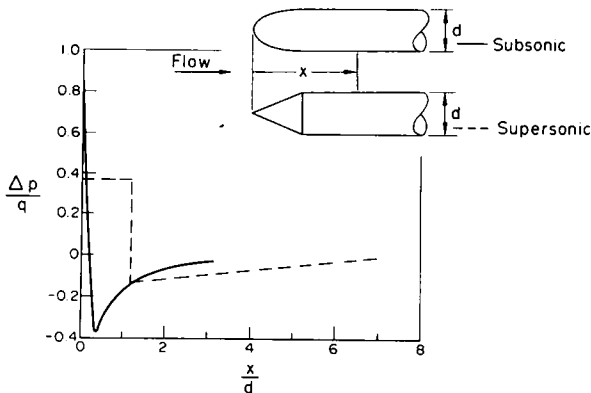


FIG. 61. Theoretical pressure distributions along cylindrical bodies with axisymmetric noses.

2.3.3. Effect of stem and collar

A static tube must necessarily have a support either in the form of a stem or an expansion collar to accommodate the stem. The stem can either join perpendicularly to the head tube or as a continuation of the head tube bent through 90° with a reasonable radius. Merriam and Spaulding⁽⁸⁸⁾ had found that the influence on the static pressure due to the stem in incompressible flow is independent of the type of bend connection for ratios of $x/D > 4$, where x is the distance between the stem and the static pressure holes and D the diameter of the stem.

The presence of the stem causes a positive error in the static pressure readings at orifices ahead of the stem (blocking effect). This error decreases rapidly with increase in distance from the stem. However, for orifices situated not directly in front of the stem, no theoretical prediction is at hand. The experimental results reported by Hubbard,⁽⁵⁷⁾ shown in Fig. 62, will be useful. These results were obtained for the stem effect on a single orifice. The

static tube was situated at the centre of a 300 mm-diameter pipe. The orifice was placed far enough from the nose of the static tube such that the error caused by the nose is small. Lock *et al.*⁽⁸¹⁾ had investigated the effects at subsonic speeds of a streamlined stem on the static pressure readings. Their results, given in Fig. 63, show that the static pressure error decreases with distance ahead of the

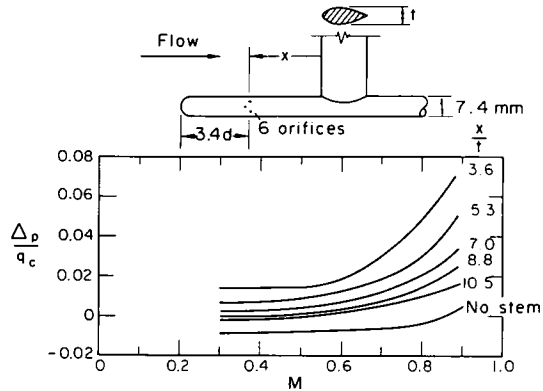


FIG. 63. Effect of stem on the static pressure measured by 6 circumferential orifices on a static tube at zero yaw.

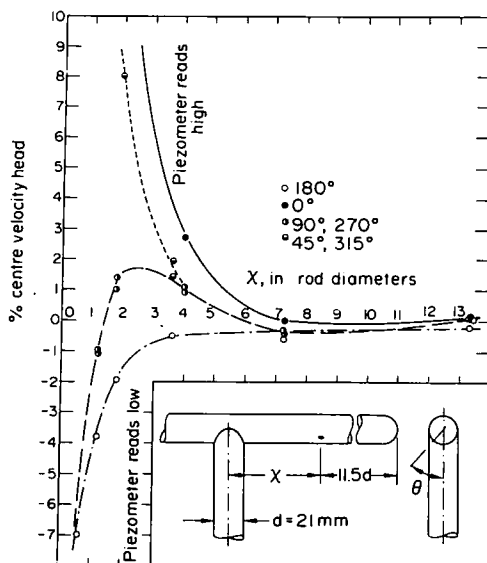


FIG. 62. Effect of stem on the static pressure read by an orifice on a static tube: showing static pressure variation as a function of orifice position.

stem. For a fixed location, the error remains substantially constant below Mach 0.5 and increases rapidly with Mach number above this critical value. For orifices located about 10 stem diameters ahead of the stem, the static pressure error will be within $\frac{1}{2}\%$ of the dynamic pressure for Mach numbers up to 0.7. However, the results were obtained with substantial nose effect as the static taps were situated only 3.4 tube diameters behind the nose. The stem effect on the measured static pressure of a static tube at supersonic speeds had also been investigated. Holder *et al.*⁽⁵⁴⁾ reported that the stem should be situated at least 13 tube diameters downstream for all the probes they had tested for the nose effect; except the square-ended one, for which 6 or 7 diameters are sufficient.

The fact that the error caused by the stem is positive is often made use of in static tube designs to compensate for the negative error due to the nose of the probe.

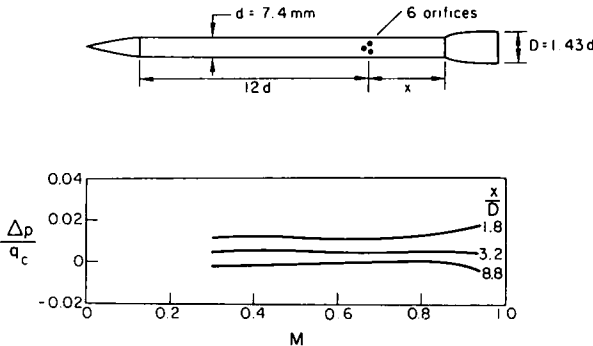


FIG. 64. Effect of collar on the static pressure measured by six circumferential orifices on a static tube at zero yaw.

The blockage effect of collars has been investigated at subsonic speeds. The results of Lock *et al.*, shown in Fig. 64, indicate that the static pressure error decreases with increase in distance of the collar from the orifice and that for $x/d > 3.2$ the variation of the static pressure error with Mach number is negligible up to Mach 0.95 at zero yaw. The test data were obtained for a collar to tube diameter ratio of 1.43, for greater ratios, the blocking effect of the collar is expected to be greater. In this series of tests, the distance of the orifices from the nose section (12 tube diameters) was chosen such that the error caused by the nose is essentially zero.

2.3.4. Effect of orifice size

The orifice geometry for a round static tube is rather rigid. The thinness of the wall does not permit other forms of construction except that of square-edged holes drilled normal to the wall. Thus, demands on workmanship and edge finish are high.

A detailed discussion of the effect of orifice size on the static pressure reading has been given in Section 2.2.2 in connection with the wall piezometer. As has been pointed out earlier, no clear-cut separation of the above results into wall piezometer and static tube applications is possible. Of all the investigations reported therein, it seems that the results of Fuhrmann and Rayle are of more direct application to the static tube, though the cavity of a static tube may not be as large as that used by Fuhrmann and the l/d ratio much smaller than that used by Rayle. It is expected that the error would be small for a static tube due to its much smaller l/d ratio, and evidence indicates that negative errors may also arise. The absolute magnitude of the static orifices seems not of great importance provided the D/d ratio is not too small to invalidate the above results—a value of about 10 is suitable.

In addition, experiments directly performed on the static tube have been reported by Bäuerle⁽⁶⁾ and Schulze *et al.*⁽¹²⁰⁾ Bäuerle studied the effect of orifice size on static pressure indication in tests of long cylindrical probes 10 to 40 mm in diameter. He concluded that the ratio of orifice depth to orifice diameter can be varied from approximately 0.1 to 4

and the ratio of orifice to probe diameters from approximately 0.01 to 0.5 without significantly affecting the static pressure measured. However, the Reynolds number range has not been reported. Schulze *et al.* studied probes of diameters 1.52, 3.18 and 6.35 mm over a Reynolds number range (based on probe diameter) of 3000 to 53,000. The ratio of orifice depth to orifice diameter was varied from 0.5 to 1.67 and the ratio of orifice to probe diameters from 0.04 to 0.33 without an appreciable change in static pressure indication.

In the application of the static tube to static pressure measurements in rarefied streams, the orifice effect reported by Potter *et al.*⁽¹⁰³⁾ has been found to influence the pressure readings also. As a check on the semi-empirical theory described in Section 1.8.6, static pressure measurements were made in the low-density, hypersonic AEDC-VKF tunnel L by means of water-cooled sharp-edged flat plate (knife-edge) and sharp-nosed static cone of 15° half-angle at a free stream Mach number of 10.15 and a total temperature of 3120 K. The gas medium used was nitrogen. The ratio of the indicated pressure to the pressure on the surface outside the orifice has been plotted against the inverse Knudsen number as shown in Fig. 65. Good agreement between theory and experiment is evident. The measured static pressure increased by roughly 30% over the range of orifice sizes investigated. Much larger orifices are found necessary to avoid the orifice effect caused by heat transfer. In this connection, Talbot⁽¹²⁶⁾ has discussed a phenomenon whereby an orifice of too large a diameter causes the static pressure to be in error because of mixing (and hence momentum transfer) between the moving stream and the orifice fluid. It is possible that both effects may be present simultaneously so that avoiding the "small-orifice" effect by using very large orifices can lead to equally undesirable results. It seems, therefore, that an optimum orifice size to minimize the total error must be sought for low density static-pressure measurements.

2.3.5. Effect of yaw and pitch

The static tube is much more sensitive to angular

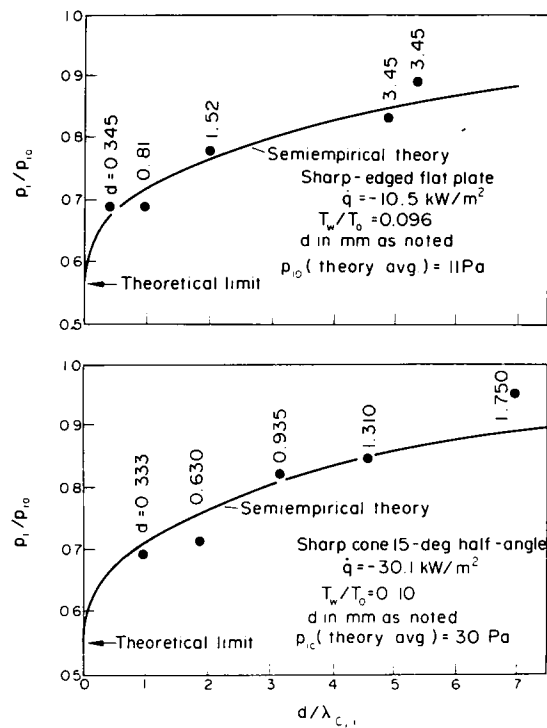


FIG. 65. Effect of orifice size on static pressure measured in low-density flows (nitrogen at $M_1 = 10.15$, $T_0 = 3120^\circ\text{K}$ and $Re_1 = 388/\text{cm}$).

deviations than the impact tube. This is probably due to the static-pressure distribution that is created on the misaligned cylindrical body of the probe by the flow component normal to the tube. As the static-pressure error is positive on the bottom, negative on the top and zero at circumferential positions about 30° from the stagnation point, it would appear that insensitivity to inclination of the static tube to flow direction might be accomplished either by locating orifices at circumferential positions of about $\pm 30^\circ$ or by placing the orifices along the top and bottom of the tube so that a compensational effect can be achieved. The first procedure can only be used if the flow direction is known beforehand. The second procedure in providing six or more static pressure orifices evenly spaced around the circumference of the static tube, however, does not provide a perfect compensation. Typical yaw characteristics for the Prandtl tube, a 10° cone and a 8° wedge have been reported by Krause and Gettelman.⁽⁶⁸⁾ These are shown in Fig. 66. As for the impact tube, the yaw characteristics depend on the nose shape of the probe. Of these three, the wedge is least sensitive to misalignment in its plane of symmetry. In all the three probes tested, there are only two static orifices at 180° apart. Mach number characteristics of these three probes at zero yaw are shown in Fig. 67. A substan-

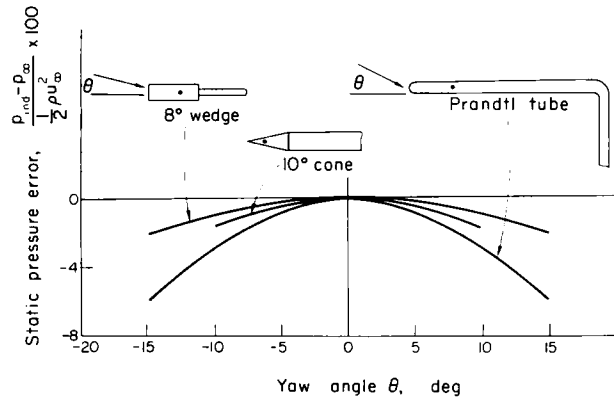


FIG. 66. Yaw characteristics of various static tubes at low speeds: all probes have only two static holes at 180° apart.

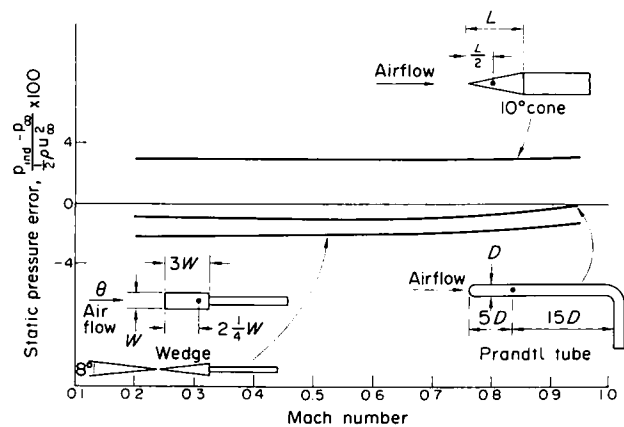


FIG. 67. Effect of compressibility on the static pressure measured by the three static tubes shown in Fig. 66 at zero yaw.

tial nose influence can be observed on the Prandtl probe.

Walchner⁽¹³⁴⁾ had investigated the effect of compressibility on the yaw characteristics in greater detail for the Prandtl probe at subsonic speeds. His results have been reported in Bryer and Pankhurst. The dependence of the yaw characteristics on the free stream Mach number has been found to persist into supersonic flows as well. However, these curves are of little practical importance because they behave somewhat erratically. In spite of this, Cooper and Webster⁽¹⁸⁾ had found that in supersonic flow the average static pressure registered by a static cone having four static orifices 90° apart corresponds closely to the static pressure of the same cone at zero angle of attack up to yaw and pitch angles of 10°. In addition, a class of static cone-cylinders having good incidence characteristics at supersonic speeds has also been reported.⁽²²⁾

2.3.6. Mach number effect

The static pressure characteristics of a probe with respect to the free-stream Mach number depends on its design. Typical Mach number characteristics for various probes at zero yaw are shown in Fig. 67. It is seen that the Mach number influence becomes felt only at rather high subsonic Mach numbers. Beyond this point, the recorded pressure rises sharply, due to the formation of local shock waves on the body of the probe. Though calibration results may continue to show a unique curve for each yaw angle, the readings may become erratic in actual operating conditions due to the possibility of larger disturbances in these situations than during calibration runs. The reading can vary by as much as 10% with slight changes in flow conditions or proximity to solid boundaries.

At supersonic speeds, a bow shock forms ahead of the tube. This allows the use of normal shock relations to predict the static pressure in front of the shock if that immediately behind the shock is measured. However, the static pressure immediately after the shock is not easily measurable; and we resort to measuring the static pressure further downstream of the shock by taking advantage of its localized character. Holder *et al.*⁽⁵⁴⁾ had reported that the effect of the shock on the static pressure reading becomes negligible when the static holes are some 10 tube diameters behind the nose.

At transonic speeds, the effect of Mach number can be delayed to close to or even past Mach one by using probes having a prolonged taper consisting of a 3° cone. Test results of two such 3° static cones have been reported in Bryer and Pankhurst. Such probes are necessarily long and hence not rigid enough if the probe size is small. Reduction in probe length can be secured by placing the static orifices at positions where the true free stream static pressure occurs. One such short head probe had been developed by Hess *et al.*⁽⁵³⁾ Its calibration is independent of Mach number over the range

$0.1 < M < 3.4$. These probes are, however, sensitive to misalignment.

Recently, a new short static probe design having good incidence characteristics at supersonic speeds has been reported by Donaldson and Richardson.⁽²²⁾ This is based on a theoretical study on supersonic flow about cone-cylinders at zero incidence, carried out by Clippinger and Giese,⁽¹⁵⁾ which shows that the surface pressure at a point 0.88 diameters aft of the base of a cone having 50° apex angle is approximately independent of Mach number for the range $1.4 < M < 5.0$, at 0.8 times the true static pressure. Two probes of the same external appearance but having different internal geometry were tested in wind tunnels at supersonic speeds between Mach numbers of 1.1 and 2.5. Detail specifications of these probes are given in Fig. 68. Test results

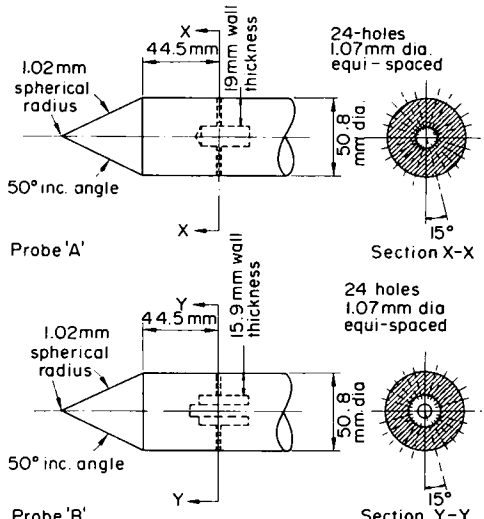


FIG. 68. Details of two versions of cone-cylinder short static tubes.

indicate that at zero incidence the probes measure a pressure within 0.95% of 0.793 times the true static pressure. Furthermore, up to almost 18° in any pitch plane in a uniform stream, the pressure difference with the zero incidence value for probe A is within -5% of the true static pressure and for probe B within -9%, showing that the internal geometry can have significant influence on the incidence characteristics of the probe. Using a mean value of 0.763 times the true static pressure allows these results to be correlated to within ±3% for the same pitch range.

2.3.7. Effect of turbulence

The analysis of Goldstein⁽³⁹⁾ mentioned earlier in relation to the pitot tube indicate that the static tube would read a pressure equal to

$$p_m = p + k\rho(\bar{v}^2 + \bar{w}^2). \quad (62)$$

On the basis of isotropic turbulence, certain theoretical arguments indicate that k might be

expected to have the value $\frac{1}{4}$, so that

$$p_m = p + \frac{1}{4}\rho\bar{q}^2. \quad (63)$$

Flow in pipes does not exhibit isotropic turbulence, Fage⁽³⁰⁾ calculated on the basis of turbulence measurements that

$$p_m = p + \frac{1}{4}\rho(\bar{v}^2 + \bar{w}^2). \quad (64)$$

However, it has been pointed out by Bradshaw and Goodman⁽⁹⁾ that Fage's result could be equally well explained by supposing that his static tube read $p + 0.003 \times \frac{1}{2}\rho U^2$ whether or not the flow is turbulent. In this respect, Fage did not calibrate his probe in non-turbulent flow, but similar hemispherical-nosed pitot-static tubes tested by Salter *et al.*⁽¹¹⁹⁾ had pressure coefficients of the order of 0.003.

Investigation on a turbulent wake gives

$$p_s = p + \frac{1}{2}\rho\bar{q}^2 \quad (65)$$

where p_s is the static pressure in the undisturbed flow and p the static pressure at any point in the wake.

It should be noted that the last equation expresses the variation of the static pressure between the undisturbed stream and a turbulent wake whereas the earlier equations relate the measured static pressure to that of the turbulent flow.

Assuming isotropic turbulence, classical analysis shows that the error given by $(p_s - p)/\frac{1}{2}\rho U^2$ is about 2% for a turbulence intensity of 14%. The corresponding error in the velocity measurement is 1%.

Another type of analysis of the turbulent error of the static openings were presented by Kronauer and Grant.⁽⁶⁹⁾ They took into consideration errors due to asymmetry in internal passages of a probe, compressibility effects resulting in higher density during inflow, and turbulent flow in the piezometer opening. Having cited other works in which the first two effects were found to be small, they then proceeded to concentrate on the effect of asymmetrical fluctuations coupled with turbulent flow internally. Their conclusion was that the error depends not only on the magnitude of the fluctuations, but also on the frequency of the pressure changes compared to a typical probe frequency. No error exists if the fluctuation frequency is much higher than the typical probe frequency, but this condition is not met for many conventional pitot-static and certain cylindrical pitot probes. However, simple modifications can satisfy this condition. Inasmuch as the non-linear effects are due to the existence of turbulent flow internally, there is also a critical amplitude of pressure fluctuation below which no error is introduced. When error does exist, it can be either positive or negative, and as much as 15% of the amplitude of the pressure fluctuation which introduces the non-linearity.

A third type of analysis has been proposed by considering turbulence as a statistical assemblage

of a vast number of eddies of various sizes. Barat⁽⁴⁾ pointed out that when thus conceived, turbulence effects depend not only on the turbulence intensity but also on the geometrical scale of the turbulence, i.e. on the sizes of the component eddies. When the size of a typical eddy is small compared with the diameter of the static tube, the pressure fluctuations at the orifices are not correlated and the tube does read high, as Goldstein's theory has indicated. Toomre⁽¹³²⁾ presented a more detailed analysis of this effect and showed that the error can either be positive or negative. The sign of the error depends on the "typical eddy size" of the turbulence in comparison with probe radius, being positive for small scale turbulence in which the fluctuations at the various holes are not in phase; and negative for large scale turbulence in which the pressure fluctuations at the orifices become increasingly correlated. This correlation results in some form of misalignment in the normal flow around the tube and manifests itself as a tendency to read low by an amount corresponding to certain average value of the angle of misalignment. Toomre further showed that the error in the limit of very large eddy scale is equal in magnitude but opposite in sign to that for very small eddies, and appears to be zero for eddies equal to or slightly greater than the tube radius. Thus, the magnitude of the turbulence error varies between the following limits:

$$-\frac{1}{2}\rho(\bar{v}^2 + \bar{w}^2) < p_m < \frac{1}{2}\rho(\bar{v}^2 + \bar{w}^2). \quad (66)$$

It is therefore seen that the maximum error given by Toomre is twice that given by Goldstein. However, the way in which the error varies with scale between the two limits has not been established.

An experimental investigation on the effect of turbulence on the readings of static tubes has been reported by Bradshaw and Goodman.⁽⁹⁾ Their study was made in the centre-line of a circular jet and confirmed the suggestion of Barat and Toomre that the error depends on the ratio of the size of the tube to the size of typical eddies, reading low when this ratio is small and high when large. They further found that in the range of tube sizes likely to be used in turbulent shear flows, the measured pressure is closer to the true static pressure than to either of the theoretical limits for very large or very small tubes; and suggested that the best course in the present state of the art is to omit any corrections due to turbulence.

2.3.8. Effect of cavitation

When the local pressure in the vicinity of a body submerged in a flowing liquid is reduced sufficiently, cavitation occurs with resulting changes in pressure distribution about downstream portions of the body. For pitot tubes of normal shape, no changes in impact head occurs; but if a pitot-static tube is used, the static pressure may change appreciably. Typical results for a tube with

a hemispherical nose have been reported by Rouse and McNoun.⁽¹¹⁸⁾ These are shown in Fig. 69.

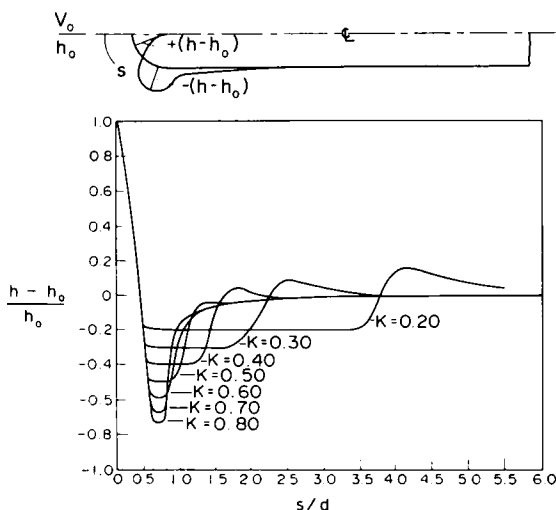


FIG. 69. Effect of cavitation on the pressure distribution over a cylindrical body with a hemispherical nose.

2.3.9. Effect of velocity gradient

A velocity gradient in the flow field gives rise to a gradient in the total pressure. The fluid stagnating at the leading edge of the probe will therefore be subjected to a pressure gradient, which increases towards the region of higher velocity. Thus, a slight downwash is created in the vicinity of the probe. The effect of this downwash on the static pressure is probably similar to a slight pitch or yaw, which is rather negligible.

In boundary layer measurements where the proximity of the wall will constrain the downwash, the effect on the probe reading is expected to be even smaller. In this connection, unpublished results of N. E. Sweeting, reported in reference 94, obtained with a small static tube 1.9 mm diameter indicate a complete absence of any systematic variations (as compared with the static pressure recorded at a hole in the surface of a flat plate) when the tube was at a number of distances from this plate, including one reading with the tube resting on the plate.

2.3.10. Effect of blockage and interference

Though the results of Sweeting discussed in the previous section indicate that the static pressure is not affected by its proximity to a wall when the flow area is large, it is, however, sensitive to the presence of flow boundaries in more confined situations, such as the "venturi effect" in pipe flow discussed in Section 2.2.1.

In open jet flows, Krause⁽⁶⁷⁾ has noted that the static probe reads low in an open jet of limited diameter as compared to an infinite stream. He further reported that for correct static pressure measurements the centre-line distance between static tubes used in a rake should be greater than 6 tube diameters for $M < 0.6$. Greater separation is necessary for $M > 0.6$.

2.4. Disc Static Probes

Disc static probes are generally of two types, having a sharp or rounded edge. The main feature of the sharp-edge disc consists of a disc of the form of a truncated cone with slant surface inclined at 10° to its base. The base diameter is some four times that of the top, which is of the same size as the stem. The results of Shaw described in Section 2.2.2 can be applied to the design as well as error correction for this type of static probe. It is rather sensitive to misalignment. Because of this, large sharp-edge discs are hardly used in single phase fluid measurements any more. However, owing to the easiness with which it can be scaled up to provide a large hole dimension, overall disc diameter up to 50 mm has been reported in use, it is useful in two-phase flow measurements since this alleviates the problem of blockage. Enkenhus⁽²⁹⁾ reported the use of a small sharp-edge disc, having diameter of 1.59 mm and hole diameter of 0.81 mm, as a free molecule static probe. In such applications, the disc has to be kept small so that the mean free path of the gas molecules should be of the same order as the disc diameter.

By rounding the edge of the disc and suitably arranging the static hole, the sensitivity of the disc static probe to angular misalignment can be greatly reduced. The features of this round-edge disc have been given in Bryer and Pankhurst, who also presented some calibration curves of this probe. Gilmer* has reported that the use of a spherical depression at the pressure tap would compensate for the streamline curvature induced by the leading edge of the disc so that the pressure reading of the probe is now within 1% of the true value over a wide Mach number range. Characteristics showing the variation of the inherent error of round-edge disc probes with and without depression with Mach number are given in Fig. 70.

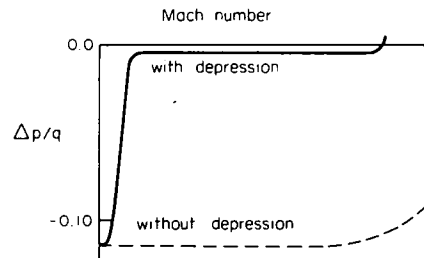


FIG. 70. Mach number characteristics for static discs.

Though the instrument tested by Bryer *et al.*⁽¹⁰⁾ is very small in size, as it is intended for use in three-dimensional flow measurements, there seems to be no reason why this cannot be scaled up to an overall dimension comparable to that reported for

*Private communication to R. P. Benedict, reported in the latter's book entitled *Fundamentals of Temperature, Pressure, and Flow Measurements*, Wiley, 1969.

the sharp-edge disc used for two-phase flow measurements. However, independent calibration in the Reynolds number range of interest is now advisable.

The effect of turbulence on the disc static probe is not known with certainty. Discussions in Section 2.3.7 indicate that the error is rather negligible unless its dimension is much larger than conventional static tubes. However, a highly turbulent stream can cause a disc static probe to flutter on its stem thus obviating its further usefulness.*

2.5. Static Pressure Cantilever Probes

2.5.1. The static cylinder

It is well known from potential flow theory that for an infinite cylinder in a cross stream, there are two points on its circumference symmetrically located with respect to the stagnation point, at which the pressure is equal to the static pressure in the free stream. We have seen earlier that for a cylinder closed at one end the effect of the closed end becomes negligible when the pressure orifices are placed some distance from it. Hence, the static pressure cantilever probe is essentially a long cylinder with two holes on the circumference separated by a critical angular distance on a diametral plane located several tube diameters below the tip. By having two static holes instead of one, it allows the true static pressure to be obtained by averaging these two readings as long as both are operating on the linear portions of the pressure distribution curve. Furthermore, this also helps in probe alignment.

In ideal flow theory, the location of the static holes are uniquely determined. However, for real fluids the location of the critical angle, i.e. the angle between the stagnation and the static points on the circumference of the cylinder, varies with both the Reynolds and the Mach numbers. In order to minimize this source of error, Glaser⁽³⁵⁾ suggested that use be made of a range of Reynolds numbers in which the rate of variation of pressure distribution with flow velocity is minimum. One such range is between Reynolds numbers of 5000 and 50,000 for incompressible or low Mach number flows, which also provides reasonable probe sizes.

In addition, the hole size seems to have an effect on the pressure distribution, as evidenced by the diversity of values of critical angles reported in the literature. This effect has been investigated by Hemke⁽⁵²⁾ using a circular cylinder 25 mm in diameter spanning a 150 mm diameter open jet with air velocities ranging from 9 to 53 m/sec. Tests with orifices 0.2 to 6.4 mm in diameter showed that hole diameters must be kept below 1.5 mm for accurate pressure distribution measurements in the front portion of the cylinder. The pressures on the rear,

however, were independent of hole size. In addition, Thom⁽¹²⁹⁾ has shown that the pressure produced in a hole drilled in a cylinder is not the pressure at the centre of the hole, but at a point half way along the hole radius toward the front of the cylinder. Thus, the static holes should be located such that

$$\theta = \theta_0 + \frac{90d}{\pi D} \quad (67)$$

where θ = designed critical angle, θ_0 = critical angle in absence of static opening, d = hole diameter, D = outer diameter of cylinder.

Values of θ_0 can be obtained from Thom's report. Sample values are

$$\theta_0 = 34.2^\circ \text{ at } Re = 8.5 \times 10^3$$

$$\theta_0 = 34.3^\circ \text{ at } Re = 17 \times 10^4.$$

As the slope in the linear portion of the pressure distribution is about 0.05 per degree, it is therefore necessary to keep θ within 0.2° in order that the systematic error in the dynamic pressure be smaller than 1%.

When extreme accuracy is not required, carefully drilled holes from the surface of the cylinder to a common central canal would facilitate probe construction. However, care still need be taken to ensure symmetry of construction.

In addition, Winternitz⁽¹³⁷⁾ recommended that the ratio of orifice depth to diameter be within 0.5 to 1.7; and that the orifice to probe diameter ratio within 0.04 to 0.3. The higher limit of the latter ratio, in view of Hemke's results, seems too high and is best kept below 0.06.

The static cylinder has been found to be able to determine static pressures to a fair degree of accuracy in turbulent flow or flows of unknown direction when the variation of the angle of flow is below 45° .

Error due to pitch in the static pressure is less than 1% if the pitch angle is smaller than 5° ; and we can ensure a small pitch angle by orientating the probe about its plane such that the impact orifice shows a maximum reading.

On the other hand, the error due to compressibility can be quite pronounced; the indicated static pressure has been reported to vary by about 12% between Mach numbers ranging from 0.3 to 0.7. Further discussion on this effect has been given by Bryer and Pankhurst.

The influence of the axial pressure gradient along the probe, referred to in Bryer and Pankhurst, could possibly be alleviated by placing the pressure taps some five probe diameters away from the tip, as it has been found that at this position the stagnation pressure reading is essentially unaffected by secondary flows about the tip.⁽¹³⁷⁾

2.5.2. The static wedge

As can be seen from Fig. 71, the static wedge is superior to the static cylinder because the indicated static pressure is much less sensitive to hole loca-

*P. Bradshaw, private communication.

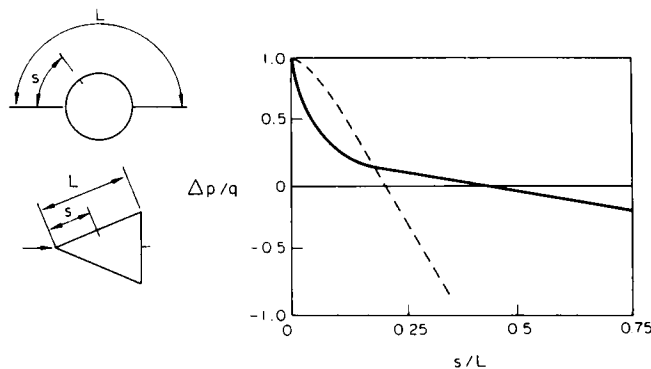


FIG. 71. Comparison of static pressure distributions for cross-flow over a cylinder and an unyawed wedge.

tion (the rate of variation for the wedge is about one-sixteenth that for the cylinder). This allows wider manufacturing tolerances and thus a lower cost for a given accuracy. Also evident from this figure is that the correct stream static pressure will be registered by the wedge at zero yaw if the pressure orifices are located 0.37 the length of the slant face from the leading edge. These orifices are to be drilled normal to the surface. No information is available at this moment with regard to the shift in the effective centre with hole size. Results obtained in connection with the cylinder are believed to be applicable.

Keast⁽⁶⁵⁾ reported that the static wedge is more yaw sensitive than the static cylinder. This is probably due to separation at the leading edge. However, the critical Mach number at which shocks first appear on the wedge is higher than for the cylinder. This is a function of the wedge angle: the smaller the angle the higher the critical Mach number. In addition, small wedge angles serve to reduce the hole spacing and hence velocity gradient errors. Even for the same hole spacing, errors due to velocity or total pressure gradient have been found to be much smaller for the wedge than the cylinder. Further discussions on this topic can be found in Bryer and Pankhurst.

2.6. The Knife Edge

Static pressure in supersonic flow has also been measured using the knife edge flat plate shown in Fig. 72a. The leading edge must be thin and sharp in order not to produce a detached shock wave, and the flat face accurately aligned with the flow. It is also important for the pressure sensing orifice to lie upstream of the Mach waves formed at the corners of the probe. This type of instrument does not greatly disturb the upstream flow, and is therefore useful for pressure explorations in the vicinity of shock waves. Misalignment errors are, however, serious; but they can be reduced by the use of two such probes, symmetrically disposed, as shown in Fig. 72b. A hollow cylindrical design can also be used instead.

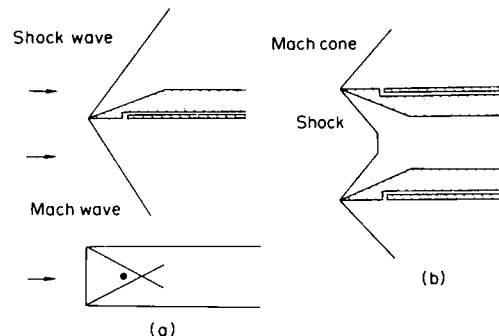


FIG. 72. The knife-edge: sharp-edged static probe for supersonic measurements.

One known effect to which this probe is subjected is the "small orifice" effect when used for measurements in rarefied gas streams. This can be corrected by means of the semi-empirical theory of Potter *et al.*⁽¹⁰³⁾ discussed earlier in Section 1.8.6. Good agreement between experimental and theoretical results can be seen in Fig. 65.

3. DYNAMIC PRESSURE MEASUREMENT

3.1. Introduction

The dynamic pressure at a point in a flow field is defined as the difference between the total and the static pressures at that point. For incompressible flow, this is identical to the kinetic or velocity pressure. In isentropic compressible flows, it is related to the Mach number of the flow. Thus, the measurement of dynamic pressure provides a means of calculating the velocity of the flow field at the point under consideration.

Three types of dynamic pressure probes have come into general use, viz. the pitot-static, conical and cantilever probes.

3.2. The Pitot-Static Tube

The use of separate pitot and static tubes can become cumbersome in practical situations for which only the dynamic measurement is required.

Fortunately, the mode of construction of these two probes permits them to be coupled together to form a compact coaxial combination. For this purpose, the effect of nose and stem on the static pressure measurement will govern the dimension of this combination probe. Generalized dimensions of some common pitot-static combinations are given in Fig. 73.

The error for the pitot-static combination are generally those occurring in both the separate impact and static tubes. For instances in which both these readings are affected simultaneously, the resulting error is given by the algebraic sum of the individual errors. For the sake of completeness, such combined errors are briefly summarized below.

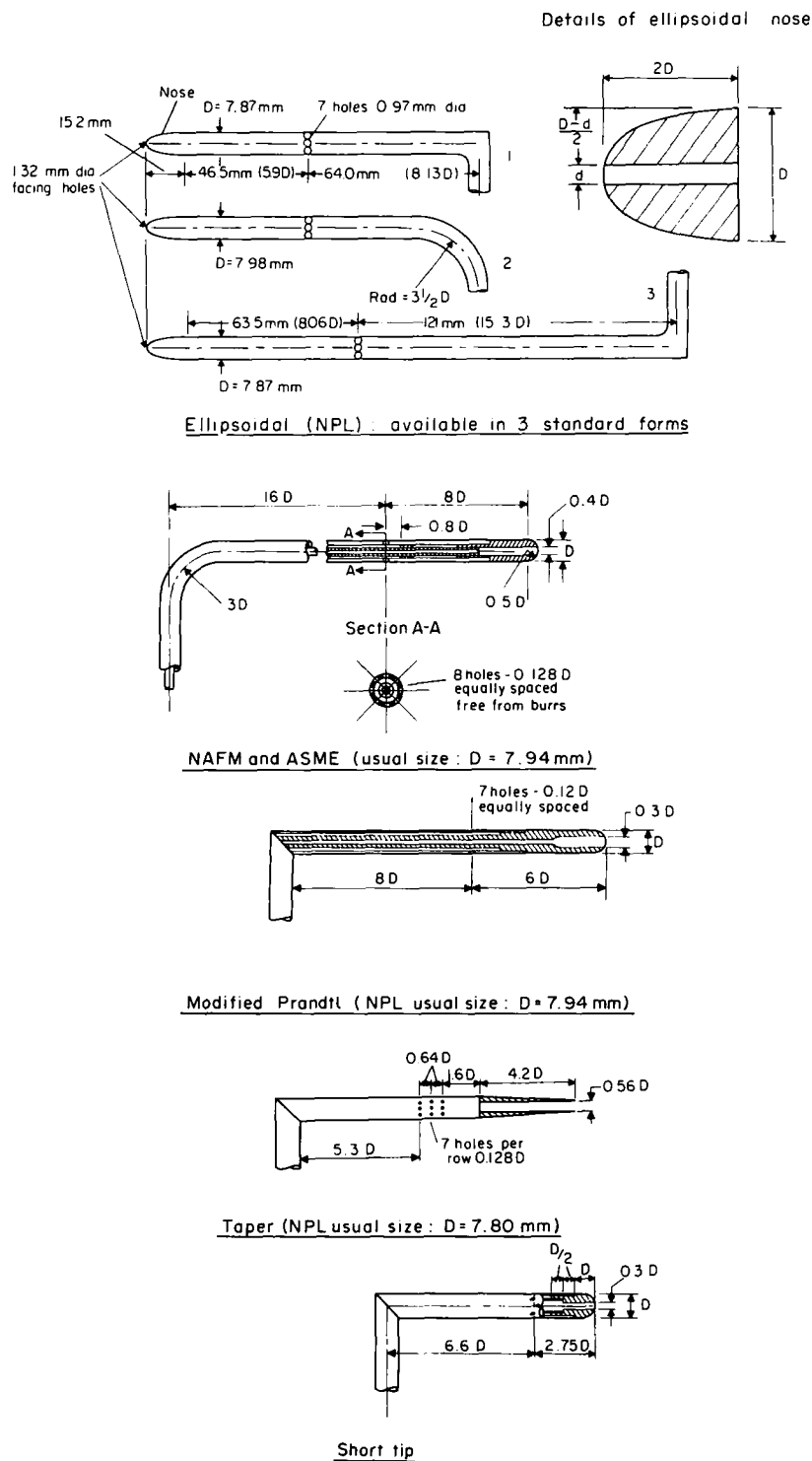


FIG. 73. Generalized dimensions of several pitot-static tubes in common use.

3.2.1. Reynolds number effect

The Reynolds number characteristics for incompressible flow of the pitot-static tube is essentially governed by that of the pitot tube, since available experimental evidence indicates that the static pressure is substantially independent of Reynolds number in the range 3000 to 53,000, based on the outer probe diameter. Moreover, some of the calibration tests reported are actually conducted for the pitot-static combination, such as the NPL standard probes and the Prandtl tube.

3.2.2. Yaw and pitch effect

It is rather fortuitous that yaw and pitch errors for the pitot and static tubes are of the same sign so that a compensating effect occurs in the pitot-static combination. Characteristics for the hemispherical (modified Prandtl), ellipsoidal and tapered nose probes have been given in Bryer and Pankhurst. In general, it can be said that the hemispherical nose probe yields velocity readings accurate to about 2% up to angles of attack of 30°. On the other hand, if the direction of the flow is known to within 15°, the ellipsoidal probe is much more superior, with an error less than 1%.

3.2.3. Turbulence effect

On the basis of isotropic turbulence, the results of Goldstein⁽³⁹⁾ indicate that the dynamic pressure measured by a pitot-static tube can be written as

$$P_m - p_m = \frac{1}{2} \rho q^2 + \frac{1}{2} \rho q'^2. \quad (68)$$

Flow in pipes does not exhibit isotropic turbulence, the results of Fage⁽³⁰⁾ given by eqn. (64) may be substituted for the static pressure to obtain an equivalent expression for the dynamic pressure. But, see the criticism of Bradshaw and Goodman on Fage's result given on p. 198.

In spite of Goldstein's analysis, present information suggests that a pitot-static tube aligned with the mean flow will record in isotropic turbulence a differential pressure of magnitude

$$\frac{1}{2} \rho u^2 + \alpha \rho q'^2 \quad (69)$$

where α varies between $\frac{1}{6}$ for indefinitely small scale turbulence and $\frac{1}{2}$ for indefinitely large-scale turbulence; and may in fact be closer to $\frac{1}{2}$ because the contribution from static pressure is rather small for practical probe sizes. Thus, even when the rms turbulent velocity fluctuation is as high as 10% of u , the error in velocity measurements, if turbulence effect is neglected, amounts to only 0.5 to 2.5%. As this magnitude of fluctuations represents a fairly turbulent stream, we may conclude that turbulence effect on dynamic pressure readings are often negligible, except in very accurate measurements or in instances where the turbulence intensity can rise to considerably higher values.

3.2.4. Mach number or compressibility effect

For low Mach numbers, the incompressible Bernoulli equation can be used for computing the flow velocity. The lower limit to the use of the pitot-static tube is determined solely by the sensitivity of the manometers used to measure the pressure difference. The error caused by neglecting the effect of compressibility amounts to about 1% at Mach 0.28, which corresponds to an air speed at normal temperature and pressure of about 90 m/sec. Using the first two terms of the binomial expansion of the isentropic Bernoulli equation gives the same accuracy to almost Mach 1, if care is exerted in avoiding disturbances on the flow. However, in most practical applications, the upper usable limit of the pitot-static tube would be reached at about Mach 0.7 for a modified Prandtl tube, a value set by the static tube. Although the isentropic Bernoulli equation remains valid on the supersonic range, it cannot be used because now it is not possible to determine the true total pressure by means of a blunt-nose pitot tube since this causes a bow shock to form ahead of the probe. However, it is possible to deduce the velocity from individual total and static pressure readings by means of the Rayleigh supersonic formula. For this purpose, additional information on the temperature of the stream is required. If we are to leave the velocity in the form of the Mach number, as is in common practice, this additional information is not needed.

Theoretical considerations by MacColl and Codd⁽⁸²⁾ indicate that the true stagnation pressure behind a normal shock will not be measured unless the impact orifice is small in comparison to the frontal area of the probe, while experimental evidence indicate that if the static pressure tap is placed some 10 diameters behind the nose, the static pressure measured corresponds closely to the free stream value.⁽⁵⁴⁾

The effect of yaw on the dynamic pressure reading of a Prandtl tube in subsonic flow has been investigated by Walchner.⁽¹³⁴⁾ His results are shown in Fig. 74, from which it is seen that a properly aligned probe is capable of registering the true dynamic pressure correctly up to above Mach 0.85.

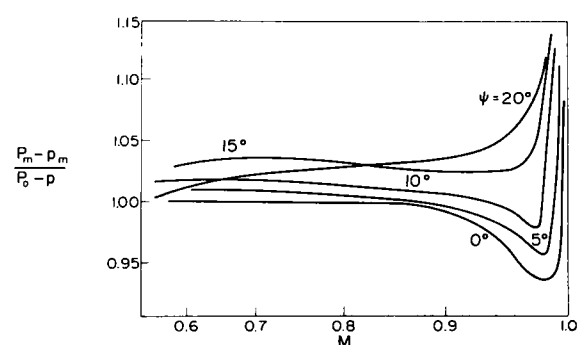


FIG. 74. Effect of yaw on the Mach number characteristics of the pitot-static tube.

3.2.5. Response rates for pitot-static tubes

The speed of reading a pitot-static tube depends on the length and diameter of the pressure passages inside the probe, the size of manometer connections and the displacement volume of the manometer. The time constant is very short for any of the standard tubes down to 3 mm diameter. However, it increases rapidly for smaller diameters. For this reason, 1.6 mm o.d. tubes is the smallest recommended size for ordinary use. This will take 15 to 60 seconds to reach equilibrium with ordinary manometer hook-ups for readings in air. Pitot-static tubes of 0.8 mm o.d. can easily have time constants as long as 15 minutes in air, and they choke up very easily with fine dirt in the air stream. If very small tubes are required, it is therefore preferable to use separate total and static tubes rather than the combined pitot-static tube.

3.2.6. Minimum probe size to achieve prescribed accuracy in a given pipe

The pitot-static tube is frequently used for measurements in pipes. The main objective of these is to provide information on the total discharge by a traverse and subsequent integration of the velocity profile over the pipe area. Obviously, accurate result could be achieved by applying all the necessary corrections before integration. However, the process is tedious and not of practical interest. It is therefore more expedient to have the combined effects of these corrections reduced to a simple selection rule, say, of the maximum probe size permissible in a given pipe in order to achieve a prescribed accuracy on the volumetric discharge.

Let us first consider the error caused by the total tube. The error significant in this connection is due to the displacement effect. Using the results of Young and Maas (which is sufficiently accurate for most practical purposes, though the discussion in Section 1.3.1 may modify the following results somewhat) Fage⁽³¹⁾ calculated the overestimation on the discharge in fully developed turbulent pipe flow, if the uncorrected measurements are used for the integration, to be

$\frac{D}{D_p}$	0.03	0.02	0.01
% overestimation	0.9	0.4	0.1

For the static tube, the data of Hubbard, as shown in Fig. 47, indicate that the static pressure measured by a static tube is lower than that of the undisturbed flow by an amount equal to the venturi effect caused by the area reduction due to probe insertion, when the probe is along the axis of the pipe. Furthermore, the lack of systematic variation in the static pressure measured by a static tube of 1.9 mm diameter over a flat plate, as reported by Sweeting, suggests that this venturi effect may remain the same with the static tube in other locations. Thus, the overestimation of the discharge

caused by the static tube is $(D/D_p)^2$. For the three D/D_p values tabulated above, the respective errors are

% overestimation	0.09	0.04	0.01
------------------	------	------	------

Thus, it can be seen that the total error contributed by the combined pitot-static tube is approximately 1%, $\frac{1}{2}\%$ and $\frac{1}{4}\%$ for D/D_p ratios of 0.03, 0.02 and 0.01 respectively. From these values, the maximum probe size that can be used in a pipe of a given diameter to achieve a prescribed accuracy can be deduced, e.g. probes 6 mm external diameter should, if possible errors are to be limited to about $\frac{1}{4}\%$, not to be used in pipes of less than 300 mm diameter, and so on.

3.3. Cantilever Probes

As for the pitot-static tube, the cantilever probe is obtained by coupling the pitot and static cylinders or wedges together onto the same coaxial stem. This arrangement produces the most compact dynamic pressure probes.

As the design procedures of Livesey and Glaser for the pitot and static cylinders respectively are independent of each other, they can easily be applied to the construction of the cantilever cylinder. It is obvious that this is beset by the more severe limitations of its two components. A well-designed probe, however, is capable of giving a pressure coefficient close to unity over a wide range of Reynolds numbers, as evidenced by their test results.

One way of facilitating the construction of the cantilever probe is to keep the static pressure orifices below the total head hole. This design is therefore recommended unless the probe is also intended for flow-direction measurement.

Further discussion on this probe, especially about its rigidity in terms of its resonance frequency due to vortex shedding and effect of compressibility, can be found in Bryer and Pankhurst.

3.4. Conical Probes

The use of an uncalibrated cone containing four static pressure and one total pressure orifices as a Mach number indicator at supersonic speeds has been reported by Cooper and Webster,⁽¹⁸⁾ using a conical probe of the form shown in Fig. 75 having $m/n = 25$. Test results obtained at Mach 1.59 show that the Mach number can be predicted to within

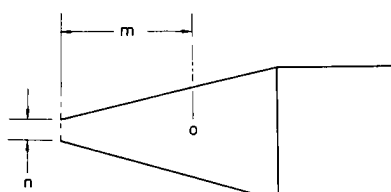


FIG. 75. Geometry of pitot-static cone combination.

1% up to incidence angles of 8° using the total pressure and mean static pressure readings for reduction. The mean static pressure is obtained by simply averaging the four static pressures. Further increase in incidence results in an overestimation of the Mach number by about 5% at an angle of attack of 16.1° . The indicated Mach number has been found to remain the same under all conceivable combination of pitch and yaw as was tested by rotating the cone at steps of 15° about its axis over the entire pitch-yaw range. The primary problem encountered in the reduction process is obviously the accuracy with which existing theories can be used to interpret the results. It has been found that for the determination of both Mach number and flow angles either the linear or the first-order non-linear theory could be used with essentially the same accuracy. In the case of Mach number determination, this observation stems from the fact that the four static pressures were arbitrarily averaged such that the evaluation of the Mach number depended only on the unyawed solution given by Taylor and MacColl.⁽¹²⁸⁾

Another satisfactory design consisting of a 60° cone having $m/n = 2.4$ has been reported in Bryer and Pankhurst.

4. FLOW DIRECTION AND VECTOR VELOCITY MEASUREMENT

4.1. Introduction

Except in the most simple flow configurations, the direction of the stream is usually unknown. Though the static and pitot-static tubes show a pronounced pressure optimum when correctly aligned, they are never used directly for accurate flow direction determinations. To this end, modifications on the standard pitot configuration is often incorporated to further improve its sensitivity. Though there appears to be a wide variety of pressure sensitive direction probes, the design principle behind these is quite simple and rather stereotyped. With the exception of the cantilever probe, all designs consist of one or two pairs of symmetrically mounted pressure taps with the faces of the open ends making equal but opposite inclinations with the fluid stream. In general, configurations built up from open-ended tubes are easier to make than those in which the pressure taps are drilled into the body of the probe. Designs with only one pair of pressure taps are for use in two-dimensional flow-direction measurements, while those having two pairs are for three-dimensional measurements. Combinations including an impact orifice have the added advantage of allowing the complete velocity vector to be determined in one positioning. Such vector velocity measuring probes are often restricted for use in subsonic streams only because in general the asymmetrical shock formed ahead of the probe in super-

sonic streams would obviate the continual use of the instrument unless the probe has a high analytical bias, such as the yawed cone.

A wide selection of flow direction and vector velocity probes has been described in Bryer and Pankhurst. In what follows we shall more or less confine ourselves to elaborations on points that have not been adequately covered by these authors and to other designs not included by them.

There are two ways in which pressure-sensitive direction probes can be used. The simpler and more direct of these is the null method. In this method, the probe is mounted in a holder and the flow angle determined by balancing the pressure measured at opposite sets of holes. Depending on whether the flow to be measured is two- or three-dimensional, the holder is required to have angular adjustment in one or two directions respectively. Orientation and traversing mechanisms for use with the null method have been described in detail in Bryer and Pankhurst.

In the alternative approach, the probe is positioned in a fixed position facing the stream and pressure differences between symmetrically opposite taps are measured and the flow direction deduced by means of prior calibration or theoretical considerations. In this connection, roll alignment for one pair of orifices in three-dimensional streams will greatly reduce the complexity of the ensuing flow geometry and calibration charts.

4.2. Effect of Viscosity, Compressibility and Total Pressure Gradient

In subsonic streams, a properly designed and constructed null-type probe should not be affected by changes in Reynolds or Mach number, as long as the flow field is symmetrical about the probe axis. The null system is well suited to the design of combination probes, since static and total pressures can be measured most accurately when the probe is aligned with the flow. On the other hand, fixed-position probes require prior calibrations in a known flow and the accuracy of these results in flow fields having different total pressure gradients is doubtful.

In supersonic streams, the accuracy of a null-probe would not be impaired if the probe axis coincides with its zero axis, i.e. the direction of the free stream when the probe is nulled in a uniformly parallel stream. This is because the shock pattern formed will be symmetrical about the zero and hence the probe axis. A fixed-probe, on the other hand, which relies on the measurement of pressure differences between the various taps may be seriously in error since the shock affecting one tap may be of different strength from that affecting its counterpart. In addition, asymmetric shocks will produce a change in the downstream flow direction, thus introducing further error into the measurement.

In transonic flow, the behaviour of a pressure-sensitive direction probe becomes indeterminate because shocks may now stand in front of one tap and behind its counterpart even on an apparently symmetric, nulled probe.

Improvement of a direction probe influenced by shocks may be achieved by reducing the tap spacing. In this connection, certain geometries may possess analytic advantages, the yawed cone being an example.

Additional results influencing the selection of probes for supersonic flow measurements have been discussed in Bryer and Pankhurst.

4.3. Two-dimensional Probes

4.3.1. Claw probe

The claw probe is constructed with two tubes inclined to the stream direction at an angle of 45° for maximum sensitivity. These tubes lie in a single plane perpendicular to the axis of rotation of the probe, which passes through a rather arbitrarily determined "measuring point".

Characteristics for the claw probe has been reported by Conrad⁽¹⁶⁾ in comparison to that of a two-tube yawmeter of his own design. Both of these are shown in Fig. 76, from which it can be seen that the Conrad probe is of higher sensitivity.

Claw probes have now largely been superseded by others of more compact designs having overall transverse dimensions smaller than 3 mm, disturbing the flow less and giving readings more nearly at a point.

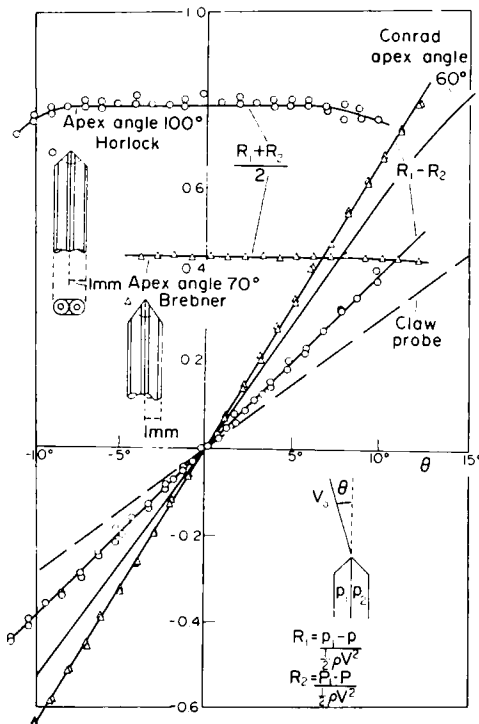


FIG. 76. Calibration curves of two-tube Conrad yawmeters.

4.3.2. Conrad or cobra probes

This is probably the best of the nulled probes for flow direction measurements. It is inexpensive and easy to construct, being formed from two or three tubes soldered together. The two-tube Conrad probe has a minimum tube spacing and is superior for use in flow fields having steep velocity gradients. The insertion of the impact tube undoubtedly destroys the superior quality of the two-tube probe by increasing the tube spacing of the yawed elements. In some cases, such as in unsteady flow in turbomachines, however, it is imperative that impact pressure be measured at the same time. Under these conditions, the three-tube cobra retains its superiority compared to other types of direction probes.

When used as a fixed probe, the yaw characteristics of the two-tube Conrad probe is related to the pressure difference measured by the two tubes; while their sum is related to the total pressure of the flow. Both the yaw and total head characteristics for two-tube Conrad probes having different apex angles are compared in Fig. 76. Apex angles between 40° and 120° (in steps of 10°) have been used by various investigators. Conrad⁽¹⁶⁾ reported that maximum sensitivity is attained with a 60° apex angle; however, the results of Horlock⁽¹⁶⁾ and Brebner (unpublished, reported by Küchemann⁽⁷⁰⁾) indicate that this may actually occur at 70°.

The main disadvantage of the two-tube Conrad probe is that it cannot give all flow parameters from its readings in one position, though Brebner had developed a method, described in detail in Bryer and Pankhurst, whereby the flow direction, velocity, static pressure and total head can be found in terms of their main stream values from the four readings taken when the probe is pointing at two directions with a known angle of rotation between them. This procedure is, to say the least, very tedious. On the other hand, all these parameters can be obtained from the pressure readings in one setting of the three-tube probe. An analysis to this effect had been given by Crabtree assuming linear relations for the differential pressures between the side tubes and the central one (unpublished results, reported in detail by Küchemann⁽⁷⁰⁾). However, this method is only applicable in a rather narrow yaw range. The use of calibration functions can considerably extend the usefulness of the probe to much wider yaw ranges. In this connection, Rajaratnam and Muralidhar⁽¹¹⁾ have reported calibration results for the three-tube Conrad probe up to a yaw angle of 60°. The probe used in obtaining these curves was made from stainless steel tubings of external diameter 3 mm and internal diameter 1.8 mm. The apex angle of this probe is 90°. The arguments used to arrive at the form of the calibration curves are as follows:

When the three-tube cobra is yawed at an angle θ to the flow direction, the pressures recorded by the

member tubes of the combination can be written as

$$p_1 = p_0 + K_1 \Delta p, \quad (70)$$

$$p_2 = p_0 + K_2 \Delta p, \quad (71)$$

$$p_3 = p_0 + K_3 \Delta p, \quad (72)$$

where p_0 is the true total pressure, recorded by the central tube at zero yaw, Δp the true dynamic pressure, the numerical subscripts refer to member tubes for the configuration shown in Fig. 77 and the K 's represent the respective calibration functions.

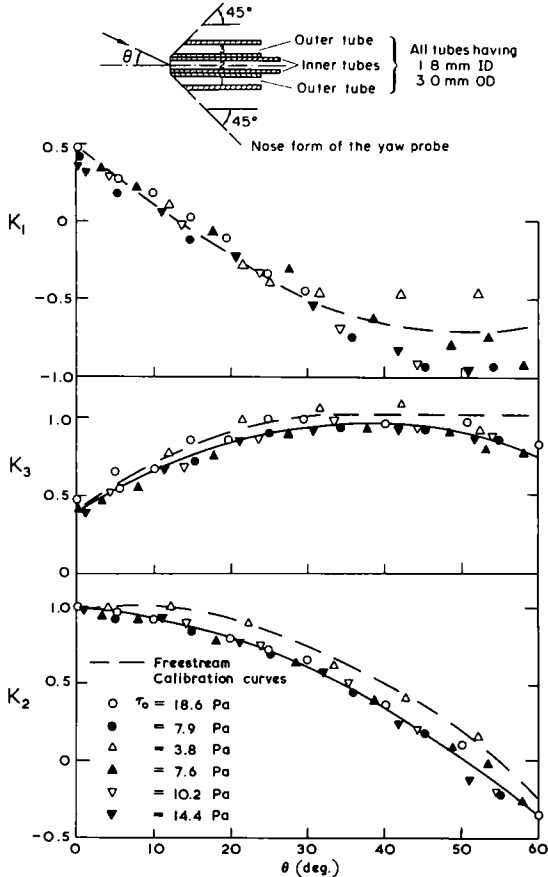


FIG. 77. Calibration functions K_1 , K_2 and K_3 for the 2-D cobra used for velocity vector and skin-friction measurements.

It has been found that the calibration factors K_i are functions of the yaw angle θ alone, both when the probe is located in the free stream and when it is resting on the wall of a plane turbulent wall jet under zero pressure gradient, produced by a deeply submerged nozzle in a rectangular channel. These functions have also been given in Fig. 77. By suitably combining eqns. (70) to (72), we obtain the following definition for K_0

$$\frac{p_3 - p_2}{p_1 - p_2} = \frac{K_3 - K_2}{K_1 - K_2} = K_0. \quad (73)$$

The variation of K_0 with θ is shown in Fig. 78.

Thus, from the readings p_1 , p_2 and p_3 obtained with the probe in a fixed position, K_0 can be computed from eqn. (73). This allows the yaw angle

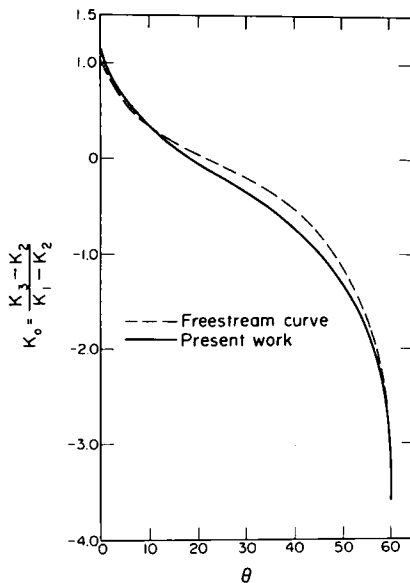


FIG. 78. Calibration function K_0 for the 2-D cobra used for velocity vector and skin-friction measurements.

θ to be read off from Fig. 78, and hence K_1 , K_2 and K_3 , from Fig. 77. The total and dynamic pressures can then be calculated using any two of the three equations (70) to (72). Because of the relatively larger difference between the free stream and wall calibration curves for K_2 , it is advisable to avoid using eqn. (71) for calculating p_0 and p .

Eichenberger⁽²⁶⁾ reported that the two-tube Conrad probe is capable of reproducing flow directions to within 0.2°. He also noticed a constant error per unit velocity gradient; of magnitude of 0.65° for probes comprising of two 0.51 mm diameter tubes yawed at 60° to the stream. In addition, Conrad probes have been found to give accurate results within a boundary layer if the pitch angle of local flow direction does not exceed 6° in steady flow.⁽¹³⁾

4.3.3. Cantilever cylinder

This is a simple, rugged, two-dimensional probe. The design of this probe has been given earlier in Sections 1.9.1 and 2.5.1. Reference should be made to these sections and to Section 3.3 for relevant discussions in Bryer and Pankhurst.

When intended for flow-direction measurement, the two static orifices have to be connected to separate channels. If both flow direction and impact or dynamic pressure are to be made, the impact and static orifices have to be kept at the same level.

Shocks will stand on this probe at Mach numbers between 0.55 and 1.0 so that direction measurement is no longer possible in this Mach number range.

The sensitivity of this instrument has been estimated to be 5% of the impact pressure per degree of yaw. This makes it useful for measurements within 0.1° with velocities over 30 m/sec.

4.3.4. Wedge

The wedge is another simple, rugged, two-

dimensional probe. It is constructed by superposing the design criteria given in Sections 1.9.2 and 2.5.2. It can be supported on either the conventional L-shape or cantilever stems. In the former configuration, it is also known as the chisel probe.

The critical Mach number at which shocks first appear on a wedge is a function of the wedge angle. For this reason, wedges of small included angles are preferred. This also reduces hole spacing and, consequently, velocity gradient errors.

Discussion on some other forms of wedge-type combination probes has been given in Bryer and Pankhurst.

4.4. Three-dimensional Probes

4.4.1. The conical probe

When used with the null system, there is little difference between this probe and the three-dimensional Conrad probe. However, because of the analytical advantage of the cone over other geometric shapes at supersonic speeds, the flow angles can also be determined with the probe in a fixed position using the indicated static pressure measurements. The use of this probe in the fixed system has been reported by Cooper and Webster⁽¹⁸⁾ for both Mach number and flow angle determinations. The former usage has already been described in Section 3.4, and we shall confine our attention here to its use as a yawmeter. The primary problem in this connection is, of course, the accuracy with which existing theory can be used in converting the pressure measurements to the free stream parameters.

Tests obtained at Mach 1.59 show that the pitch and yaw angles can be predicted to within 0.5° for various combinations of pitch and yaw, with yaw smaller than pitch, up to an incidence angle of 10°.

It has also been found that in the reduction of both the Mach number and flow angles from the pressure measurements either the linear or the first-order non-linear theory can be used with essentially the same accuracy. For the case of flow-angle determination, this follows from the fact that the pressure coefficients for both these cases are approximately the same in the range of flow angles reported.

In addition, the reader is referred to Section 3.4 for relevant discussions in Bryer and Pankhurst.

4.4.2. The cantilever cylinder

This is the only three-dimensional probe to retain the compact and rugged construction of its two-dimensional counterpart. However, it differs from the latter in that the plane of the impact and static orifices is now located much closer to the hemispherical cap, on which another pressure tap is drilled on the same axial plane as the stagnation orifice. The resultant configuration of this four-hole cylinder is shown in Fig. 79. This additional orifice

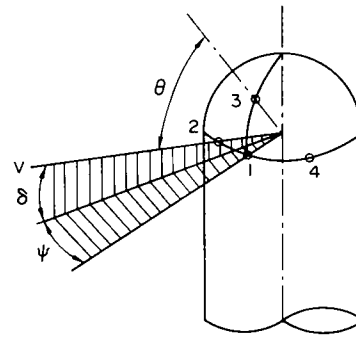


FIG. 79. Geometry and nomenclature for the four-hole cantilever cylinder.

is required to provide, together with the impact orifice, the extra information on the pitch angle of the flow. Because of its proximity to the cap, prior calibration of the probe is necessary due to flow distortion about the orifices caused by the end effect. Prior calibration is also required because the probe is capable of giving only the yaw angle directly by the null method; and the pitch angle has to be determined from the pressure readings using calibration curves. These have been reported by Markowski and Moffatt⁽⁸⁶⁾ in terms of the parameters M_R and θ_R , defined by

$$M_R = \frac{p_1 - p_2}{p_1}, \quad (74)$$

$$\theta_R = \frac{p_1 - p_3}{p_1 - p_2}. \quad (75)$$

These definitions allow the Mach number of the flow to be determined from Fig. 80a. This, together with θ_R , determines the complementary pitch angle θ (i.e. pitch angle = $90^\circ - \theta$) and the two pressure parameters p_{0r} and p_{sr} from Fig. 80b. From these pressure parameters, the free stream impact and static pressure can be calculated using the following relations

$$p_0 = p_1 + p_{0r}(p_1 - p_2), \quad (76)$$

$$p_s = p_1 + p_{sr}(p_1 - p_2). \quad (77)$$

Markowski and Moffatt reported that the pitch angle may be obtained to within $\pm 2^\circ$, and p_0 and p_s to within 2% of the velocity pressure, in the range of θ from 40° to 120° .

In view of the large tap spacing of this probe, it cannot be used in flows having large velocity gradients.

4.4.3. Five-hole pressure probes

In essence, these probes consist of an axisymmetric body having five pressure taps on the nose of the body. Of these, the centre tap indicates the impact pressure; while the other four peripheral holes, which are spaced 90° apart, serve as direction indicators. Spherical (hemispherical) ellipsoidal and other nose shapes have been used. The five-tube Conrad probe is yet another conceivable configura-

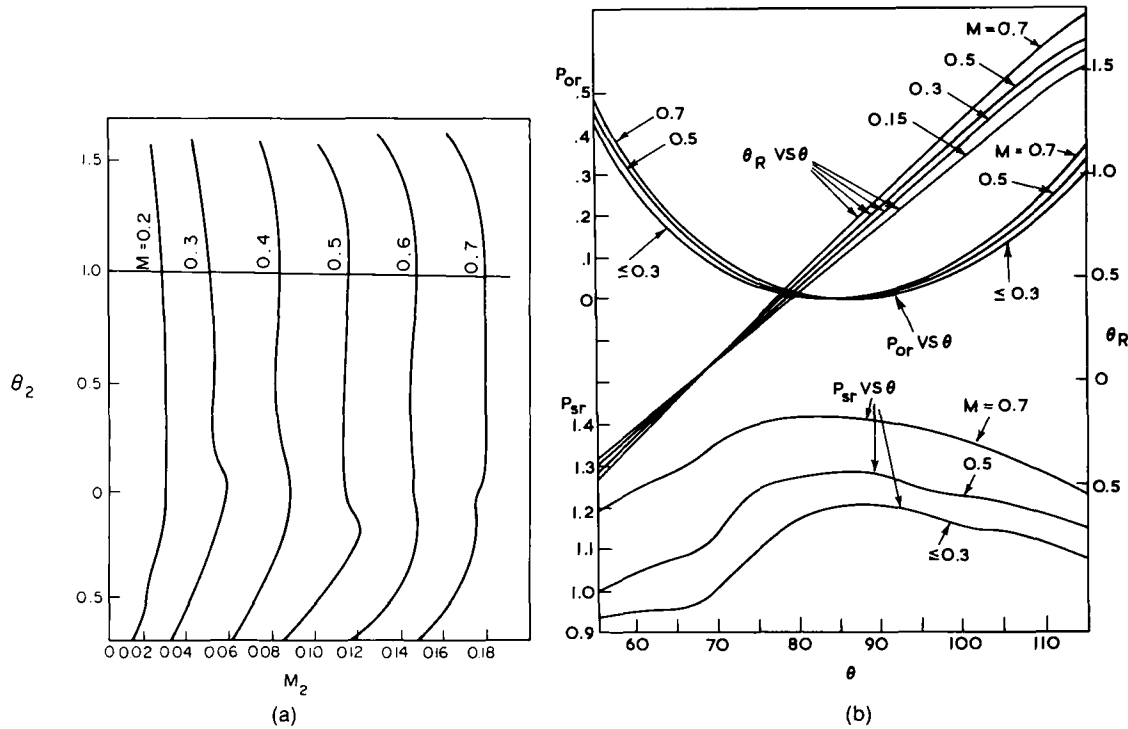


FIG. 80. Calibration charts for the four-hole cantilever cylinder: (a) Mach number characteristics, (b) characteristics for total-, static-pressure parameters and complementary pitch angle.

tion. Of these, the conical probe has been discussed separately in Section 4.4.1 because of its importance in supersonic measurements.

The spherical probe consists of a small sphere supported by a stem which can be placed either parallel or perpendicular to the mean flow direction. The latter configuration retains the compactness of the four-hole cantilever cylinder, but has much smaller tap spacing. However, because of its asymmetry in the pitch plane, the pitch pressure taps have to be calibrated before use, even for the null system. Complete calibration curves for this probe had been obtained by Van der Hegge Zijnen. These have been reproduced in Bryer and Pankhurst.

When the axis of the stem is placed along the flow direction, the most compact configuration ensuing is the hemispherical probe having size of the sphere equal to the minimum size of the stem required to accommodate the various pressure lines. This probe retains the property of being used in the null system without prior calibration because of its symmetrical construction.

Emmons²⁷ described the use of an uncalibrated sphere (or hemisphere) for flow angle measurement with the probe used in a fixed position. When the pitch angle, ψ , is zero, the yaw angle, α , can be written as

$$\alpha = \frac{p_1 - p_3}{p_0 - p_3} \lambda \quad (78)$$

where the numerical subscripts refer to pressure-tap arrangement as shown in Fig. 81b; and p_0 represents the true impact pressure. The parameter

λ is defined by the following expression:

$$\lambda = \frac{1}{4.5 \sin 2\theta} \quad (79)$$

where θ is the angle subtended by a peripheral hole and the impact orifice at the centre of the sphere.

For small pitch angles, λ becomes

$$\frac{1}{\lambda} = -4.5 \sin 2\theta \{1 - 2\cos^2(\psi\theta)\}. \quad (80)$$

Equation (80) shows that the parameter λ varies by about 4% over a pitch range of 10° for $\theta = 45^\circ$.

Combining eqns. (78) and (80), the calibrated function for the spherical or hemispherical probe can be written as

$$\frac{p_1 - p_3}{p_0 - p_3} = 4.5\alpha \sin 2\theta (1 - 2\psi^2\theta^2) \quad \text{for small } \psi. \quad (81)$$

Emmons suggested using p_1 as p_0 without correction. There is no doubt that correction on this is necessary in the presence of velocity gradients due to the large tap spacing inherent in the probe construction. Correction due to compressibility at high subsonic, transonic and low supersonic speeds has been discussed in Bryer and Pankhurst.

In order to completely describe the flow, the dynamic pressure is also required. This enables the free stream static pressure to be found since the impact pressure is measured directly. For the case of incompressible flow, the dynamic head can be evaluated from p_i at any peripheral hole using the

potential flow relation

$$P_0 - p = \frac{p_s - p_i}{\frac{q}{4} \sin^2 \theta}. \quad (82)$$

Equation (82) is applicable only at operating Reynolds numbers large enough that the viscous effect is negligible and within the range of yaw and pitch angles for which the total and static pressures can adequately compensate each other.

For large angles of incidence, experimental calibrations become inevitable. Jegorow⁽⁶¹⁾ has reported families of curves for the spherical probe used in the fixed system over a pitch and yaw range of $\pm 60^\circ$, with accuracy up to $\pm 0.3^\circ$ for pitch angle, $\pm 1\%$ for velocity pressure and $\pm 1\%$ for stream static pressure. The yaw angle can be determined to greater accuracy due to the symmetry in the yaw plane.

Dau *et al.*⁽¹⁹⁾ reported the use of the ellipsoidal five-hole probe shown in Fig. 81a. The probe is so

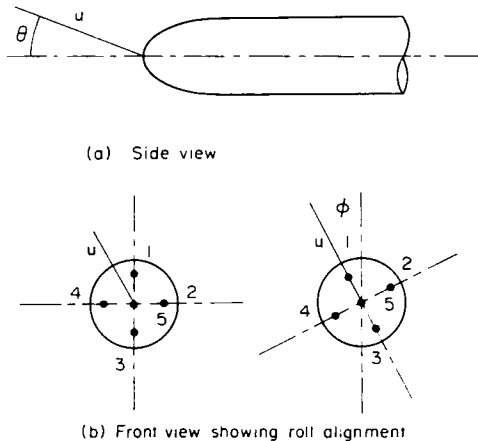


FIG. 81. Geometry of and nomenclature for the five-hole pressure probe.

mounted that it can be rolled about its longitudinal axis rather than yawed in its yaw plane. When placed in the flow, the roll angle ϕ can be measured directly by rolling the probe until the pressure difference between the holes 2 and 4 is zero. This presupposes that the flow in the neighbourhood of the probe tip is reasonably uniform. After aligning the probe thus, the pressures at all the five pressure orifices depend on the local values of θ , p and q , which constitute the remaining flow parameters. These parameters represent the local pitch angle, the local static pressure and the local dynamic pressure respectively. Defining the pressure coefficient for hole i by the expression

$$C_{pi} = \frac{p_i - p_r}{q} \quad (83)$$

where p_r is a convenient reference pressure. It can be shown that, since these coefficients are functions of θ only,

$$\frac{C_{p1} - C_{p3}}{C_{p5} - C_{p3}} = \frac{p_1 - p_3}{p_5 - p_3} = F(\theta). \quad (84)$$

Taking the inverse of eqn. (84), we have

$$\theta = f\left\{\frac{p_1 - p_3}{p_5 - p_3}\right\}. \quad (85)$$

Similarly, we can also show that

$$\frac{q}{p_s - p_3} = g\left\{\frac{p_1 - p_3}{p_5 - p_3}\right\} \quad (86)$$

and

$$\frac{p - p_s}{p_s - p_3} = h\left\{\frac{p_1 - p_3}{p_5 - p_3}\right\}. \quad (87)$$

Calibration functions for f , g and h had been reported by Dau *et al.* and are being reproduced in Fig. 82. Accuracies, for an automated probe using a servomotor fed by pressure signals from holes 2 and 4 to roll the probe and an analogue computer and plotter programmed to plot the local flow parameters in a continuous manner as the probe was being traversed, have been reported to range from 2% to 5% for the static and dynamic pressure coefficients, about 2° for θ and 3° for ϕ depending on the value for θ .

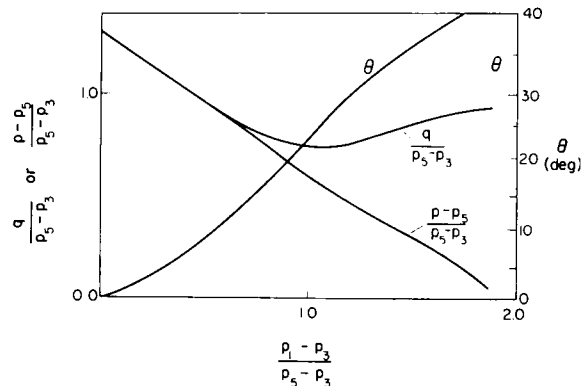


FIG. 82. Experimental calibration curves for the five-hole pressure probe.

Bryer and Pankhurst reported families of calibration curves for the five-hole Conrad probe used in the fixed position. Such curves are somewhat complex since it now requires differential pressures from both pairs of side tubes to specify the flow parameters. Calibrations involving a roll alignment, as has been used by Dau *et al.* for the ellipsoidal probe, would greatly simplify the results and is therefore preferred.

5. SKIN FRICTION MEASUREMENT

5.1. Introduction

Direct measurement of skin friction is of considerable interest in experimental fluid mechanics. This is because knowledge of the skin friction enables the drag on a body to be calculated. Also, the skin friction defines the velocity gradient at the wall and this serves as a check on the velocity traverse.

The first attempt in using a modified form of the pitot tube for skin friction measurement was that of

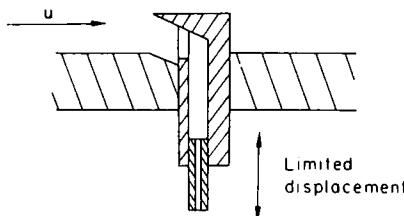


FIG. 83. The Stanton tube.

Stanton *et al.*⁽¹²⁴⁾ This form of probe, shown in Fig. 83, has since been known as the Stanton tube. Essentially it is a rectangular surface probe having the wall as the bottom surface. The top surface of the probe is in the form of a lip which is capable of being displaced through a small distance thus enabling the velocity profile close to the wall to be measured. This in turn permits the calculation of the skin friction. The pitot tube in the form of the Stanton tube suffers from one severe limitation. It is extremely inflexible and cannot be used as a general-purpose instrument because of its special construction. We shall, therefore, refrain from discussing it further.

The next attempt to extend the pitot tube to skin friction measurement was that of Preston,⁽¹⁰⁴⁾ who suggested that a conventional round pitot resting on the surface can be used to determine the skin friction. In recognition of Preston's insight, a pitot thus used has been called a Preston tube. This is, however, a rather poor terminology as it conveys the idea that a Preston tube is some modified form of the conventional pitot, which it is not. Rather, it represents only one way of using the pitot tube.

Since the introduction of the Preston tube into the boundary layer may cause too much flow disturbance, especially in instances where the boundary layer is very thin, other surface probes have since been developed for the measurement of skin friction. Examples of these include the static-hole pair and the razor-blade technique. The former comes as a direct consequence of investigations on the static-hole error problem while the latter is essentially a simplified version of the Stanton tube.

5.2. The Preston Tube

5.2.1. Theoretical background

Based on the well-established concept of universality of the wall region in turbulent wall shear layers, Preston has suggested a method for measuring skin friction using a pitot tube resting on the wall surface. His arguments run briefly as follows:

Dimensional analysis has led to a wall law of the form:

$$\frac{u}{u^*} = f\left(\frac{yu^*}{\nu}\right). \quad (88)$$

If instead of the mean velocity we substitute the pressure difference recorded by a pitot resting on the wall and the local static pressure, Δp , the above

relation can be written as

$$\frac{\Delta p}{\tau_0} = g\left(\frac{u^* D}{\nu}\right) \quad (89)$$

where D is the outer pitot diameter; alternatively, this can be written as

$$\frac{\tau_0 D^2}{4\rho\nu^2} = h\left(\frac{\Delta p D^2}{4\rho\nu^2}\right). \quad (90)$$

This last relation provides a convenient way for determining the skin friction since the shear stress is now uniquely related to the pressure head measured by the pitot-wall-static-hole combination. For a pitot of given geometry the function h can now be simply and accurately determined from pipe flow experiments where the skin friction can be deduced from the measurement of pressure drop. In view of the fact that the wall laws for pipe and boundary layer flows are identical, the calibration is therefore expected to hold also in boundary layer flows.

5.2.2. Calibration results for round pitot

After some years in which the validity of Preston's assumption of universality of the wall region were questioned, it is now generally accepted that the Preston tube provides a simple and yet accurate device for skin-friction measurement. The investigations of Head and Rechenberg,⁽⁵⁰⁾ Rechenberg⁽¹¹⁵⁾ and Patel⁽⁹⁶⁾ contributed greatly to dispel the uncertainties that had been raised and to firmly entrench the Preston tube as a reliable skin friction meter.

In most of the investigations reported, use was made of round pitots. Of these, the particular pitot having a d/D ratio of 0.6 had been used more extensively than others. The effect of the d/D ratio on the calibration had been found to be negligible for symmetrically built round pitots.^(96,115) However, in view of the results of the latter, it is advisable to keep $d/D > 0.2$.

In his pioneer investigation, Preston has demonstrated that

- (i) the calibration curve, i.e. the function h , determined in a 50 mm diameter pipe is independent of the pitot diameter.
- (ii) When a series of pitot tubes of widely different diameters were used at any particular station in the boundary layer, the values of skin friction determined by the use of this calibration curve were found to be identical.

The results of Head and Rechenberg showed that for a given skin friction the pitot reading was the same for both boundary-layer and pipe flows thus vindicating Preston's conclusions and provide evidence on the existence of an identical wall law for both boundary layer and pipe flows.

Patel's results not only confirmed Preston's first conclusion that the calibration curve is independent of the ratio of Preston tube to pipe diameters as long as the former lies entirely within the wall region of the wall shear layer, but also went further to establish a definitive calibration curve. This has

been divided into three regions corresponding to the conventional notions of sublayer, transition and fully turbulent layers.

Before listing the calibration curves for these regions, we shall first define the following parameters:

$$x^* \equiv \log \left(\frac{\Delta p D^2}{4 \rho v^2} \right), \text{ common logarithm of the independent variable,} \quad (91)$$

$$y^* \equiv \log \left(\frac{\tau_0 D^2}{4 \rho v^2} \right), \text{ common logarithm of the dependent variable.} \quad (92)$$

(i) *Fully turbulent region:*

$$55 < \frac{u^* D}{2v} < 800$$

or $3.5 < y^* < 5.3$ and $5.6 < x^* < 7.6$,

the calibration curve is given by

$$x^* = y^* + 2 \log (1.95 y^* + 4.10) \quad (93)$$

to within $\pm 1\%$ of τ_0 . The results of Patel in this region are in excellent agreement with those of Head and Rechenberg.

(ii) *Transition region:*

$$5.6 < \frac{u^* D}{2v} < 55$$

or $1.5 < y^* < 3.5$ and $2.9 < x^* < 5.6$,

the calibration curve can be represented by the empirical relation

$$y^* = 0.8287 - 0.1381 x^* + 0.1437 x^{*^2} - 0.0060 x^{*^3} \quad (94)$$

to within $\pm 1\frac{1}{2}\%$ of τ_0 .

(iii) *Sublayer:*

$$\frac{u^* D}{2v} < 5.6$$

or $0 < y^* < 1.5$ and $0 < x^* < 2.9$,

the calibration curve is given by the linear relation

$$y^* = \frac{1}{2} x^* + 0.037. \quad (95)$$

Further, using his calibration results in region (iii), Patel demonstrated that the sublayer wall law is compatible with a displacement of the effective centre of the pitot tube given by MacMillan, i.e. with $\delta = 0.15D$ for a round pitot having $d/D = 0.6$. Using this displacement together with calibration results of region (i) he deduced the coefficients of the semi-logarithmic law of the wall for the fully turbulent region to be $A = 5.5$ and $B = 5.45$. These results certainly go a long way to dispel uncertainties associated with the velocity or total pressure gradient effect on the pitot reading in pipe flow. For a fuller discussion on this effect, the reader is referred to Section 1.3.1.

Head and Ram⁽⁵¹⁾ pointed out that the calibration results of Patel in the form of eqns. (93) to (95) are rather inconvenient to use, particularly eqn. (93),

which is implicit in the unknown parameter y^* . They reported two alternative presentations which are of more direct application.

The first form is based on the expression

$$\frac{\Delta p}{\tau_0} = F \left(\frac{\Delta p D^2}{\rho v^2} \right) \quad (96)$$

which can be easily shown to be equivalent to eqn. (90). This form of presentation has the advantage that the dependent variable varies by a factor of only about 25 over the entire calibration range reported; whereas the parameter y^* used by Patel varies over four orders of magnitude. Results in the form of eqn. (96) have been tabulated by Head and Ram. These are reproduced below in Table 1.

In the course of their tabulation, Head and Ram found that Patel's expression do not match well at their joining points and they have to fair these results graphically in the neighbourhood of these points. Table 1 has been constructed with intervals of $\Delta p D^2 / \rho v^2$ so chosen that consecutive values of $\Delta p / \tau_0$ differ by no more than 2%. Thus, even without interpolation, values of $\Delta p / \tau_0$ can be read off with an accuracy less than $\pm 1\%$.

In view of the fact that in boundary-layer measurements, the skin friction coefficient c_f rather than the skin friction itself is of direct interest, Head and Ram have also reported results in the form which gives c_f directly. The functional relationship for c_f can be derived from eqn. (96) as follows:

$$c_f = \frac{\tau_0}{\frac{1}{2} \rho U_*^2} = \frac{\Delta p}{\frac{1}{2} \rho U_*^2} / F \left\{ \frac{\Delta p}{\frac{1}{2} \rho U_*^2} \times \frac{1}{2} \left(\frac{U_* D}{v} \right)^2 \right\}$$

or

$$c_f = \left(\frac{u_p}{U_*} \right)^2 / F \left\{ \left(\frac{u_p}{U_*} \right)^2 \times \frac{1}{2} \left(\frac{U_* D}{v} \right)^2 \right\} \quad (97)$$

where u_p represents the velocity corresponding to the dynamic pressure Δp recorded by the Preston tube and U_* the free-stream velocity.

Alternatively, we can write this as

$$c_f = G \left(\frac{u_p}{U_*}, \frac{U_* D}{v} \right) \quad (98)$$

which forms the basis of their second presentation. These results are shown in Fig. 84. The range of the variables reported in this figure is such that each contour of c_f covers almost the entire range of Patel's calibration. The free-stream velocity required in using Fig. 84 can be easily obtained by pushing the Preston tube outside the boundary layer. This procedure for obtaining U_* is recommended because it can provide at the same time the much needed information on whether the pitot tube lies wholly within the universal wall region of the boundary layer.

5.2.3. Limitations on the use of the Preston tube

Up to now, experimental evidence indicates that the calibration results are substantially unaffected by transverse curvature of the surface, the pres-

TABLE I. $\Delta p/\tau_w$ as a function of $\Delta pD^2/\rho\nu^2$

$\frac{\Delta pD^2}{\rho\nu^2} \times 10^{-2}$	$\frac{\Delta p}{\tau_w}$	$\frac{\Delta pD^2}{\rho\nu^2} \times 10^{-3}$	$\frac{\Delta p}{\tau_w}$	$\frac{\Delta pD^2}{\rho\nu^2} \times 10^{-3}$	$\frac{\Delta p}{\tau_w}$	$\frac{\Delta pD^2}{\rho\nu^2} \times 10^{-4}$	$\frac{\Delta p}{\tau_w}$	$\frac{\Delta pD^2}{\rho\nu^2} \times 10^{-5}$	$\frac{\Delta p}{\tau_w}$	$\frac{\Delta pD^2}{\rho\nu^2} \times 10^{-6}$	$\frac{\Delta p}{\tau_w}$
4.0	9.18	1.30	16.56	4.6	30.23	2.0	52.32	1.4	86.8	5.0	139.5
4.2	9.41	1.34	16.81	4.8	30.79	2.1	53.15	1.5	88.0	6.0	142.7
4.4	9.63	1.38	17.06	5.0	31.33	2.2	53.93	1.6	89.1	7.0	145.4
4.6	9.85	1.42	17.31	5.2	31.84	2.3	54.68	1.7	90.2	8.0	147.8
4.8	10.06	1.46	17.55	5.4	32.34	2.4	55.40	1.8	91.2	9.0	150.0
5.0	10.27	1.50	17.79	5.6	32.84	2.5	56.62	1.9	92.1		
5.2	10.47	1.54	18.02	5.8	33.31	2.6	56.80	2.0	93.0		
5.4	10.67	1.58	18.25	6.0	33.78	2.7	57.45	2.2	94.7	$\frac{\Delta pD^2}{\rho\nu^2} \times 10^{-7}$	$\frac{\Delta p}{\tau_w}$
5.6	10.87	1.62	18.48	6.2	34.23	2.8	58.07	2.4	96.2		
5.8	11.06	1.66	18.71	6.4	34.68	2.9	58.68	2.6	97.6		
6.0	11.25	1.70	18.94	6.6	35.11	3.0	59.28	2.8	98.8		
6.2	11.44	1.74	19.16	6.8	35.52	3.2	60.40	3.0	99.9	1.0	151.9
6.4	11.62	1.78	19.38	7.0	35.94	3.4	61.46	3.2	100.9	1.2	155.3
6.6	11.80	1.82	19.59	7.2	36.34	3.6	62.47	3.5	102.4	1.4	158.1
6.8	11.98	1.86	19.80	7.4	36.72	3.8	63.43	4.0	104.5	1.6	160.6
7.0	12.16	1.90	20.01	7.6	37.11	4.0	64.34	4.5	106.4	1.8	162.8
7.2	12.33	1.95	20.27	7.8	37.50	4.2	65.20	5.0	108.0	2.0	164.9
7.4	12.50	2.00	20.53	8.0	37.87	4.4	66.01	5.5	109.3	2.2	166.8
7.6	12.67	2.05	20.79	8.5	38.74	4.6	66.80	6.0	110.4	2.5	169.3
7.8	12.83	2.10	21.05	9.0	39.58	4.8	67.57	6.5	111.4	3.0	172.8
8.0	12.99	2.15	21.30	9.5	40.40	5.0	68.32	7.0	112.2	3.5	175.8
8.2	13.15	2.20	21.54			5.2	69.05	7.5	113.0	4.0	178.5
8.4	13.31	2.25	21.78	$\frac{\Delta pD^2}{\rho\nu^2}$	$\frac{\Delta p}{\tau_w}$	5.5	70.00	8.0	113.7	4.5	180.9
8.6	13.47	2.30	22.02	$\frac{\Delta pD^2}{\rho\nu^2}$	$\frac{\Delta p}{\tau_w}$	6.0	71.55	9.0	114.9	5.0	183.1
8.8	13.63	2.40	22.49	$\times 10^{-4}$		6.5	73.00			6.0	186.8
9.0	13.78	2.50	22.96			7.0	74.35			7.0	190.0
9.2	13.93	2.6	23.41	1.00	41.18	7.5	75.60	$\frac{\Delta pD^2}{\rho\nu^2} \times 10^{-6}$	$\frac{\Delta p}{\tau_w}$	8.0	182.8
9.4	14.08	2.7	23.86	1.05	41.93	8.0	76.80			9.0	195.3
9.6	14.23	2.8	24.30	1.10	42.65	8.5	77.95				
9.8	14.38	2.9	24.73	1.15	43.34	9.0	78.95				
		3.0	25.08	1.20	44.00	9.5	79.90	1.0	116.0	$\frac{\Delta pD^2}{\rho\nu^2}$	$\frac{\Delta p}{\tau_w}$
		3.1	25.43	1.25	44.64			1.1	117.1		
		3.2	25.78	1.30	45.27			1.2	118.1	$\times 10^{-8}$	
		3.3	26.13	1.35	45.87			1.4	119.8		
		3.4	26.48	1.40	46.45			1.6	121.5	1.0	197.5
1.0	14.53	3.5	26.82	1.45	47.01			1.8	123.1	1.2	201.4
1.02	14.67	3.6	27.16	1.50	47.56			2.0	124.6	1.4	204.7
1.06	14.95	3.7	27.50	1.55	48.09	1.0	80.80	2.2	126.0	1.6	207.5
1.10	15.23	3.8	27.83	1.60	48.61	1.05	81.70	2.5	127.8	1.8	210.1
1.14	15.51	3.9	28.15	1.65	49.12	1.10	82.55	3.0	130.7	2.0	212.5
1.18	15.78	4.0	28.46	1.70	49.62	1.15	83.35	3.5	133.3	2.5	217.4
1.22	16.04	4.2	29.07	1.8	50.56	1.20	84.1	4.0	135.6	3.0	221.6
1.26	16.30	4.4	29.66	1.9	51.46	1.30	85.5	4.5	137.7	3.5	225.0

ence of modest external pressure gradients, the absolute thickness of the turbulent layer and wall roughness, provided the Preston tube lies entirely in the universal wall region and the roughness height is small compared with the least pitot dimension.

The first condition has been irrevocably established for internal or concave transverse curvatures, since pipe-flow measurements reveal an identical law of the wall irrespective of pipe diameter.

For the case of external or convex curvature, the same universal velocity profile is believed to be equally applicable. Quarmby⁽¹⁰⁸⁾ has reported the use of flattened Preston tubes in concentric annuli. He found that in fully developed flows, the pressure gradient obtained from shear stress measurements at the inner and outer walls checked very well with that obtained from direct measurement. Such an observation should confirm the validity of the use

of flattened Preston tubes in situations having convex transverse curvature only. Though Quarmby's results had generated some controversy in the literature, the good agreement in the pressure-gradient values could be quoted as a convincing proof of the validity of measurements made by the Preston tube under such conditions. In order to provide a theoretical justification for this, the velocity profile measurements reported by Quarmby in reference 109 have been examined in depth. It is found that though the velocity profiles on the inner and outer walls in the log-linear region belong to two different parametric families of universal profiles of the form

$$u^+ = A \log y^+ + B \quad (99)$$

with values of A smaller and B higher for inner profiles, all velocity profiles within the inner layer are in close agreement with each other as well as

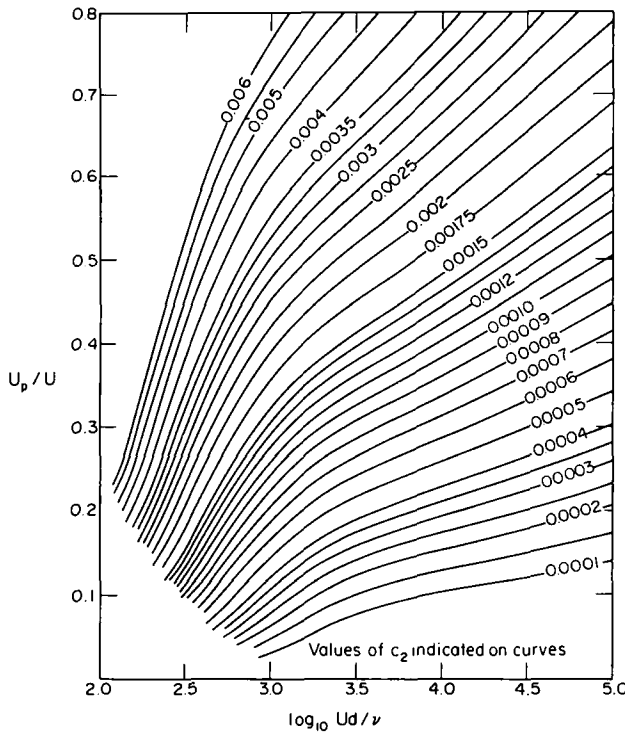


FIG. 84. Calibration curves for the Preston tube showing u_p/U as functions of tube Reynolds number and wall skin friction coefficient.

with Deissler's empirical correlation. In fact, the scatter about this correlation may be said to be of the same order as that seen in Deissler's own comparison with pipe flow data. In view of this, it can be said that the use of Preston tubes in concentric annuli will yield the same accuracy as in pipe or boundary flows as long as the tubes are small enough to stay submerged in the sub- or transitional layer of the flow. In this respect, it is fortuitous for Quarmby to have selected flattened pitots for his measurements since their small thickness would enable them to satisfy the above restriction at all times.

Regarding the second condition, it is expected that the Preston tube becomes inapplicable in severe pressure gradients, both favourable and adverse, since the law of the wall breaks down under such conditions. In both severe favourable and adverse pressure gradients, Patel reported that the Preston tube overestimates the skin friction. In this connection, he found that the inner pressure gradient parameter, defined by $\Pi \equiv (\nu/\rho u^*) (dp/dx)$, was insufficient to define a single parametric family of calibration curves, thus obviating the use of the Preston tube under these conditions. Nevertheless, he was able to suggest the following limits in terms of this parameter within which the calibration curves can be used with prescribed accuracy:

(a) Adverse pressure gradients:

maximum error 3%: $0 < \Pi < 0.01$, $u^*D/\nu \leq 200$,
maximum error 6%: $0 < \Pi < 0.015$, $u^*D/\nu \leq 250$.

(b) Favourable pressure gradients:

maximum error 3%: $0 < -\Pi < 0.005$, $u^*D/\nu \leq 200$, $d\Pi/dx < 0$,

maximum error 6%: $0 < -\Pi < 0.007$, $u^*D/\nu \leq 200$, $d\Pi/dx < 0$.

The additional restriction of $d\Pi/dx < 0$ in favourable pressure gradients is imposed to ensure that the flow is sufficiently far from the commencement of relaminarization.

Assuming Blasius' skin friction law

$$c_f = 0.079 Re^{-1/4} \quad (100)$$

to hold in pipe flow, where Re is the Reynolds number based on pipe diameter and mean velocity, the relation between Π and Re can be easily shown to be

$$\Pi = -20.1 Re^{-7/8}. \quad (101)$$

Thus, a 3% accuracy of τ_0 corresponds to a pipe flow Reynolds number of 13,000. Patel cautioned the use of the Preston tube at Reynolds numbers smaller than this value because in this region the scatter of the calibration data becomes significant.

With regard to the last condition, Preston suggested that the extent of the region in which local dynamical similarity exists appears to vary from one-fifth to one-twentieth of the boundary-layer thickness for conditions remote from and close to separation, respectively.

In addition, Head and Rechenberg reported the presence of large and more or less regular spanwise variations in the skin friction in a growing boundary layer. This would considerably complicate the

measurement of surface shear. They suggested that the Preston tube, because of the ease with which it can be traversed across the surface, should be extremely useful under these circumstances.

Recent experiments reported by Patel and Head⁽⁹⁷⁾ indicate that the velocity distribution in the wall region of fully developed flow does not conform precisely to the universal wall law when the pipe Reynolds number is smaller than about 6000. These results cast some doubt on the accuracy of Preston tube calibrations carried out in pipes at low Reynolds numbers. However, its effect, like the discrepancies noted earlier at the cross-over points in the expressions given by Patel, may reasonably be regarded as insignificant for practical purposes.

5.2.4. Results for pitots of other cross sections

The only other form of pitot used in this connection was the flattened oval-shaped pitot. Now, owing to its small thickness, there is no need for the pitot to rest on the surface as it can be easily located within the wall region. The displacement of the effective centre due to the velocity gradient effect can thus be made negligibly small by locating the pitot far enough from the wall, though now its position has to be accurately determined. This inconvenience will discourage this mode of usage in practice.

Results obtained by Preston indicate that essentially the same calibration applies to the fully turbulent region. The difference between these results and those for the round pitot had been attributed to the displacement of the effective centre of the round pitot in the presence of a transverse velocity gradient. However, the effective centre displacement deduced by Preston was a function of its wall distance. Though this does provide some dependence on the velocity gradient and hence the shear parameter as required by theoretical considerations discussed in Section 1.3.1, his proposed correction for the velocity gradient effect should not be taken too seriously in view of the uncertain nature of the Young and Maas correction he used for the rectangular pitot and also the poorer accuracy of his data as compared to those of later investigators.

More recently, Quarmby and Das⁽¹⁰⁷⁾ had confirmed Preston's observation that calibration results are essentially the same for both flattened and round pitots. Their results were obtained for near geometrically similar flattened pitots having $h/H \approx 0.6$, $h/w \approx 0.5$ and $H/W \approx 0.6$. These results showed that within the range $4.6 < x^* < 6.0$ (the upper limit being the highest x^* value reported) the calibration curve (based on external height) almost coincides with Patel's calibration for the round pitot (based on outside diameter). Such results imply that for $x^* > 4.6$ the difference in the displacement effect between flattened and round pitots becomes negligible for practical purposes. For $x^* < 4.6$, results for the flattened pitot are higher than

Patel's by some 5%. It was found that the relation

$$y^* = 0.5152 + 0.1693x^* + 0.0651x^{*2} \quad (102)$$

fits the results over the entire range for $3.38 < x^* < 6$ within 1½% of τ_0 .

5.3. Measuring Wall Shear Stress of Unknown Direction

The Preston tube is a convenient method for measuring skin friction when its direction is known. However, when the shear stress is at an unknown angle with the free-stream direction, as in some three-dimensional boundary layers where the law of the wall remains valid in the inner region, the performance of the Preston tube becomes rather poor, because of the insensitivity of the probe to the angle of attack, as is evident from Fig. 85. To overcome the difficulties encountered by the conventional Preston tube, Rajaratnam and Muralidhar⁽¹¹¹⁾ had suggested the use of a three-tube Conrad probe instead.

For the present application, the analysis is similar to that used in Section 4.3.2. However, it is now necessary to seek a means whereby the dynamic pressure recorded at the wall can be converted into a parameter involving the wall shear stress. This can be accomplished as follows:

Rewriting eqn. (96) in the inverted form

$$\frac{\Delta p D^2}{\rho v^2} = f\left(\frac{\Delta p}{\tau_0}\right) \quad (103)$$

and substituting into eqns. (70) to (72) the following set of equations can be obtained:

$$p_i = p_0 + K_i \frac{\rho v^2}{D^2} f\left(\frac{\Delta p}{\tau_0}\right), \quad i = 1, 2, 3 \quad (104)$$

where K_i represents the calibration factors of the member tubes of the probe configuration shown in Fig. 77. The calibration tests were performed at six values of τ_0 in a plane turbulent wall jet under zero pressure gradient, produced by a deeply submerged nozzle in a rectangular channel.

By suitably combining any two of the three equations, for instance, for $i = 1$ and 2, it could be shown that

$$\frac{1}{K_1 - K_2} \times \frac{(p_2 - p_1)D^2}{\rho v^2} = \frac{\Delta p D^2}{\rho v^2} = f\left(\frac{\Delta p}{\tau_0}\right) \quad (105)$$

whence

$$\Delta p = \frac{p_2 - p_1}{K_2 - K_1}. \quad (106)$$

Thus, from the readings p_1 , p_2 and p_3 read with the probe in an arbitrary direction, K_0 can be calculated using eqn. (73). This allows the estimation of θ from Fig. 78, and hence K_1 , K_2 and K_3 from Fig. 77. Using eqn. (105), $\Delta p/\tau_0$ can be estimated from the calibration results for the Preston tube tabulated in Table 1. From this, τ_0 can be determined with the help of eqn. (106).

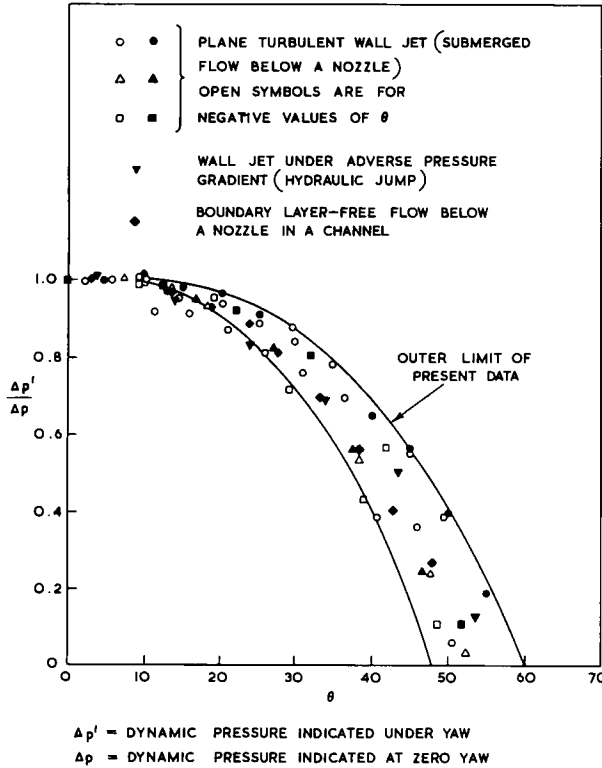


FIG. 85. Variation of $\Delta p'/\Delta p$ with yaw angle of the Preston tube. (Inner curve from ref. 123).

There appears to be some restrictions on the use of the three-tube-Conrad probe for vector shear stress measurements. This is because the wall region of the three-dimensional turbulent boundary layer is much thinner than its two-dimensional counterpart.

5.4. Wall Shear Measurement in Two-phase Flow

Calibration data for the Preston tube in air-water mixtures having gas mass fraction lying between 0.059 and 0.701 have been reported by Schraub *et al.*⁽¹²⁵⁾ Their results, shown in Fig. 86, indicate that

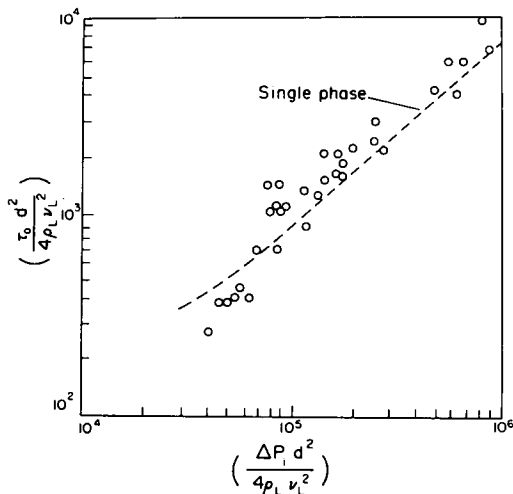


FIG. 86. Skin-friction correlation for air-water mixtures as compared to single-phase relation of Patel.

accuracy up to within $\pm 30\%$ of the single phase curve can be attained with most of the points evaluated with liquid properties. In cases where the liquid films were thinner than the height of the probe, they noted that the scatter can be reduced by using air properties. Probably, some mixed mean properties would be better suited to non-dimensionalize the data.

5.5. The Static Hole Pair

For deep static holes of a particular wall fitting design, eqn. (58) can be reduced to the simple form of eqn. (89) where D now denotes the static hole diameter, d , and Δp the static pressure error. It is therefore evident that a static hole pair can be used as a skin friction meter. Rajaratnam⁽¹¹⁰⁾ has reduced the deep static hole results of Shaw⁽¹²¹⁾ in the form of eqn. (96). He found that within the range $0 < \log(\Delta p d^2 / \rho v^2) < 5.5$, these can be represented by the expression

$$\frac{\tau_0 d^2}{\rho v^2} = 129 \left(\frac{\Delta p d^2}{\rho v^2} \right)^{0.555}. \quad (107)$$

Using eqn. (107), it can be shown that if p' and p'' are static pressures registered by holes of diameters d_1 and d_2 respectively, then the true static pressure under measurement is given by

$$p = \frac{\alpha p' - p''}{\alpha - 1} \quad (108)$$

where

$$\alpha = \left(\frac{d_2}{d_1} \right)^{1.60}.$$

Once p is known, τ_0 can be found from eqn. (107) using either static pressure reading. Contrary to what Rajaratnam has stated, this method of measuring skin friction should not be dependent on the universality of the law of the wall, since only local properties at the wall are involved—unlike the Preston tube which requires a velocity measurement. It does depend, as has been pointed out in Section 2.2.2, on the geometry of the wall fitting. Thus, the results of Livesey *et al.*⁽⁸⁰⁾ would give a different relation for eqn. (107). However, Shaw's hole configuration could be fabricated much more easily and would enjoy wider application.

Test results of Duffy and Norbury⁽²³⁾ have indicated that the static hole pair is capable of measuring skin friction within about 2%; but a number of practical difficulties are involved, including the necessity to measure very small pressure differences of the order of 0.01 cm alcohol and to keep below an acceptable level the error due to spanwise variation of skin friction. They further pointed out that when spanwise variation in skin friction exists, neglecting the difference of skin friction at the two holes can result in substantial errors if the diameter ratio of the holes is not large enough. A large diameter ratio of the hole pair is also desirable because this will increase the pressure difference measured. However, there are practical limitations: the last dimensionless group in eqn. (58) will limit the large hole diameter to smaller than about one-fifth the boundary-layer thickness and the small hole should be large enough to give reasonable response time.

In spite of what has been said by Duffy and Norbury, the static-hole pair is in fact the most suitable device for skin friction measurements in the presence of skin friction gradients, as the following analysis will show:

Using the result of Shaw given in eqn. (107), the reading at a static hole can be shown to be

$$\Delta p = \frac{A}{(\rho v^2)^{1.8}} \tau_0^{1.8} d^{1.6} \quad (109)$$

where

$$A = \frac{1}{129^{1.8}}.$$

Now, suppose that a static hole of diameter d_1 is located at a position a and another of diameter d_2 at b , then, the pressure difference across the static hole pair is

$$\Delta p' = \Delta p'_1 - \Delta p'_2 = \frac{A}{(\rho v^2)^{1.8}} \tau_a^{1.8} d_1^{1.6} \left\{ 1 - \left(\frac{\tau_b}{\tau_a} \right)^{1.8} \left(\frac{d_2}{d_1} \right)^{1.6} \right\}. \quad (110)$$

Interchanging the position of these two holes will give

$$\Delta p'' = \Delta p''_1 - \Delta p''_2 = \frac{A}{(\rho v^2)^{1.8}} \tau_b^{1.8} d_1^{1.6} \times \left\{ 1 - \left(\frac{\tau_a}{\tau_b} \right)^{1.8} \left(\frac{d_2}{d_1} \right)^{1.6} \right\}. \quad (111)$$

Dividing eqn. (110) by eqn. (111) and rearranging yields

$$\frac{\tau_a}{\tau_b} = \left\{ \frac{\frac{\Delta p'}{\Delta p''} + \left\{ \frac{d_2}{d_1} \right\}^{1.6}}{1 + \frac{\Delta p'}{\Delta p''} \left(\frac{d_2}{d_1} \right)^{1.6}} \right\}^{0.555}. \quad (112)$$

Thus, knowing the pressure differences of the static hole pair at two given locations allows the shear stress ratio for these positions to be computed, and hence τ_a or τ_b can be evaluated using eqns. (110) or (111). For the particular case in which the shear stress is equal at the two locations, the two pressure differential readings should be equal. This is evident from eqn. (112).

A form of the disc static probe suitable for use in this manner is shown in Fig. 87.

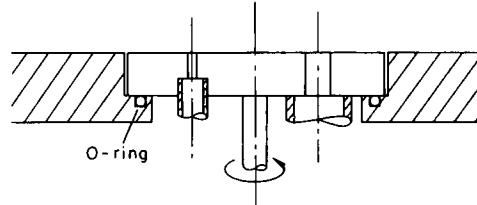


FIG. 87. A form of static-hole pair suitable for use in situations having skin friction gradients.

5.6. The Razor-blade Technique

The razor-blade technique represents an attempt in simplifying the construction of the Stanton tube. Essentially, it consists of the building up of a surface total-head tube by covering a static pressure hole with a segment of a razor blade. East⁽²⁵⁾ secured the blade in place by means of a magnet while Pai and Whitelaw⁽⁹⁵⁾ reported the use of adhesive tape or cement. In using cement, care should be taken that it does not leak between the blade and the wall. Test results of Pai and Whitelaw indicate that the influence of hole diameter is small provided that the blade is completely covering the static hole. Only visual alignment of the blade with the upstream edge of the hole is necessary. A slight protrusion of the blade edge is to be preferred for reproducibility. They have demonstrated that the calibration remains valid if the blade is removed and relocated over the same or a different, similar-sized hole: for individually calibrated blades, values of shear stress remains within $\pm 3\%$ of the original calibration. For all the blade segments (having thicknesses within the range 0.101 ± 0.0025 to 0.229 ± 0.013 mm) secured with cement or tape, shear stress values can be predicted within $\pm 9\%$ of the following calibration

functions:

$$y^* = \begin{cases} -0.464 & \text{cement} \\ -0.512 & \text{tape} \end{cases} + 0.741x^* \quad 1.17 \leq y^* \leq 2.30.$$

The expression for cement has been found to agree closely with East's calibration, given by

$$y^* = -0.23 + 0.618x^* + 0.0165x^{*2} \quad 1.2 \leq y^* \leq 3.8$$

over the common y^* range. In the above formulas, the parameters x^* and y^* are to be evaluated with h , the height of the blade edge above the wall, replacing D , the diameter of the Preston tube, in their definitions given by eqns. (91) and (92).

6. FLOW MEASUREMENT

6.1. Introduction

When used as a flowmeter, the pitot tube is by no means inferior to many of the commercially available direct reading instruments. This is evident from the development of the micrometer-pitot calibrating pipe which is the most accurate method for measuring gas-flow rate in small pipes—since gases cannot be easily collected and weighed as liquids.

The use of the pitot tube as a flow-metering device consists of first plotting the velocity profile by means of a pitot traverse and the subsequent integration of this profile over the flow area. Undoubtedly, this method is too tedious to be of significance in practice except for accurate calibration work. In order to simplify the procedures involved in the application of this method, many methods have been devised to reduce the amount of work required in the process of integration and/or to reduce the number of measurements.

In the following discussions, the methods are developed for application along one diameter only. This is generally satisfactory if the flow is known to be symmetrical. When the flow is asymmetrical, it is advisable to make measurements along two perpendicular diameters. In addition, it should be noted that the errors quoted are inherent to the method due to the approximations involved. To achieve the prescribed accuracies given below, other errors caused by the probe should be kept to a minimum. In this connection, the probe size should be kept within the limits suggested in Section 3.2.6.

6.2. Pipes of Circular Cross-sections

6.2.1. Equal-area methods

In these methods, the pipe is subdivided into n zones of equal area, and the mean velocity of each zone is measured with a pitot-static tube. It can be readily shown that the total discharge is related to the individual zone discharge by

$$Q = A\bar{u} = \sum a_i \bar{u}_i = a \sum \bar{u}_i. \quad (113)$$

Alternatively, the mean velocity can be written as

$$\bar{u} = \frac{1}{n} \sum \bar{u}_i \quad (114)$$

where A = cross-section area of pipe, a_i = area of zone i , Q = total volumetric discharge, \bar{u}_i = mean velocity of zone i , \bar{u} = mean velocity of pipe.

Two methods have been suggested for measuring the mean velocities. In the first method, known as the tangential method, the mean velocity of zone i is assumed to be equal to that at a radius which in turn divides this zone into two equal parts. There is no reason why this should be so. It is merely an assumption to facilitate computation. Of course, the error incurred will be less the greater the number of zones the pipe is subdivided into. In practice, n is generally taken to be 5, so that ten readings will be taken across a diameter at the following positions:

$$0.026d, \quad 0.082d, \quad 0.146d, \quad 0.226d, \quad 0.342d, \\ 0.658d, \quad 0.774d, \quad 0.854d, \quad 0.918d, \quad 0.974d.$$

The second method was developed by Winternitz and Fischl^[138] using a fully developed pipe flow velocity profile in the form of

$$u = A + B \log \frac{y}{d} + C \frac{y}{d}. \quad (115)$$

Because of the form of the profile used, this method has been termed the log-linear method. The locations of the measuring stations have been worked out to correspond exactly to the mean zone velocities of the above profile. These positions are given below for 2, 4, 6, 8 and 10 measurements per diameter:

2:0.112d,	0.888d.
4:0.043d,	0.290d, 0.710d, 0.957d.
6:0.032d,	0.135d, 0.321d, 0.679d, 0.865d, 0.968d.
8:0.021d,	0.117d, 0.184d, 0.345d, 0.655d, 0.816d, 0.883d, 0.979d.
10:0.019d,	0.076d, 0.153d, 0.217d, 0.361d, 0.639d, 0.783d, 0.847d, 0.924d, 0.981d.

Winternitz and Fischl had made extensive comparison of the tangential and log-linear methods with a large number of pitot-static traverses consisting of up to 100 measuring points per diameter in fully developed as well as developing flows in both smooth and rough pipes including some highly irregular velocity profiles. In the roughest pipes included in their investigations, the average height of the equivalent sand roughness was about one-thirtieth the pipe diameter. They concluded that, for fully developed pipe flow, the 4-point log-linear method gave an error of less than $\frac{1}{2}\%$, whereas the 10-point tangential method overestimated by about 1%. For pipe flow that was not fully developed and for irregular velocity distributions, including some that were markedly asymmetric, the 4-point log-linear method was inferior, the 6-point about equivalent, and the 8- and 10-point superior, to the 10-point tangential method. The error of the 10-

point log-linear method was about half that of the 10-point tangential method, which has an error of about 1%.

6.2.2. Rapid methods

If high accuracies are not required, even fewer measurements need be made. Winternitz and Fischl had recommended that the mean velocity can be computed from three observations per diameter using the following equation:

$$\bar{u} = \frac{1}{3}\{u_{0.500} + 2(u_{0.081} + u_{0.919})\} \quad (116)$$

where the subscripts represent the specified positions from a wall along a diameter at which measurements are to be made.

An even simpler method using two measurements has been suggested by Aichelen⁽¹⁾ after analysing the data of Nikuradse. The mean velocity is given by

$$\bar{u} = \frac{1}{2}(u_{0.119} + u_{0.881}). \quad (117)$$

This is, in fact, quite close to the 2-point log-linear method.

For fully developed flow in smooth and rough pipes, these quick methods give accuracies comparable to the 4-point log-linear and 10-point tangential methods. However, for asymmetric profiles, the errors are considerably higher. Winternitz and Fischl's method overestimated the mean velocity of profiles A and B of Fig. 88 by 3.6% and 1.3%, and

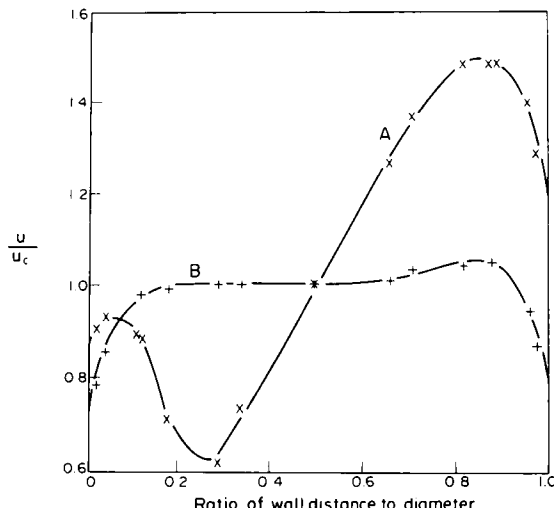


FIG. 88. Two representative asymmetric velocity profiles used for testing accuracies of various equations used for flow measurement.

Aichelen's method by 6.8% and 4.3% respectively; whereas the 4- and 6-point log-linear methods gave errors not exceeding 1% for both profiles.

6.3. Rectangular Pipes

For rectangular pipes, B.S. 1042 recommends the subdivision of the cross-sectional area into a grid of

geometrically similar parts which should not be less than sixteen in number, and that no part should exceed 230 cm^2 in area. The mean velocity through each part is to be determined as follows: for all parts not adjacent to any wall, the mean velocity is taken to be that at the centre of the part. For parts adjacent to a wall, the B.S. recommends that additional readings at one-sixth and five-sixths the width or depth of the part from the wall should be taken, and the mean of these three readings used as the mean velocity through the part. Thus, five readings need be taken at each corner part and three in all others bounded on one side by a wall. It is therefore seen that the minimum number of measurements specified is forty-eight. Even with this large number of measurements, the error can be much larger than that in circular pipes using much fewer measurements. For instance, for a square section subdivided into sixteen parts, an error of 2% or more can be incurred in certain types of asymmetric velocity distributions.

To reduce the tedium of the B.S. method, it may be of value to extend the tangential method in circular flow to rectangular pipes. However, it does not seem that the accuracy of this is known at the present.

6.4. Flow Measurement from Pressure Gradient

All the methods discussed so far involve the measurement of the velocity head of the flow using a pitot-static tube. As an alternative, we can also obtain the total discharge from the pressure gradient producing the flow. This method can be carried out much more readily than the above methods, since now the information required can be obtained directly from one differential pressure reading from two static orifices along a known length of pipe. For the purpose of computation, we have to distinguish between laminar and turbulent flows.

When the flow is laminar, the well-known Hagen-Poiseulle solution gives the mean velocity as

$$\bar{u} = \frac{R^2}{8\mu} \frac{dp_D}{dx}. \quad (118)$$

In turbulent flow, it can be easily shown that the Prandtl-Nikuradse skin friction formula for smooth pipes can be rewritten as

$$\frac{1}{\sqrt{f}} = 4 \log \left\{ \frac{2R}{\nu} \sqrt{\left(\frac{R}{\rho} \frac{dp_D}{dx} \right)} \right\} - 0.4. \quad (119)$$

Thus, knowing the dynamic pressure gradient and other relevant parameters, the skin friction coefficient can be obtained by direct calculation, and the mean velocity can then be computed using the expression

$$\bar{u} = \sqrt{\left(\frac{1}{f} \frac{R}{\rho} + \frac{dp_D}{dx} \right)}. \quad (120)$$

This procedure can be directly extended to rough pipes using the Colebrook skin friction formula in the following form:

$$\frac{1}{\sqrt{f}} = -4 \log \left\{ \frac{0.6275}{R} \sqrt{\left(\frac{R dp_D}{\rho dx} \right)} + \frac{\epsilon}{3.7D} \right\} \quad (121)$$

Equations (119) and (121) are capable of giving accuracies as high as the skin friction laws themselves. They are therefore highly accurate when applied to fully developed pipe flows for which these laws were obtained. Their acceptability in non-fully developed flows and in situations having irregular profiles has not been tested. It should also be noted that in non-horizontal pipe-lines, the elevation head should be deducted, since only the dynamic pressure gradient is of significance in the above formulas.

NOTES ADDED TO PROOF

A recent article by H. A. Becker and A. P. G. Brown entitled Response of Pitot probes in turbulent streams (*J. Fluid Mech.* **62**(1) (1974) 85–114) reported a new theoretical study on impact pressure response in incompressible turbulent streams for which viscous ($Re_D > 1000$) and mean velocity gradient corrections are negligible and for which the turbulence scale is large compared with probe diameter ($\Lambda > 5D$). Using their directional response parameters, these authors showed that two pitots having different directional characteristics can be used for the measurement of turbulence intensities. Results obtained on the centre-line of round jets, both free and confined, were found to agree closely with results from hot-wire anemometry. With this breakthrough, it may be said that pressure probes have finally recovered the last important field of fluid measurement—the measurement of turbulence characteristics—for which they have been shut out for a long time in the past, and that this review can be ended on the happy note that at this moment no other methods developed for fluid measurement have been as successfully applied as pressure probes to all these seven areas of fluid measurement discussed here.

REFERENCES

1. AICHELEN, W., Der geometrische Ort für die mittlere Geschwindigkeit bei turbulenter Strömung in glatten und rauen Röhren. *Z. Naturforschung*, **2**, 106 (1947).
2. ALLEN, C. M. and HOOPER, L. J., Piezometer investigation. *Trans. ASME*, **54**, Paper Hyd-54-1 (1932).
3. ASHKENAS, H. and SHERMAN, F. S., The structure and utilization of supersonic free jets in low density wind tunnels. *Proc. 4th Int. Symp. on Rarefied Gas Dynamics*, Vol. II, pp. 84–105, Academic Press, 1966.
4. BARAT, M., Influence de la turbulence sur le prises de pression statique. *Comptes Rendus*, **246**, 1156 (1958).
5. BARKER, M., On the use of very small pitot-tubes for measuring wind velocities. *Proc. Roy. Soc. A*, **101**, 435–45 (1922).
6. BÄUERLE, H., Measuring instruments for pressure, velocity and direction measurements. *Repts. & Transl. No. 951*, Brit. M.A.P. Völknerode, Mar. 15, 1947.
7. BLUE, R. E. and LOW, G. M., Factors affecting laminar boundary layer measurements in a supersonic stream. NACA TN 2891, 1953.
8. BRADFIELD, W. S., DE COURSIN, D. G. and BLUMER, C. B., The effect of leading-edge bluntness on a laminar supersonic boundary layer. *J. Aeronaut. Sci.* **21**, 373 (1954).
9. BRADSHAW, P. and GOODMAN, D. G., The effect of turbulence on static pressure tubes. *Brit. ARC R&M* 3527, 1968.
10. BRYER, D. W., WALSCHE, D. E. and GARNER, H. C., Pressure probes for three-dimensional flow. *Brit. ARC R&M* 3037, 1958.
11. CHAMBRE, P. L. and SCHAAF, S. A., The theory of the impact tube at low pressures. *J. Aeronaut. Sci.* **15**(12) (1948).
12. CHANG, J. H. and FENN, J. B., Viscous effects on impact pressure measurements in low density flows at high Mach numbers. *Proc. 6th Int. Symp. on Rarefied Gas Dynamics*, Vol. I, pp. 335–8, Academic Press, 1969.
13. CHUE, S. H., HANUS, N. and WINTER, E. R. F., Analytical and experimental study of heat transfer in a simulated Martian atmosphere. NASA-CR-108920, 1970.
14. CLAUSING, P., Ueber die Strömung sehr verdünnter Gase durch Röhren von beliebiger Länge. *Ann. der Physik*, **5**(12), 961 (1932).
15. CLIPPINGER, R. F. and GIESE, J. H., Tables of supersonic flow about cone-cylinders, Part I: surface data. Ballistics Res. Lab. Rept. No. 729, 1950.
16. CONRAD, O., Geräte zur Messung von Strömungsrichtungen. *Archiv für Technisches Messen*, V 116–2, Oct. 1950.
17. COOKE, J. R., The use of quartz in the manufacture of small diameter pitot tubes. *Brit. ARC CP* 193, Dec. 1954.
18. COOPER, M. and WEBSTER, R. A., The use of an uncalibrated cone for determination of flow angles and Mach numbers at supersonic speeds. NACA TN 2190, 1951.
19. DAU, K., MCLEOD, M. and SURRY, D., Two probes for the measurement of the complete velocity vector in subsonic flow. *Aeronaut. J.* **72**, 1066–8 (1968).
20. DAVIES, F. V., Some effects of pitot size on the measurement of boundary layers in supersonic flow. *Brit. ARC* 15430, Aug. 1952.
21. DAVIES, P. O. A. L., The behavior of a pitot tube in transverse shear. *J. Fluid Mech.*, **3**, 441–56 (1958).
22. DONALDSON, I. S. and RICHARDSON, D. J., A short static probe with good incidence characteristics at supersonic speed. *Brit. ARC CP* 1099, 1970.
23. DUFFY, J. and NORBURY, J. F., Measurement of skin friction in pressure gradients using static hole pair. *I. Mech. E. Proc.* **182**, pt 3H, pp. 76–83 (1967/8).
24. DUSSOURD, J. L. and SHAPIRO, A. H., Deceleration probe for measuring stagnation pressure and velocity of a particle-laden gas stream. *Heat Transfer & Fluid Mechanics Inst.*, Univ. of Calif., 1955.
25. EAST, L. F., Measurement of skin friction at low subsonic speeds by the razor blade technique. *Brit. ARC R&M* 3525, 1967.
26. EICHENBERGER, H. P., The shear flow in bends, Sc.D. Thesis, M.I.T., 1952.
27. EMMONS, H., Preliminary report on the theory, calibration and use of a 5-hole axial yaw probe. Rept. 110, Harvard Univ.

28. ENKENHUS, K. R., Pressure probes at very low density. UTIA Rept. No. 43, Jan. 1957.
29. ENKENHUS, K. R., The design, instrumentation and operation of the UTIA low density wind tunnel. UTIA Rept. No. 44, June 1957.
30. FAGE, A., On the static pressure in fully turbulent flow. *Proc. Roy. Soc. A* **155**, 576-96 (1936).
31. FAGE, A., The estimation of pipe delivery from pitot-tube measurements. *Engng.* **145**, 616 (1938).
32. FOLSOM, R. G., Review of the pitot tube. *Trans. ASME*, **78**, 1447-60 (1956).
33. FRY, J. D. and TYNDALL, A. M., On the value of the pitot constant. *Phil. Mag.*, Series 6, **21**, 348-66 (1911).
34. FUHRMANN, G., Theoretische und experimentelle Untersuchungen an Ballon-modellen, Dissertation at Göttingen Univ., 1912; also in *Jahrbuch Motorluftschiffstudiengesellschaft*, **5**, 63 (1911/12).
35. GLASER, A. H., The pitot cylinder as a static pressure probe in turbulent flow. *J. Sci. Instr.* **29**, 219 (1952).
36. GLAUERT, M. B., The method of images in shear flow. *J. Fluid Mech.*, **9**, 561-80 (1960).
37. GOLDBERG, L., General Electric MSD Report R 655D59, Nov. 1959.
38. GOLDMAN, I. B. and MARCHELLO, J. M., Impact tube size in fluid velocity measurement. *AICHE J.* **10**, 775-6 (1964).
39. GOLDSTEIN, S., A note on measurement of total head and static pressure in a turbulent stream. *Proc. Roy. Soc. A* **155**, 570-5 (1936).
40. GRACEY, W., LETKO, W. and RUSSELL, W. R., Wind tunnel investigations of a number of total-pressure tubes at high angles of attack—subsonic speeds. NACA TN 2331, 1951.
41. GRACEY, W., COLETTI, D. E. and RUSSELL, W. R., Wind tunnel investigations of a number of total pressure tubes at high angle of attack—supersonic speeds. NACA TN 2261, 1951.
42. GRACEY, W., Wind tunnel investigations of a number of total pressure tubes at high angles of attack—subsonic, transonic and supersonic speeds. NACA Tech. Rept. 1303, 1957.
43. GRACEY, W., PEARSON, A. D. and RUSSELL, W. R., Wind tunnel investigation of a shielded total pressure tube at transonic speeds. NACA Rm L51K19, 1952.
44. GRAVES, J. C. and QUIEL, N. R., Impact pressure and total temperature interpretation at hypersonic Mach number. GALCIT Hypersonic Res. Project, Memorandum No. 20, July 1954.
45. HAHN, J. F., The effect of Mach number, incidence, and hole position on the static pressure measured by a square-ended probe. *J. Roy. Aeronaut. Soc.* **68**, 54 (1964).
46. HALL, I. M., The displacement effect of a sphere in a two dimensional shear flow. *J. Fluid Mech.*, **1**, 142 (1956).
47. HANSEN, C. F. and NOTHWANG, G. J., Condensation of air in supersonic wind tunnels and its effects on flow about models. NACA TN 2690, 1952.
48. HARRIS, E. L., Investigation of the time response and outgassing effects of pressure probes in free molecule flow. UTIA TN No. 6, Apr. 1956.
49. HARRIS, E. L. and PATTERSON, G. N., Properties of impact pressure probes in free molecule flows. UTIA Rept. No. 52, Apr. 1958.
50. HEAD, M. R. and RECHENBERG, I., The Preston tube as a means of measuring skin friction. *J. Fluid Mech.*, **14**, 1-17 (1962).
51. HEAD, M. R. and RAM, V. V., Simplified presentation of Preston tube calibration. *Aeron. Quart.* **22**, 295-300 (1971).
52. HEMKE, P. E., Influence of the orifice on measured pressures. NACA TN 250, 1926.
53. HESS, J. L., SMITH, A. M. O. and RIVELL, T. L., Development of an improved static pressure sensing probe for all Mach numbers: Phase I. Douglas Aircraft Co., Rept. ES 40336, 1961.
54. HOLDER, D. W., NORTH, R. J. and CHINNECK, A., Experiments with static tubes in a supersonic air-stream—Parts I and II. *Brit. ARC R&M* 2782, 1953.
55. HOMANN, F., The effect of high viscosity on the flow around a cylinder and a sphere. NACA Tech. Memorandum 1334, 1952. 1334, 1952.
56. HORLOCK, J. H., Instrumentation used in measurement of the three-dimensional flow in an axial flow compressor. *Brit. ARC CP* 321, 1957.
57. HUBBARD, C. W., Investigation of errors of pitot tubes. *Trans. ASME*, **61**, 477-92 (1939).
58. HUGHES, P. C. and DE LEEUW, J. H., Theory for the free molecule impact probe at an angle of attack. *Proc. 4th Symp. on Rarefied Gas Dynamics*, Vol. I, pp. 653-76. Academic Press, 1965.
59. HURD, C. W., CHESKY, K. P. and SHAPIRO, A. H., Influence of viscous effects on impact tubes. *J. Appl. Mech.* pp. 253-6 (1953).
60. HUSTON, W. B., Accuracy of airspeed measurements and flight calibration proceedings, NACA Tech. Rept. 919, 1948.
61. JEGOROW, G., Measurement of direction, velocity and pressure in a three-dimensional current. RTP transl. No. 2498, Durrand Reprinting Commission, Caltech.
62. JENSEN, V. G., Viscous flow around a sphere at low Reynolds numbers. *Proc. Roy. Soc. A* **249**, 346 (1959).
63. KANE, E. D. and MASLACH, G. J., Impact pressure interpretations in a rarefied flow at supersonic speeds. NACA TN 2210, 1950.
64. KANTROWITZ, A., Heat-capacity lag in gas dynamics. *J. Chem. Phys.* **14**, 150-64 (1946).
65. KEAST, F. H., High speed cascade testing techniques. *Trans. ASME*, **74**, 685 (1952).
66. KENNARD, E. H., *Kinetic Theory of Gases*, pp. 330-2, McGraw Hill, 1938.
67. KRAUSE, L. N., Effects of a pressure-rake design parameter on static pressure measurement for rakes used in subsonic free jets. NACA TN 2520, 1951.
68. KRAUSE, L. N. and GETTELMAN, C. C., Considerations entering into the selection of probes for pressure measurement in jet engines. *ISA Proc.* **7**, 134 (1952).
69. KRONAUER, R. E. and GRANT, H. P., Pressure probe response in fluctuating flows. *Proc. 2nd U.S. National Congr. Appl. Mech.*, 1954, pp. 163-9.
70. KÜCHEMANN, D., Boundary layers on swept wings. Their effects and their measurement. AGARD paper No. AG 19/P9, June 1955 (Ottawa meeting), pp. 69-100.
71. LEE, V. A., Interference effects from total pressure rakes in supersonic flow. M.S. Thesis, Univ. Texas, Aug. 1955.
72. LEES, L., Hypersonic flow. Inst. of Aeron. Sci., Preprint No. 554, June 1955.
73. LESTER, W. G. S., The flow past a pitot tube at low Reynolds numbers. *Brit. ARC R&M* 3240, 1961.
74. LEVINSKY, E. S. and YOSHIHARA, H., Rarefied hypersonic flow over a sphere. *Hypersonic Flow Research* (ed. RIDDELL, F. R.), pp. 81-106. Academic Press, 1962.
75. LIGHTHILL, M. J., Contribution to the theory of the pitot tube displacement effect. *J. Fluid Mech.*, **2**, 493 (1957).
76. LIGHTHILL, M. J., The fundamental solution for

- small steady three-dimensional disturbances to a two-dimensional parallel shear flow. *J. Fluid Mech.* **3**, 113 (1957).
77. LIN, T. C. and SCHAAF, S. A., The effect of slip on flow near a stagnation point and in a boundary layer. NACA TN 2568, 1951.
 78. LIVESEY, J. L., Design of total pressure probes for minimum interference with measured flow. *J. Aeronaut. Sci.* **21**, 641 (1954).
 79. LIVESEY, J. L., The behaviour of transverse cylindrical and forward facing total pressure probes in transverse total pressure gradient. *J. Aeronaut. Sci.* **23**, 949-55 (1956).
 80. LIVESEY, J. L., JACKSON, J. D. and SOUTHERN, C. J., The static hole error problem. *Aircraft Engng.* **34**, 43-47 (1962).
 81. LOCK, C. N. E., KNOWLER, A. E. and PEARCEY, H. H., The effect of compressibility on static heads. Brit. ARC R&M 2386.
 82. MACCOLL, J. W. and CODD, T., Theoretical investigation of the flow around various bodies in the sonic region of velocities. Min. of Supply Theoret. Res. Rept. 17/45, ARC 45/19, 1945.
 83. MACMILLAN, F. A., Viscous effects on pitot tubes at low speeds. *J. Roy. Aeronaut. Soc.* **58**, 570-2 (1954).
 84. MACMILLAN, F. A., Viscous effects on flattened pitot tubes at low speeds. *J. Roy. Aeronaut. Soc.* **58**, 837-9 (1954).
 85. MACMILLAN, F. A., Experiments on pitot tubes in shear flow. Brit. ARC R&M 3028, 1956.
 86. MARKOWSKI, S. J. and MOFFATT, E. M., Instrumentation for the development of aircraft power plant components involving fluid flow. *Quart. Trans. SAE*, **2**, 104-16 (1948).
 87. MATTHEWS, M. L., An experimental investigation of viscous effects on static and pressure probes in hypersonic flow. GALCIT Hypersonic Res. Proj., Memo. No. 44, June 1958.
 88. MERRIAM, K. G. and SPAULDING, E. R., Comparative tests of pitot-static tubes, NACA TN 546, 1935.
 89. MONAGHAN, R. J., An approximate solution of the compressible laminar boundary layer on a flat plate. Brit. ARC R&M 2760, 1949.
 90. MONAGHAN, R. J., The use of pitot tubes in the measurement of laminar boundary layers in supersonic flow. Brit. ARC R&M 3056, 1957.
 91. MYADZU, A., Influence of type and dimensions of pressure holes on the recorded static pressure. *Ing. Arch.* **7**, 35 (1936).
 92. O'DONNELL, R. M., Experimental investigation at a Mach number of 2.41 of average skin friction coefficients and velocity profiles for laminar and turbulent boundary layers and an assessment of probe effects. NACA TN 3122, 1954.
 93. OWER, E. and JOHANSON, F. L., The design of pitot-static tubes. Brit. ARC R&M 981, 1925.
 94. OWER, E. and PANKHURST, R. C., *The Measurement of Air Flow*, 4th ed., Pergamon Press, 1966.
 95. PAI, B. R. and WHITELAW, J. H., Simplification of the razor blade technique and its application to the measurement of wall shear stress in wall jet flows. *Aeronaut. Quart.* **20**, 355-64 (1969).
 96. PATEL, V. C., Calibration of the Preston tube and limitations on its use in pressure gradients. *J. Fluid Mech.* **23**, 185-208 (1965).
 97. PATEL, V. C. and HEAD, M. R., Some observations of skin friction and velocity profiles in fully developed pipe and channel flows. *J. Fluid Mech.* **38**, 181 (1969).
 98. PATTERSON, G. N., Theory of free molecule orifice-type pressure probes in isentropic and non-isentropic flow. UTIA Rept. No. 41, Nov. 1956.
 99. PEARCEY, H. H., The effect of the condensation of atmospheric water vapour on total head and other measurements in the NPL high speed tunnels. Brit. ARC R&M 2249, 1951.
 100. POLLARD, M. G., Interpretation of impact pressures in rarefied gas flows, *Proc. 6th Int. Symp. on Rarefied Gas Dynamics*, Vol. I, pp. 811-34, Academic Press, 1969.
 101. POND, H. L., The effect of entrance velocity on the flow of a rarefied gas through a tube. *J. Aerosp. Sci.* **29**, 917-20 (1962).
 102. POTTER, J. L. and BAILEY, A. B., Pressures in the stagnation regions of blunt bodies in the viscous-layer to merged-layer regimes of rarefied flow. Arnold Engng. Development Center, TDR-63-168, Sept. 1963, also see *AIAA J.* **2**, 743-5 (1964).
 103. POTTER, J. L., KINSLAW, M. and BOYLAN, D. E., An influence of the orifice on measured pressures in rarefied flow. *Proc. 4th Int. Symp. on Rarefied Gas Dynamics*, Vol. II, pp. 175-94. Academic Press, 1966.
 104. PRESTON, J. H., The determination of turbulent skin friction by means of pitot tubes. *J. Roy. Aeronaut. Soc.* **58**, 109-21 (1954).
 105. PROBSTEN, R. F. and KEMP, N. H., Viscous aerodynamic characteristics in hypersonic rarefied gas flow. *J. Aerosp. Sci.* **27**, 174-92 (1960).
 106. QUARMBY, A. and DAS, H. K., Displacement effect on pitot tubes with rectangular mouths. *Aeronaut. Quart.* **20**, 129-39 (1969).
 107. QUARMBY, A. and DAS, H. K., Measurement of skin friction using a rectangular mouthed Preston tube. *Aeronaut. J.* **73**, 228-30 (1969).
 108. QUARMBY, A., On the use of the Preston tube in concentric annuli. *Aeronaut. J.* **71**, 47-49 (1967).
 109. QUARMBY, A., An experimental study of turbulent flow through concentric annuli. *Inter. J. Mech. Sci.* **9**, 205-22 (1967).
 110. RAJARATNAM, N., A note on the static error problem. *J. Roy. Aeronaut. Soc.* **70**, 370 (1966).
 111. RAJARATNAM, N. and MURALIDHAR, D., Yaw probe used as Preston tube. *Aeronaut. J.* **72**, 1059-60 (1968).
 112. RAJASOORIA, G. P. D. and BRUNDIN, C. L., An experimental investigation of the laminar near wake behind a circular cylinder in a Mach 6 rarefied air stream. Dept. of Engng. Sci. Rept. No. 1108/70, Univ. of Oxford, June 1970.
 113. RAY, A. K., On the effect of orifice size on static pressure reading at different Reynolds number. *Ing. Arch.* **24**, 171 (1956).
 114. RAYLE, R. E., JR., An investigation of the influence of orifice geometry on static pressure measurements, M.S. Thesis, M.I.T., 1949.
 115. RECHENBERG, I., Messung der turbulenten Windschubspannung. *A. Flugwiss.* **11**, 429 (1963).
 116. ROGERS, E. W. E. and BERRY, C. J., Tests on the effect of incidence on some pressure heads at high subsonic speeds. Brit. ARC CP 41, 1950.
 117. ROTHE, D. E. and DE LEEUW, J. H., A numerical solution of the free molecule impact pressure probe relations for tubes of arbitrary length, UTIA Rept. No. 88, Sept. 1962; also *AIAA J.* **1**, 220-1 (1963).
 118. ROUSE, H. and MCNOUN, J. S., Cavitation and pressure distribution, head forms at zero angle of yaw. *Stat Univ. of Iowa, Stud. Engng Bull.* **32**, 1948.
 119. SALTER, C., WARSAP, J. H. and GOODMAN, D. G., A discussion of pitot-static tubes and of their calibration factors with a description of various versions of a new design. Brit. ARC R&M 3365, 1962.
 120. SCHULZE, W. M., ASHBY, G. C., JR. and ERWIN, J. R., Several combination probes for surveying static and total pressure and flow direction. NACA TN 2830, 1952.
 121. SHAW, R., The influence of hole dimensions on static pressure measurements. *J. Fluid Mech.* **7**(4), 550-64 (1960).

122. SHERMAN, F. S., New experiments on impact pressure interpretation in supersonic and subsonic rarefied airstreams. NACA TN 2995, 1953.
123. SIGALLA, A., Experiments with pitot tubes used for skin friction measurement, The Brit. Iron and Steel Assoc. Rept., Mar. 1958.
124. STANTON, T. E., MARSHALL, D. and BRYANT, C. N., On the conditions at the boundary of a fluid in turbulent motion. *Proc. Roy. Soc. A97*, 413 (1920).
125. STRAUB *et al.* Two phase flow and heat transfer in multirod geometries. GEAP-5161 and 5207, 6th & 7th General Electric Quarterly Progress Repts. on Project Agreement 44 to USAEC, May and Aug. 1966.
126. TALBOT, L. M., Viscosity corrections to cone probes in rarefied supersonic flow at a nominal Mach number of 4. NACA TN 3219, 1954.
127. TAYLOR, G. I., Pitot pressure in moist air. Brit. ARC R&M 2248, 1945.
128. TAYLOR, G. I. and MACCOLL, J. W., The air pressure on a cone moving at high speeds, *Proc. Roy. Soc., A* 139, 278-311 (1933).
129. THOM, A., An investigation of fluid flow in two dimensions. Brit. ARC R&M 1194, 1929.
130. THOM, A. and APELT, C. J., The pressure in a two-dimensional static hole at low Reynolds numbers. Brit. ARC R&M 3090, 1958.
131. THWAITES, B. (ed.), *Incompressible Aerodynamics*, Oxford, 1960.
132. TOOMRE, A., The effect of turbulence on static pressure measurements. Brit. ARC 22010, 1960.
133. TSIEN, H. S., Notes on aerodynamics of compressible fluids. Aeron. Engng. Dept. Notes, M.I.T., 1949.
134. WALCHNER, O., Ueber den Einfluss der Kompressibilität auf die Druckanzeige eines Prandtl-Rohres bei Strömungen mit unterschallgeschwindigkeit. *Jahrbuch der deutschen Luftfahrtforschung*, 1, 578 (1938), English version: NACA Tech. Memorandum 917, 1939.
135. WALSCHE, D. E. and GARNER, H. C., Usefulness of various pressure probes in fluctuating low speed flows. Brit. ARC 21714, 1960.
136. WILSON, L. N., An experimental investigation of Reynolds number effects on supersonic static probes. UTIA TN 3, 1954.
137. WINTERNITZ, F. A. L., Cantilevered pitot cylinder. *The Engineer*, 199, 729-32 (1955).
138. WINTERNITZ, F. A. L. and FISCHL, C. F., A simplified integration technique for pipe flow measurement. *Water Power*, 9, 225 (1957).
139. YOUNG, A. D. and MAAS, J. N., The behaviour of a pitot tube in a transverse total pressure gradient. Brit. ARC R&M 1770, 1936.
140. ZAHM, A. F., Pressure of air on coming to rest from various speeds. NACA TN 247, 1926.